

Bayesian Modeling with Spatial Curvature Processes

Aritra Halder^a, Sudipto Banerjee^b and Dipak K. Dey^c

^aDepartment of Biostatistics,
Drexel University, Philadelphia, PA, USA.

^bDepartment of Biostatistics,
University of California, Los Angeles, CA, USA.

^cDepartment of Statistics,
University of Connecticut, Storrs, CT, USA.

February 13, 2023

Abstract

Spatial process models are widely used for modeling point-referenced variables arising from diverse scientific domains. Analyzing the resulting random surface provides deeper insights into the nature of latent dependence within the studied response. We develop Bayesian modeling and inference for rapid changes on the response surface to assess directional curvature along a given trajectory. Such trajectories or curves of rapid change, often referred to as *wombling* boundaries, occur in geographic space in the form of rivers in a flood plain, roads, mountains or plateaus or other topographic features leading to high gradients on the response surface. We demonstrate fully model based Bayesian inference on directional curvature processes to analyze differential behavior in responses along wombling boundaries. We illustrate our methodology with a number of simulated experiments followed by multiple applications featuring the Boston Housing data; Meuse river data; and temperature data from the Northeastern United States.

Keywords— Bayesian modeling, Directional Curvature, Gaussian Processes, Wombling.

1 Introduction

Spatial data science manifests in a variety of domains including environmental and geographical information systems (GIS) ([Webster & Oliver 2007](#), [Burrough et al. 2015](#), [Schabenberger & Gotway 2017](#), [Plant 2018](#)), digital cartography and terrain modeling ([Law et al. 2000](#), [Santner et al. 2003](#), [Jones 2014](#), [Vaughan 2018](#)), imaging ([Winkler 2003](#), [Chiu et al. 2013](#),

Dryden & Mardia 2016), spatial econometrics and land use (LeSage & Pace 2009), public health and epidemiology (Elliot et al. 2000, Waller & Gotway 2004, Lawson 2013) and public policy (Haining 1993, Wise & Craglia 2007). Spatial data analysis seeks to estimate an underlying spatial surface representing the process generating the data. Specific inferential interest resides with local features of the surface including rates of change of the process at points and along “spatial boundaries” to understand the behavior of the underlying process and identify lurking explanatory variables or risk factors. This exercise is often referred to as “wombling”, named after a seminal paper by Womble (1951); (also see Gleyze et al. 2001). For regionally aggregated data, it identifies boundaries delineating neighboring regions and has been used to study health disparities (Lu & Carlin 2005, Li et al. 2015, Gao et al. 2022) and ecological boundaries (Fitzpatrick et al. 2010). For point-referenced data, where variables are mapped at locations within an Euclidean coordinate frame with a sufficiently smooth spatial surface, it refers to estimating spatial gradients and identifying boundaries representing large gradients (Banerjee et al. 2003, Banerjee & Gelfand 2006, Qu et al. 2021).

Our current contribution develops Bayesian inference for spatial curvature along curves on Euclidean domains. Modeling curvature will require smoothness considerations of the process (Adler 1981, Kent 1989, Stein 1999, Banerjee & Gelfand 2003). Observations over a finite set of locations from these processes cannot visually inform about smoothness. Therefore, smoothness of the process is specified from mechanistic considerations which can be introduced through prior specifications as needed. While Bayesian inference for first order derivatives and directional gradients have received considerable attention (see, e.g., Morris et al. 1993, Banerjee et al. 2003, Majumdar et al. 2006, Liang et al. 2009, Heaton 2014, Terres & Gelfand 2015, Wang & Berger 2016, Terres & Gelfand 2016, Wang et al. 2018, Qu et al. 2021, for inferential developments involving spatial gradients from diverse modeling and application perspectives) such processes inform about directional change, but do not enable inference on curvature (departure from flatness) of the spatial surface.

Analyzing surface roughness from sampling considerations can be traced at least as far back as [Greenwood \(1984\)](#). We offer full inference with uncertainty quantification about spatial curvature at a point and average curvature along a curve from observed data after accounting for explanatory variables. Considering second-order finite differences we establish a valid spatial curvature process as a limit of such finite difference processes. When formulating directional curvature, we favor the normal direction corresponding to a chosen curve and devise a “wombling” measure to track curvature of the surface along the curve. We derive and exploit analytical expressions of higher order processes to avoid numerical finite differences. The Bayesian inferential framework delivers exact posterior inference for the above constructs on the response as well as latent (or residual) processes.

Section 2 develops the directional curvature processes through a differential operator. Section 3 develops the vector analytic framework for curvilinear wombling using curvature processes. Section 4 builds a hierarchical model to exploit the preceding distribution theory and conduct curvature analysis on the response and the latent process. Section 5 presents detailed simulation experiments for assessing directional gradients and curvatures. Section 6 considers applications to three different data sets: Boston housing data, Meuse river data, and Northeastern US Temperatures (the third data is presented in the Supplement).

2 Spatial Curvature Processes

Let $\{Y(\mathbf{s}) : \mathbf{s} \in \mathcal{S} \subset \mathbb{R}^d\}$ be a univariate weakly stationary random field with zero mean, finite second moment and a positive definite covariance function $K(\mathbf{s}, \mathbf{s}') = \text{Cov}(Y(\mathbf{s}), Y(\mathbf{s}'))$ for locations $\mathbf{s}, \mathbf{s}' \in \mathbb{R}^d$. In particular, under *isotropy* we assume $K(\mathbf{s}, \mathbf{s}') = \tilde{K}(\|\mathbf{s} - \mathbf{s}'\|)$, where $\|\mathbf{s} - \mathbf{s}'\|$ is the Euclidean distance between the locations \mathbf{s}, \mathbf{s}' ([Matérn 2013](#)). Building upon notions of mean square smoothness (see, e.g., [Stein 1999](#)) at an arbitrary location \mathbf{s}_0 in \mathbb{R}^d , we focus upon second order differentiability, $Y(\mathbf{s}_0 + h\mathbf{u}) = Y(\mathbf{s}_0) + h\mathbf{u}^\top \nabla Y(\mathbf{s}_0) + h^2 \mathbf{u}^\top \nabla^2 Y(\mathbf{s}_0) \mathbf{u} / 2 + r_2(\mathbf{s}_0, h^2 \|\mathbf{u}\|)$, where $r_2(\mathbf{s}_0, h^2 \|\mathbf{u}\|) / h^2 \rightarrow 0$ as $h \rightarrow 0$ in the L_2 sense and

∇ and ∇^2 are the gradient and Hessian operators, respectively.

For the scalar h and unit vectors \mathbf{u} , \mathbf{v} , we define $Y_{\mathbf{u},\mathbf{v},h}^{(2)} = (Y(\mathbf{s}_0 + h(\mathbf{u} + \mathbf{v})) - Y(\mathbf{s}_0 + h\mathbf{u}) - Y(\mathbf{s}_0 + h\mathbf{v}) + Y(\mathbf{s}_0))/h^2$ to be the second order finite difference processes in the directions \mathbf{u} , \mathbf{v} at scale h . Being a linear function of stationary processes it is well-defined. Passing to limits, $D_{\mathbf{u},\mathbf{v}}^{(2)}Y(\mathbf{s}_0) = \lim_{h \rightarrow 0} Y_{\mathbf{u},\mathbf{v},h}^{(2)}(\mathbf{s}_0)$. Provided the limit exists, $D_{\mathbf{u},\mathbf{v}}^{(2)}Y(\mathbf{s}_0)$ is defined as the directional curvature process. If $Y(\mathbf{s})$ is a mean square second order differentiable process in \mathbb{R}^d for every $\mathbf{s} \in \mathbb{R}^d$ then $D_{\mathbf{u},\mathbf{v}}^{(2)}Y(\mathbf{s}) = \mathbf{u}^\top \nabla^2 Y(\mathbf{s}) \mathbf{v}$ is well-defined with $D_{\mathbf{u},\mathbf{v}}^{(2)}Y(\mathbf{s}) = \lim_{h \rightarrow 0} (h^2 \mathbf{u}^\top \nabla^2 Y(\mathbf{s}) \mathbf{v} + \tilde{r}_2) / h^2 = \mathbf{u}^\top \nabla^2 Y(\mathbf{s}) \mathbf{v}$, where $\tilde{r}_2 = r_2(\mathbf{s}, h^2 \|\mathbf{u} + \mathbf{v}\|) - r_2(\mathbf{s}, h^2 \|\mathbf{u}\|) - r_2(\mathbf{s}, h^2 \|\mathbf{v}\|)$. In practice, we need only work with computing these derivatives for an orthonormal basis of \mathbb{R}^d , say the Euclidean canonical unit vectors along each axis $\{\mathbf{e}_1, \dots, \mathbf{e}_d\}$. If $\mathbf{u} = \sum_{i=1}^d u_i \mathbf{e}_i$, and $\mathbf{v} = \sum_{i=1}^d v_i \mathbf{e}_i$ are arbitrary unit vectors, we can compute $D_{\mathbf{u},\mathbf{v}}^{(2)}Y(\mathbf{s}) = \sum_{i=1}^d \sum_{j=1}^d u_i D_{\mathbf{e}_i, \mathbf{e}_j}^{(2)}Y(\mathbf{s}) v_j$. The directional curvature process is linear in the sense that $D_{-\mathbf{u}, -\mathbf{v}}^{(2)}Y(\mathbf{s}) = D_{\mathbf{u}, \mathbf{v}}^{(2)}Y(\mathbf{s})$, $D_{\mathbf{u}, -\mathbf{v}}^{(2)}Y(\mathbf{s}) = D_{-\mathbf{u}, \mathbf{v}}^{(2)}Y(\mathbf{s}) = -D_{\mathbf{u}, \mathbf{v}}^{(2)}Y(\mathbf{s})$. Since $D_{\mathbf{w}, \mathbf{w}}^{(2)}Y(\mathbf{s}) = \|\mathbf{w}\|^2 D_{\mathbf{u}, \mathbf{u}}^{(2)}Y(\mathbf{s})$, where $\mathbf{w} = \|\mathbf{w}\| \mathbf{u}$ and \mathbf{u} is a unit direction, we henceforth only consider unit directions. First order directional gradient processes, $D_{\mathbf{u}}^{(1)}Y(\mathbf{s})$, are reviewed in [Banerjee & Gelfand \(2006\)](#) and in Section S1.1 of the Supplement. Choosing a direction is emphasized with respect to interpreting the directional curvature processes. Directional curvature is the change in the normal to the surface $Y(\mathbf{s})$ at \mathbf{s}_0 when moving along a slice of the surface in the direction \mathbf{w} . The associated algebraic sign locally classifies the nature of curvature at \mathbf{s}_0 —for instance, convex or concave ellipsoids (see [Stevens 1981](#)). A detailed discussion, with illustration, is available in Section S2 of the Supplement.

Since $\nabla^2 Y(\mathbf{s})$ is a symmetric matrix, to avoid singularities arising from duplication we modify $D_{\mathbf{u},\mathbf{v}}^{(2)}Y(\mathbf{s})$ as follows. If $vech$ is the usual half-vectorization operator for symmetric matrices and \mathcal{D}_d is the duplication matrix ([Magnus & Neudecker 1980](#)) of order $d^2 \times d(d+1)/2$ then, $D_{\mathbf{u},\mathbf{v}}^{(2)}Y(\mathbf{s}) = \mathbf{c}_{\mathbf{u},\mathbf{v}}^\top vech(\nabla^2 Y(\mathbf{s}))$ where $\mathbf{c}_{\mathbf{u},\mathbf{v}}^\top = (\mathbf{u} \otimes \mathbf{v})^\top \mathcal{D}_d$ and \otimes is the Kronecker product for matrices. If $\mathbf{u} = (u_1, u_2)^\top$, $\mathbf{v} = (v_1, v_2)^\top \in \mathbb{R}^2$, then

$\mathbf{c}_{\mathbf{u}, \mathbf{v}} = (\mathbf{u} \otimes \mathbf{v})^\top \mathcal{D}_2 = (v_1 u_1, v_1 u_2 + v_2 u_1, v_2 u_2)^\top$. The process $vech(\nabla^2 Y(\mathbf{s}))$ in $\mathbb{R}^{d(d+1)/2}$ consists of the pure and mixed second order derivatives in $\nabla^2 Y(\mathbf{s})$. The distributions needed for inference on directional curvature processes depend on $vech(\nabla^2 Y(\mathbf{s}))$ rather than $\nabla^2 Y(\mathbf{s})$. We refer to $(\nabla Y(\mathbf{s})^\top, vech(\nabla^2 Y(\mathbf{s}))^\top)^\top$ as the differential process and $\{\mathbf{u}^\top \nabla Y(\mathbf{s}), \mathbf{c}_{\mathbf{u}, \mathbf{u}}^\top vech(\nabla^2 Y(\mathbf{s}))\}$ as the directional differential processes induced by $Y(\mathbf{s})$ along \mathbf{u} .

Inference for differential processes requires $(Y(\mathbf{s}), \nabla Y(\mathbf{s})^\top, vech(\nabla^2 Y(\mathbf{s}))^\top)$ to be a valid multivariate process. Its existence is derived from the limit of corresponding finite difference approximations, which yields the cross-covariance matrix depending on fourth (and lower) order derivatives of K . We investigate the parent and differential processes using a differential operator $\mathcal{L} : \mathbb{R}^1 \rightarrow \mathbb{R}^m$, $m = 1 + d + d(d+1)/2$, where $\mathcal{L}Y = (Y, \nabla Y^\top, vech(\nabla^2 Y)^\top)^\top$. The resulting process $\mathcal{L}Y(\mathbf{s})$ is also stationary with a zero mean and a cross-covariance matrix

$$V_{\mathcal{L}Y}(\Delta) = \begin{pmatrix} K(\Delta) & -(\nabla K(\Delta))^\top & vech(\nabla^2 K(\Delta))^\top \\ \nabla K(\Delta) & -\nabla^2 K(\Delta) & \nabla^3 K(\Delta)^\top \\ vech(\nabla^2 K(\Delta)) & -\nabla^3 K(\Delta) & \nabla^4 K(\Delta) \end{pmatrix}, \quad (1)$$

where $\Delta = \mathbf{s} - \mathbf{s}'$, $\nabla K(\Delta)$ is the $d \times 1$ gradient, $\nabla^2 K(\Delta)$ is the $d \times d$ Hessian, $\nabla^3 K(\Delta)$ is the $d(d+1)/2 \times d$ matrix of third derivatives and $\nabla^4 K(\Delta)$ is the $d(d+1)/2 \times d(d+1)/2$ matrix of fourth order derivatives associated with $K(\Delta)$. Under isotropy, $\nabla K(\Delta) = \frac{\nabla \tilde{K}(\|\Delta\|)}{\|\Delta\|} \Delta$, if $A_0 = \left(\nabla^2 \tilde{K}(\|\Delta\|) - \frac{\nabla \tilde{K}(\|\Delta\|)}{\|\Delta\|} \right)$ then, $\nabla^2 K(\Delta) = \frac{\nabla \tilde{K}(\|\Delta\|)}{\|\Delta\|} I_d + A_0 \frac{\Delta \Delta^\top}{\|\Delta\|^2}$, $\nabla^3 K(\Delta) = A_0 \left\{ \frac{vech(I_d)^\top \otimes \Delta}{\|\Delta\|^2} - 3 \frac{vech(\Delta \Delta^\top)^\top \otimes \Delta}{\|\Delta\|^4} + \frac{1}{\|\Delta\|^2} \left(\frac{\partial vech(\Delta \Delta^\top)}{\partial \Delta} \right) \right\} + \nabla^3 \tilde{K}(\|\Delta\|) \cdot \frac{vech(\Delta \Delta^\top)^\top \otimes \Delta}{\|\Delta\|^3}$, where $\tilde{K}(\Delta)$ and its derivatives are analytically computed for our covariance functions of interest in Section S3 of the Supplement. Let $A_1 = \frac{\partial \Delta \otimes vech(I_d)^\top}{\partial \Delta}$, $A_2 = \frac{\partial \Delta \otimes vech(\Delta \Delta^\top)^\top}{\partial \Delta}$, $A_3 = \frac{\partial}{\partial \Delta} \left(\frac{\partial vech(\Delta \Delta^\top)}{\partial \Delta} \right)$ be reordered tensors (matrices) of order $d(d+1)/2 \times d(d+1)/2$ conforming to the order of corresponding elements in $vech$. Let A_4 be the element-wise product of Δ with $\left(\frac{\partial vech(\Delta \Delta^\top)}{\partial \Delta} \right)$ in the same

order, $B_1 = \text{vech}(\Delta\Delta^\top)\text{vech}(I_d)^\top$ and $B_2 = \text{vech}(\Delta\Delta^\top)\text{vech}(\Delta\Delta^\top)^\top$. Then, $\nabla^4 K(\Delta)$ is,

$$A_0 \left\{ \frac{A_1}{\|\Delta\|^2} - 3\frac{A_2}{\|\Delta\|^4} + \frac{A_3}{\|\Delta\|^2} - (1 + A_4) \left(\frac{2B_1}{\|\Delta\|^4} + \frac{B_1}{\|\Delta\|^3} \right) + 3 \left(\frac{4B_2}{\|\Delta\|^6} + \frac{B_2}{\|\Delta\|^5} \right) \right\} \\ + \nabla^3 \tilde{K}(\|\Delta\|) \left(\frac{B_1}{\|\Delta\|^3} + \frac{A_2}{\|\Delta\|^3} + \frac{A_4}{\|\Delta\|^3} - 6\frac{B_2}{\|\Delta\|^5} \right) + \nabla^4 \tilde{K}(\|\Delta\|) \frac{B_2}{\|\Delta\|^4}. \quad (2)$$

The resulting multivariate differential process, $\mathcal{L}Y$, is stationary but not isotropic. Evidently, for the differential operator to be well-defined under isotropy, $\nabla^4 K(\mathbf{0})$ must exist since $\text{var}(D_{\mathbf{u},\mathbf{u}}^{(2)} Y(\mathbf{s})) = \nabla^4 \tilde{K}(\mathbf{0})$ (analogous to results in [Banerjee et al. 2003](#), Section 3). The directional differential operator is defined analogously as $\mathcal{L}_{\mathbf{u}} Y(\mathbf{s})$ such that $\mathcal{L}_{\mathbf{u}} : \mathbb{R} \rightarrow \mathbb{R}^3$. If $a_0 = \left(1 - \frac{(\mathbf{u}^\top \Delta)^2}{\|\Delta\|^2}\right)$, then analogous to (2) the covariance function of the directional curvature process, $\text{Cov}(\mathbf{c}_{\mathbf{u},\mathbf{u}}^\top \text{vech}(\nabla^2 Y(\mathbf{s})), \mathbf{c}_{\mathbf{u},\mathbf{u}}^\top \text{vech}(\nabla^2 Y(\mathbf{s}'))) = \frac{3}{\|\Delta\|^2} (5a_0 - 4)a_0 A_0 + \frac{6}{\|\Delta\|} (1 - a_0)a_0 \nabla^3 \tilde{K}(\|\Delta\|) + (1 - a_0)^2 \nabla^4 \tilde{K}(\|\Delta\|)$. To characterize covariance functions that admit such processes, we turn to spectral theory. Recall that for a positive definite function K defined in \mathbb{R} , Bochner's theorem (see e.g., [Williams & Rasmussen 2006](#)) establishes the existence of a finite positive spectral measure \mathcal{F} on \mathbb{R} . K can be expressed as the inverse Fourier transform of \mathcal{F} , $K(t) = \int_{\mathbb{R}} e^{-i\lambda t} \mathcal{F}(d\lambda)$. In cases where \mathcal{F} admits a spectral density, $K(t) = \int e^{-i\lambda t} f(\lambda) d\lambda$. For $\nabla^4 K$ to exist, a trivial extension of the result in [Wang et al. \(2018\)](#) requires that f possess a finite fourth moment. Examples of covariance kernels that satisfy this condition are (a) the squared exponential covariance kernel with $K(t) = \exp(-t^2)$ ($\sigma^2 = \phi = 1$), and $f(\lambda) = 1/2\sqrt{\pi} \exp(-\lambda^2/4)$ then, $\frac{1}{2\sqrt{\pi}} \int_{\mathbb{R}} \lambda^4 \exp(-\lambda^2/4) d\lambda = 3(\sqrt{2})^4 = 12$; and (b) the Matérn class with fractal parameter, ν ; $f(\lambda)$ is known to belong to the t -family (see e.g., [Stein 1999](#)) with $f(\lambda) = C(\phi, \nu)/(c(\phi, \nu) + \lambda^2)^{\nu+1/2}$ then, $\int_{\mathbb{R}} \lambda^4 C(\phi, \nu)/(c(\phi, \nu) + \lambda^2)^{\nu+1/2} d\lambda < \infty$, for all $\nu > 2$ (since the fourth central moment for the t -distribution exists if $\nu > 2$). Here, we consider formulating the directional differential processes using these two classes of covariance functions (a) the squared exponential, $\tilde{K}(\|\Delta\|) = \sigma^2 \exp(-\phi\|\Delta\|^\nu)$, $\nu = 2$; and (b) members of the Matérn class, $\tilde{K}(\|\Delta\|) = \sigma^2 (\phi\|\Delta\|)^\nu K_\nu(\phi\|\Delta\|)$, where K_ν is the modified Bessel function of order ν (see e.g., [Abramowitz et al. 1988](#)), and ν controls the smoothness

of process realizations. We are particularly interested in $\nu = 5/2$.

The multivariate process, $\mathcal{L}Y(\mathbf{s})$, is valid under the above assumptions without any further specific parametric assumptions over what has been outlined above. To facilitate inference for $\mathcal{L}Y(\mathbf{s})$, a probability distribution is specified for the parent process. We assume that $Y(\mathbf{s}) \sim GP(\mu(\mathbf{s}, \boldsymbol{\beta}), K(\cdot; \sigma^2, \phi))$ is a stationary process specified on \mathbb{R}^d . In what follows we also assume that $K = K(\cdot; \sigma^2, \phi)$ admits four derivatives. There are some immediate implications of a Gaussian assumption on the parent process. If $Y_1(\cdot)$ and $Y_2(\cdot)$ are zero mean, independent stationary Gaussian processes on \mathbb{R}^d , then (i) the differential processes $\mathcal{L}Y_1$ and $\mathcal{L}Y_2$ are independent of each other; (ii) if $c_1, c_2 \in \mathbb{R}$ are scalars, then $\mathcal{L}(c_1Y_1 + c_2Y_2) = c_1\mathcal{L}Y_1 + c_2\mathcal{L}Y_2$ is stationary and (iii) any sub-vector of $\mathcal{L}Y$, for example Y or $(Y, \nabla Y^\top)^\top$, is a stationary Gaussian processes.

If K is k -times mean square differentiable (i.e. $\nabla^{2k}K$ exists), the proposed differential operator can be extended to include higher order derivatives of $\nabla^k Y(\mathbf{s})$ (Mardia et al. 1996). Differential operators characterizing change in the response (and gradient) surface also follow valid stationary Gaussian processes. For instance, at an arbitrary location \mathbf{s}_0 the divergence operator, $\text{div}(Y(\mathbf{s}_0)) = \sum_{i=1}^d \frac{\partial}{\partial \mathbf{e}_i} Y(\mathbf{s}_0) = \mathbf{c}_1^\top \mathcal{L}Y(\mathbf{s}_0)$, where \mathbf{c}_1 is an $m \times 1$ vector with 0's in all places except for first order derivatives where it takes a value of 1, and the Laplacian, defined as the divergence operator for gradients, $\Delta(Y(\mathbf{s}_0)) = \sum_{i=1}^d (\nabla^2 Y(\mathbf{s}_0))_{ii} = \sum_{i=1}^d \frac{\partial^2}{\partial \mathbf{e}_i^2} Y(\mathbf{s}_0) = \mathbf{c}_2^\top \mathcal{L}Y(\mathbf{s}_0)$, where \mathbf{c}_2 is a $m \times 1$ vector with 0's in all places except for pure second order derivatives where it takes a value of 1. Furthermore, they follow valid Gaussian processes with $\text{var}(\text{div}(Y(\mathbf{s}_0))) = \mathbf{c}_1^\top V_{\mathcal{L}} \mathbf{c}_1$ and $\text{var}(\Delta(Y(\mathbf{s}_0))) = \mathbf{c}_2^\top V_{\mathcal{L}} \mathbf{c}_2$.

Let $Y(\mathbf{s})$ be a Gaussian parent process with a twice-differentiable mean function $\mu(\mathbf{s}, \boldsymbol{\beta})$, i.e. $\nabla \mu(\mathbf{s}, \boldsymbol{\beta})$ and $\nabla^2 \mu(\mathbf{s}, \boldsymbol{\beta})$ exist, and let $K(\cdot)$ be a covariance function with variance σ^2 and range ϕ . Let $\mathbf{Y} = (Y(\mathbf{s}_1), \dots, Y(\mathbf{s}_L))^\top$ be the observed realization over \mathcal{S} with mean $\boldsymbol{\mu} = (\mu(\mathbf{s}_1, \boldsymbol{\beta}), \dots, \mu(\mathbf{s}_L, \boldsymbol{\beta}))^\top$ and $\Sigma_{\mathbf{Y}}$ be the associated $L \times L$ covariance matrix with elements $K(\mathbf{s}_i, \mathbf{s}_j)$, and \mathbf{s}_0 be an arbitrary location. Let $\nabla \mathbf{K}_1 = (\nabla K(\delta_1)^\top, \dots, \nabla K(\delta_L)^\top)^\top$ and

$\nabla\mathbf{K}_2 = (\text{vech}(\nabla^2 K(\delta_1))^\top, \dots, \text{vech}(\nabla^2 K(\delta_L))^\top)^\top$ be $L \times d$ and $L \times d(d+1)/2$ matrices, respectively, and $\delta_i = \mathbf{s}_i - \mathbf{s}_0$, $i = 1, \dots, L$. The distribution $P(\mathbf{Y}, \nabla Y(\mathbf{s}_0), \text{vech}(\nabla^2 Y(\mathbf{s}_0)) \mid \boldsymbol{\theta})$, where $\boldsymbol{\theta} = \{\boldsymbol{\beta}, \sigma^2, \phi\}$, is the $m_0 = L + d + d(d+1)/2$ -dimensional Gaussian,

$$\mathcal{N}_{m_0} \left(\begin{pmatrix} \boldsymbol{\mu} \\ \nabla\boldsymbol{\mu}(\mathbf{s}_0) \\ \text{vech}(\nabla^2\boldsymbol{\mu}(\mathbf{s}_0)) \end{pmatrix}, \begin{pmatrix} \Sigma_{\mathbf{Y}} & -\nabla\mathbf{K}_1 & \nabla\mathbf{K}_2 \\ \nabla\mathbf{K}_1^\top & -\nabla^2 K(\mathbf{0}) & \nabla^3 K(\mathbf{0}) \\ \nabla\mathbf{K}_2^\top & -\nabla^3 K(\mathbf{0})^\top & \nabla^4 K(\mathbf{0}) \end{pmatrix} \right), \quad (3)$$

which is well-defined as long as the fourth order derivative of K exists. The posterior predictive distribution for the differential process at \mathbf{s}_0 is

$$P(\nabla Y(\mathbf{s}_0), \text{vech}(\nabla^2 Y(\mathbf{s}_0)) \mid \mathbf{Y}) = \int P(\nabla Y(\mathbf{s}_0), \text{vech}(\nabla^2 Y(\mathbf{s}_0)) \mid \mathbf{Y}, \boldsymbol{\theta}) P(\boldsymbol{\theta} \mid \mathbf{Y}) d\boldsymbol{\theta}. \quad (4)$$

Posterior inference for curvature proceeds by sampling from $P(\text{vech}(\nabla^2 Y(\mathbf{s}_0)) \mid \mathbf{Y}) = \int P(\text{vech}(\nabla^2 Y(\mathbf{s}_0)) \mid \nabla Y(\mathbf{s}_0), \mathbf{Y}, \boldsymbol{\theta}) P(\nabla Y(\mathbf{s}_0) \mid \mathbf{Y}, \boldsymbol{\theta}) P(\boldsymbol{\theta} \mid \mathbf{Y}) d\boldsymbol{\theta} d\nabla Y$. We sample from (4) by drawing one instance of $(\nabla Y(\mathbf{s}_0), \text{vech}(\nabla^2 Y(\mathbf{s}_0)))$ for each sample of $\boldsymbol{\theta}$ obtained from $P(\boldsymbol{\theta} \mid \mathbf{Y})$. The conditional predictive distribution of the differential process is given by $\nabla Y(\mathbf{s}_0), \text{vech}(\nabla^2 Y(\mathbf{s}_0)) \mid \mathbf{Y}, \boldsymbol{\theta} \sim \mathcal{N}_{m_1}(\boldsymbol{\mu}_1, \Sigma_1)$ where $m_1 = d + d(d+1)/2$, and

$$\boldsymbol{\mu}_1 = \begin{pmatrix} \nabla\boldsymbol{\mu}(\mathbf{s}_0) \\ \text{vech}(\nabla^2\boldsymbol{\mu}(\mathbf{s}_0)) \end{pmatrix} - \begin{pmatrix} \nabla\mathbf{K}_1 \\ \nabla\mathbf{K}_2 \end{pmatrix}^\top \Sigma_{\mathbf{Y}}^{-1}(\mathbf{Y} - \boldsymbol{\mu}), \quad (5)$$

$$\Sigma_1 = \begin{pmatrix} -\nabla^2 K(\mathbf{0}) & \nabla^3 K(\mathbf{0})^\top \\ -\nabla^3 K(\mathbf{0}) & \nabla^4 K(\mathbf{0}) \end{pmatrix} - \begin{pmatrix} \nabla\mathbf{K}_1 \\ \nabla\mathbf{K}_2 \end{pmatrix}^\top \Sigma_{\mathbf{Y}}^{-1} \begin{pmatrix} -\nabla\mathbf{K}_1 \\ \nabla\mathbf{K}_2 \end{pmatrix}. \quad (6)$$

Analogous results follow for posterior predictive inference on the curvature process.

If $\mu(\mathbf{s}, \boldsymbol{\beta}) = \mu$ is a constant, as in simple ‘‘kriging’’, then $\nabla\mu(\mathbf{s}) = \nabla^2\mu(\mathbf{s}) = 0$. More generally, if $\mu(\mathbf{s}, \boldsymbol{\beta}) = \mathbf{x}(\mathbf{s})^\top \boldsymbol{\beta}$, where $\mathbf{x}(\mathbf{s})$ is a vector of spatially indexed covariates and $\mathbf{x}(\mathbf{s})^\top \boldsymbol{\beta}$ produces a twice differentiable trend surface then explicit calculation of $\nabla\mu(\mathbf{s}_0)$ and $\nabla^2\mu(\mathbf{s}_0)$ are possible. In case $Y(\mathbf{s}) = \mu(\mathbf{s}, \boldsymbol{\beta}) + Z(\mathbf{s}) + \epsilon(\mathbf{s})$, where $Z(\mathbf{s}) \sim GP(\mathbf{0}, K(\cdot; \sigma^2, \phi))$ and $\epsilon(\mathbf{s}) \sim$

$N(0, \tau^2)$ is a white noise process, inference on gradients for the residual spatial process, $Z(\mathbf{s})$, can be performed from the posterior predictive distribution, $P(\nabla Z(\mathbf{s}_0), \text{vech}(\nabla^2 Z(\mathbf{s}_0)) \mid \mathbf{Y})$. We address this in Section 4 in the context of curvature wombling.

3 Wombling with Curvature Processes

Bayesian wombling deals with inference for line integrals

$$\Gamma(C) = \int_C g(\mathcal{L}Y) \, d\ell \quad \text{or,} \quad \bar{\Gamma}(C) = \frac{1}{\ell(C)} \int_C g(\mathcal{L}Y) \, d\ell, \quad (7)$$

where C is a geometric structure of interest, such as lines or planar curves, residing within the spatial domain of reference, ℓ is an appropriate measure, often taken to be the arc-length measure, g is a linear function (or functional) of the differential operator $\mathcal{L}Y$. Γ and $\bar{\Gamma}$ are referred to as the total and average *wombling measures* respectively. The structure C is defined to be a *wombling boundary* if it yields a large total (or average) wombling measure. Depending on the spatial domain, geometric structures of interest constructed within them may vary. For example, if we are dealing with surfaces in \mathbb{R}^3 , choices of C are curves and lines within the surface, with the local co-ordinate being \mathbb{R}^2 . In higher dimensions they would be planes (curves) or hyperplanes (hypercurves). Specifically, Bayesian curvilinear wombling involves estimating integrals in (7) over curves, which tracks rapid change over the spatial domain by determining boundaries (curves) with large gradients normal to the curve (see for e.g., [Banerjee & Gelfand 2006](#)). The integrand in (7) inherently involves a direction, in particular change measured is always in a direction normal to C . Hence, $g(\mathcal{L}Y)$ can equivalently be expressed as a linear function (functional) of $\mathcal{L}_{\mathbf{n}}Y(\mathbf{s})$, where $\mathbf{n} = \mathbf{n}(\mathbf{s})$ denotes the unit normal vector to C at \mathbf{s} . The next few paragraphs provide more detail.

With wombling measures for directional gradients discussed the Supplement, Section S1.2, we construct wombling measures for curvature. Given C , depending on the smoothness of the surface, the rate at which gradients change along the curve may present sufficient

heterogeneity while traversing the curve. If C forms a wobbling boundary with respect to the gradient, then wobbling boundaries for curvature are subsets of C that feature segments with large positive (negative) directional curvature along a normal direction to the curve. Leveraging only gradients, we develop wobbling measures for curvature that further characterize such boundaries located for gradients. The wobbling measure for curvature in $Y(\mathbf{s})$ along C ascertains whether C also forms a wobbling boundary with respect to curvature. We associate a directional curvature to each $\mathbf{s} \in C$, $g(\mathcal{L}Y(\mathbf{s})) = D_{\mathbf{n},\mathbf{n}}^{(2)}Y(\mathbf{s}) = \mathbf{c}_{\mathbf{n},\mathbf{n}}^\top \text{vech}(\nabla^2 Y(\mathbf{s}))$ (a linear function of $\mathcal{L}Y(\mathbf{s})$) along the direction of a unit normal $\mathbf{n} = \mathbf{n}(\mathbf{s})$ to C at \mathbf{s} . Using (7) we define *wobbling measures* for total and average curvature as,

$$\Gamma^{(2)}(C) = \int_C D_{\mathbf{n},\mathbf{n}}^{(2)}Y(\mathbf{s})d\ell = \int_C \mathbf{n}(\mathbf{s})^\top \nabla^2 Y(\mathbf{s})\mathbf{n}(\mathbf{s})d\ell, \quad \bar{\Gamma}^{(2)}(C) = \Gamma^{(2)}(C)/\ell(C), \quad (8)$$

respectively, where $\ell(C)$ denotes the arc-length of C . Parameterized curves, $C = \{\mathbf{s}(t) = (s_1(t), s_2(t)) : t \in \mathcal{T} \subset \mathbb{R}\}$, offer further insights. As t varies over its domain, $\mathbf{s}(t)$ outlines the curve C . Implicitly assuming that C is regular, i.e., $\|\mathbf{s}'(t)\| \neq 0$, allows the tangent and normal to exist at all points on the curve. The unit tangent and normal at each point of the curve are $\mathbf{s}'(t)/\|\mathbf{s}'(t)\|$ and $\mathbf{n} = \mathbf{n}(\mathbf{s}(t)) = (s_2'(t), -s_1'(t))^\top / \|\mathbf{s}'(t)\|$, respectively, while $\mathbf{c}_{\mathbf{n},\mathbf{n}} = \mathbf{c}_{\mathbf{n}(\mathbf{s}(t)),\mathbf{n}(\mathbf{s}(t))} = (\mathbf{n}(\mathbf{s}(t)) \otimes \mathbf{n}(\mathbf{s}(t)))^\top \mathcal{D}_d$ from Section 2.

The arc-length of C is $\ell(C) = \int_{\mathcal{T}} \|\mathbf{s}'(t)\| dt$ or $d\ell = \|\mathbf{s}'(t)\| dt$. If $\mathcal{T} = [t_0, t_1]$, then $\ell(C) = \int_{t_0}^{t_1} \|\mathbf{s}'(t)\| dt$ and $\Gamma^{(2)}(C) = \int_{t_0}^{t_1} \mathbf{n}(\mathbf{s}(t))^\top \nabla^2 Y(\mathbf{s}(t))\mathbf{n}(\mathbf{s}(t))\|\mathbf{s}'(t)\| dt$. If C is an open curve, then $\ell(C)^{-1} \int_C \mathbf{n}(\mathbf{s})^\top \nabla^2 Y(\mathbf{s})\mathbf{n}(\mathbf{s})d\mathbf{s} = \ell(C)^{-1} \int_C \mathbf{n}(\mathbf{s}(t))^\top \nabla^2 Y(\mathbf{s}(t))\mathbf{n}(\mathbf{s}(t))\|\mathbf{s}'(t)\| dt$ is the average directional curvature. For example, $C = \{\mathbf{s}(t) = (r \cos t, r \sin t), t \in [0, \pi/4]\}$ is the arc of a parameterized circle of radius r . It follows that $\|\mathbf{s}'(t)\| = r$, $\mathbf{n}(\mathbf{s}(t)) = (\cos t, \sin t)^\top$ and $\ell(C)^{-1} \int_0^{\pi/4} \mathbf{n}(\mathbf{s}(t))^\top \nabla^2 Y(\mathbf{s}(t))\mathbf{n}(\mathbf{s}(t))r dt = \frac{4}{\pi} \int_0^{\pi/4} \mathbf{n}(\mathbf{s}(t))^\top \nabla^2 Y(\mathbf{s}(t))\mathbf{n}(\mathbf{s}(t)) dt$. The average curvature in the tangential direction of C is $\frac{1}{\ell(C)} \int_C \mathbf{u}(\mathbf{s}(t))^\top \nabla^2 Y(\mathbf{s}(t))\mathbf{u}(\mathbf{s}(t))\|\mathbf{s}'(t)\| dt = \ell(C)^{-1} \int_{t_0}^{t_1} \frac{\mathbf{s}'(t)}{\|\mathbf{s}'(t)\|}^\top \nabla^2 Y(\mathbf{s}(t)) \frac{\mathbf{s}'(t)}{\|\mathbf{s}'(t)\|} \|\mathbf{s}'(t)\| dt = \mathbf{u}(\mathbf{s}(t_1))^\top \nabla Y(\mathbf{s}(t_1)) - \mathbf{u}(\mathbf{s}(t_0))^\top \nabla Y(\mathbf{s}(t_0))$. Hence, the average directional curvature remains path independent and is the difference of

directional gradient at the end points of C .

For a closed curve C , $\oint_C \mathbf{n}(\mathbf{s})^\top \nabla^2 Y(\mathbf{s}) \mathbf{n}(\mathbf{s}) ds = \oint_C \mathbf{n}(\mathbf{s}(t))^\top \nabla^2 Y(\mathbf{s}(t)) \mathbf{n}(\mathbf{s}(t)) \|s'(t)\| dt$. If the surface admits up to three derivatives, i.e. $\nabla^3 Y(\mathbf{s})$ exists, the average curvature of the region, \mathcal{D} , enclosed by C , is free of t . If $\mathbf{F}(\mathbf{s}) = \nabla^2 Y(\mathbf{s}) = (F_{ij}(\mathbf{s}))_{i,j=1,2}$, with $F_{12}(\mathbf{s}) = F_{21}(\mathbf{s})$ and $F_{ij} = F_{ij}(\mathbf{s}) = \frac{\partial^2}{\partial s_i \partial s_j} Y(\mathbf{s})$ then, $\oint_C \mathbf{n}(\mathbf{s})^\top \nabla^2 Y(\mathbf{s}) \mathbf{n}(\mathbf{s}) ds = \oint_C \mathbf{n}(\mathbf{s})^\top \mathbf{F}(\mathbf{s}) \mathbf{n}(\mathbf{s}) ds = \oint_C \mathbf{n}(\mathbf{s}(t))^\top \mathbf{F}(\mathbf{s}(t)) \mathbf{n}(\mathbf{s}(t)) \|s'(t)\| dt = \oint_C \|s'(t)\|^{-1} (F_{11} s_2'(t)^2 - 2F_{12} s_1'(t) s_2'(t) + F_{22} s_1'(t)^2) dt = \iint_{\mathcal{D}} \left\{ \frac{\partial F_{11} n_2}{\partial s_1} + \left(\frac{\partial F_{12} n_2}{\partial s_2} + \frac{\partial F_{12} n_1}{\partial s_1} \right) + \frac{\partial F_{22} n_1}{\partial s_2} \right\} ds_1 ds_2$. The last equality is obtained using Green's theorem (see for e.g., [Rudin 1976](#)). This can be interpreted as “flux” in the gradient within \mathcal{D} . Since, $F_{ij}(\mathbf{s}) = \nabla_{ij}^2 Y(\mathbf{s})$, the integrand in the last equality require the existence of $\nabla_{ijk}^3 Y(\mathbf{s})$, $i, j, k = 1, 2$. Denoting, $\tilde{\nabla}^3 Y(\mathbf{s}) = (\nabla_{ijk}^3 Y(\mathbf{s}))_{i,j,k=1,2}^\top$, vector of unique third derivatives, and $\mathbf{n}_0(\mathbf{s}) = (n_2(\mathbf{s}), n_2(\mathbf{s}), n_1(\mathbf{s}), n_1(\mathbf{s}))^\top$ then,

$$\frac{1}{\ell(C)} \oint_C \mathbf{c}_{\mathbf{n}, \mathbf{n}}^\top \text{vech}(\nabla^2 Y(\mathbf{s})) ds = \frac{1}{\ell(C)} \iint_{\mathcal{D}} \mathbf{n}_0(\mathbf{s})^\top \tilde{\nabla}^3 Y(\mathbf{s}) ds. \quad (9)$$

This extends the development in Section 3.2 of [Banerjee & Gelfand \(2006\)](#) to study the behavior of spatial curvature over closed curves on surfaces in \mathbb{R}^3 . Sampling along C is generally harder than sampling inside \mathcal{D} . Hence, the computational implications of (9) are more appealing. When studying the same behavior along a tangential direction to C with $\mathbf{s}(t_0) = \mathbf{s}(t_1) = \mathbf{s}_0$, $\oint_C \mathbf{u}(\mathbf{s})^\top \nabla^2 Y(\mathbf{s}) \mathbf{u}(\mathbf{s}) ds = \oint_{\mathbf{s}(t_0)}^{\mathbf{s}(t_1)} F_{11}(\mathbf{s}) n_1 ds_1 + F_{12}(\mathbf{s}) n_1 ds_2 + F_{21}(\mathbf{s}) n_2 ds_1 + F_{22}(\mathbf{s}) n_2 ds_2 = \mathbf{u}(\mathbf{s}(t_1))^\top \nabla Y(\mathbf{s}(t_1)) - \mathbf{u}(\mathbf{s}(t_0))^\top \nabla Y(\mathbf{s}(t_0)) = 0$, again a consequence of path independence. This validates the choice of a normal direction to C when measuring change in the gradient. Using the rectilinear approximation to curvature wobbling, as discussed later, provides a more computationally tractable and simpler approach, where double integrals manifest when computing variances of the wobbling measures.

Curvature wobbling requires predictive inference performed using gradient measures on the interval \mathcal{T} , to include $\Gamma^{(2)}(C)$ (or $\bar{\Gamma}^{(2)}(C)$) in (8). Leveraging inference for differential processes in Section 2, we obtain joint inference on the wobbling measures. Suppose $C =$

$\{\mathbf{s}(t) : t \in [0, T]\}$ is generated over $\mathcal{T} = [0, T]$. For any $t^* \in [0, T]$, let C_{t^*} denote the curve restricted to $[0, t^*]$ and $\ell(C_{t^*})$ its arc-length. Line integrals for curvilinear gradient and curvature wobbling measures are $\Gamma^{(1)}(C_{t^*}) = \int_0^{t^*} D_{\mathbf{n}}^{(1)} Y(\mathbf{s}(t)) \|\mathbf{s}'(t)\| dt$, $\bar{\Gamma}^{(1)}(C_{t^*}) = \frac{1}{\ell(C_{t^*})} \Gamma^{(1)}(C_{t^*})$, $\Gamma^{(2)}(C_{t^*}) = \int_0^{t^*} D_{\mathbf{n}, \mathbf{n}}^{(2)} Y(\mathbf{s}(t)) \|\mathbf{s}'(t)\| dt$ and $\bar{\Gamma}^{(2)}(C_{t^*}) = \frac{1}{\ell(C_{t^*})} \Gamma^{(2)}(C_{t^*})$. Since $D_{\mathbf{n}}^{(1)} Y(\mathbf{s}(t))$ and $D_{\mathbf{n}, \mathbf{n}}^{(2)} Y(\mathbf{s}(t))$ are Gaussian processes on \mathcal{T} , $\Gamma^{(1)}(C_{t^*})$ and $\Gamma^{(2)}(C_{t^*})$ are valid *dependent* Gaussian processes on \mathcal{T} . Therefore, $\mathbf{\Gamma}(C_{t^*}) = (\Gamma^{(1)}(C_{t^*}), \Gamma^{(2)}(C_{t^*}))^\top \sim \mathcal{N}_2(\boldsymbol{\mu}_{\mathbf{\Gamma}}(t^*), \mathbf{K}_{\mathbf{\Gamma}}(t^*, t^*))$, where $\boldsymbol{\mu}_{\mathbf{\Gamma}}(t^*) = \left(\int_0^{t^*} D_{\mathbf{n}}^{(1)} \mu(\mathbf{s}(t)) \|\mathbf{s}'(t)\| dt, \int_0^{t^*} D_{\mathbf{n}, \mathbf{n}}^{(2)} \mu(\mathbf{s}(t)) \|\mathbf{s}'(t)\| dt \right)^\top = (m_1(t^*), m_2(t^*))^\top$ and $\mathbf{K}_{\mathbf{\Gamma}}(t^*, t^*) = \{k_{ij}(t^*, t^*)\}_{i,j=1,2}$ whose elements are evaluated as

$$k_{ij}(t^*, t^*) = (-1)^j \int_0^{t^*} \int_0^{t^*} \mathbf{a}_i^\top(t_1) \nabla^{i+j} K(\Delta(t_1, t_2)) \mathbf{a}_j(t_2) \|\mathbf{s}'(t_1)\| \|\mathbf{s}'(t_2)\| dt_1 dt_2, \quad (10)$$

where $\mathbf{a}_1(t) = \mathbf{n}(\mathbf{s}(t))$ and $\mathbf{a}_2(t) = \mathbf{c}_{\mathbf{n}(\mathbf{s}(t)), \mathbf{n}(\mathbf{s}(t))}$. Simplifications arise in $d = 2$. For example, $\mathbf{c}_{\mathbf{n}, \mathbf{n}}(t) = (s_2'(t)^2, -2s_2'(t)s_1'(t), s_1'(t)^2)^\top$, while $\nabla^k K$, for $k = 2, 3, 4$, are matrices of orders 2×2 , 2×3 and 3×3 , respectively, of partial and mixed second, third and fourth derivatives of K and $\Delta(t_1, t_2) = \mathbf{s}(t_2) - \mathbf{s}(t_1)$. For any two points $t_1^*, t_2^* \in \mathcal{T}$, the dependence is

specified through $\begin{pmatrix} \mathbf{\Gamma}(C_{t_1^*}) \\ \mathbf{\Gamma}(C_{t_2^*}) \end{pmatrix} \sim \mathcal{N}_4 \left(\begin{pmatrix} \mathbf{m}_1 \\ \mathbf{m}_2 \end{pmatrix}, \begin{pmatrix} \mathbf{k}_{11} & \mathbf{k}_{12} \\ \mathbf{k}_{21} & \mathbf{k}_{22} \end{pmatrix} \right)$, where $\mathbf{m}_i = (m_i(t_1^*), m_i(t_2^*))^\top$,

$\mathbf{k}_{ij} = \begin{pmatrix} k_{ij}(t_1^*, t_1^*) & k_{ij}(t_1^*, t_2^*) \\ k_{ij}(t_2^*, t_1^*) & k_{ij}(t_2^*, t_2^*) \end{pmatrix}$, $i, j = 1, 2$. Generally, for n_P points partitioning \mathcal{T} the

above can be analogously extended. Clearly, $\mathbf{\Gamma}(C_{t^*})$ is a mean squared continuous process.

However, stationarity of $Y(\mathbf{s})$ does not imply stationarity of $\mathbf{\Gamma}(C_{t^*})$. For any $\mathbf{s}_j \in \mathcal{S}$ with

$\text{Cov}(Y(\mathbf{s}_j), \mathbf{\Gamma}(C_{t^*})) = \boldsymbol{\gamma}_j(t^*)$ and $\Delta_j(t) = \mathbf{s}(t) - \mathbf{s}_j$ we have,

$$\boldsymbol{\gamma}_j(t^*) = \left(\int_0^{t^*} D_{\mathbf{n}}^{(1)} K(\Delta_j(t)) \|\mathbf{s}'(t)\| dt, \int_0^{t^*} D_{\mathbf{n}, \mathbf{n}}^{(2)} K(\Delta_j(t)) \|\mathbf{s}'(t)\| dt \right)^\top. \quad (11)$$

A valid *joint distribution* can be specified over \mathcal{T} by,

$$\begin{pmatrix} \mathbf{Y} \\ \mathbf{\Gamma}(C_{t^*}) \end{pmatrix} \sim \mathcal{N}_{L+2} \left(\begin{pmatrix} \boldsymbol{\mu} \\ \boldsymbol{\mu}_{\mathbf{\Gamma}}(t^*) \end{pmatrix}, \begin{pmatrix} \Sigma_{\mathbf{Y}} & \boldsymbol{\gamma}_{\mathbf{\Gamma}}(t^*) \\ \boldsymbol{\gamma}_{\mathbf{\Gamma}}^\top(t^*) & \mathbf{K}_{\mathbf{\Gamma}}(t^*, t^*) \end{pmatrix} \right), \quad (12)$$

where $\boldsymbol{\gamma}_{\mathbf{\Gamma}}^{\top}(t^*) = [\boldsymbol{\gamma}_1(t^*) \ \boldsymbol{\gamma}_2(t^*) \ \cdots \ \boldsymbol{\gamma}_L(t^*)]$ is the $2 \times L$ cross-covariance matrix.

In practical applications curvilinear wombling is performed by approximating the curve C using linear segments. These measures at the segment level are then aggregated to produce a wombling measure for the curve. The curve is segmented using a partition. Consequently, the accuracy of estimated wombling measures for the curve depend on the choice of partition. Figures S2 and S3 in the online Supplement illustrate this concept. Explicitly, let C be a regular rectifiable curve and $[a, b] \subset \mathcal{T}$ be a compact interval. Let g be a uniformly continuous function. For any partition, P of $[a, b]$, $a = t'_0 < t'_1 < \dots < t'_{n_P} = b$, with its norm defined as $|P| = \max_{i=1, \dots, n_P} (t'_i - t'_{i-1})$. A polygonal (piecewise-linear) approximation to the curve is, $\tilde{C}_P = \bigcup_{i=1}^{n_P} C_{t_i}$, where $C_{t_i} = \{\mathbf{s}(t'_{i-1}) + t\mathbf{u}_i, t \in [0, t_i]\}$, $t_i = \|\mathbf{s}(t'_i) - \mathbf{s}(t'_{i-1})\|$ and $\mathbf{u}_i = \|\mathbf{s}(t'_i) - \mathbf{s}(t'_{i-1})\|^{-1}(\mathbf{s}(t'_i) - \mathbf{s}(t'_{i-1}))^{\top}$. Note that $\mathbf{s}(t) = \mathbf{s}(t'_{i-1}) + t\mathbf{u}_i$ for $t \in [0, t_i]$ and, hence, $\|\mathbf{s}'(t)\| = \|\mathbf{u}_i\| = 1$. Wombling measure for \tilde{C}_P is, $\Gamma(\tilde{C}_P) = \sum_{i=1}^{n_P} \int_{C_{t_i}} g(\mathcal{L}Y(\mathbf{s}(t))) \|\mathbf{s}'(t)\| dt$. As $|P| \rightarrow 0$ we have, $\Gamma(\tilde{C}_P) \xrightarrow{a.s.} \Gamma(C) = \int_a^b g(\mathcal{L}Y(\mathbf{s}(t))) \|\mathbf{s}'(t)\| dt$. This provides us with an estimate, $\Gamma(\tilde{C}_P)$ for curvilinear wombling measures associated with any general curve C . Further details are provided in the Supplement, at the end of Section S5.

The choices of g for our wombling measures result in, $\mathbf{u}^{\top} \nabla Y$ and $\mathbf{c}_{\mathbf{u}, \mathbf{u}}^{\top} \text{vech}(\nabla^2 Y)$, which are linear and therefore uniformly continuous over any compact interval. Since predictive inference is performed iteratively on individual line segments, it is sufficient to show the inferential procedure for an arbitrary curve segment C_{t_i} . The normal to C_{t_i} is free of t and denoted as, \mathbf{u}_i^{\perp} , which is the normal to \mathbf{u}_i . The associated wombling measures with C_{t_i} are $\mathbf{\Gamma}(t_i) = \left(\int_0^{t_i} D_{\mathbf{u}_i^{\perp}}^{(1)} Y(\mathbf{s}(t)) dt, \int_0^{t_i} D_{\mathbf{u}_i^{\perp}, \mathbf{u}_i^{\perp}}^{(2)} Y(\mathbf{s}(t)) dt \right)^{\top}$. For a point \mathbf{s}_j define $\Delta_{i-1, j} = \mathbf{s}_{i-1} - \mathbf{s}_j$, $j = 1, 2, \dots, L$. Their joint distribution is specified by (12), where $\boldsymbol{\gamma}_j(t_i)$ is obtained from (11) by replacing $\Delta_j(t)$ with $\Delta_{i-1, j} + t\mathbf{u}_i$ and $\mathbf{K}_{\mathbf{\Gamma}}(t_i, t_i)$ is obtained from (10) replacing $\Delta(t_1, t_2) = (t_2 - t_1)\mathbf{u}_i$ in the integrand. The analytic tractability of the line integrals in $\boldsymbol{\gamma}_j(t_i)$ is not a concern. Given choices of $\mu(\cdot)$ and $K(\cdot)$, they are all one or two dimensional integrals which are efficiently computed using simple quadrature. For example, let $Y(\mathbf{s})$ be the isotropic Gaus-

sian process with mean $\mu(\mathbf{s}) = \mu$ and $K(\|\Delta\|; \sigma^2, \phi) = \sigma^2 \exp(-\phi\|\Delta\|^2)$, where $\Delta = (\delta_1, \delta_2)^\top$. $\nabla^k K(\Delta)$, $k = 2, 3, 4$ is obtained from (2) and related results. $\gamma_j(t_i) = \gamma_j(t_i; \sigma^2, \phi) = \{\Phi(\sqrt{2\phi}(t_i + \mathbf{u}_i^\top \Delta_{i-1,j})) - \Phi(\sqrt{2\phi}\mathbf{u}_i^\top \Delta_{i-1,j})\} (c_1, c_2)^\top$ where, $c_1 = c_1(\sigma^2, \phi, \mathbf{u}_i^\perp, \Delta_{i-1,j}) = -2\sigma^2\sqrt{\pi\phi}\mathbf{u}_i^{\perp\top} \Delta_{i-1,j} e^{-\phi(\mathbf{u}_i^{\perp\top} \Delta_{i-1,j})^2}$, $c_2 = c_2(\sigma^2, \phi, \mathbf{u}_i^\perp, \Delta_{i-1,j}) = c_1(1 - 2\phi\mathbf{u}_i^{\perp\top} \Delta_{i-1,j} \Delta_{i-1,j}^\top \mathbf{u}_i^\perp)$, and $\Phi(\cdot)$ denotes the standard Gaussian cumulative distribution function. These are simple computations with quadrature required only for computing $K_\Gamma(t_i, t_i)$.

4 Bayesian Hierarchical Model

We operate under a Bayesian hierarchical model, which is specified as

$$Y(\mathbf{s}) = \mu(\mathbf{s}, \boldsymbol{\beta}) + Z(\mathbf{s}) + \epsilon(\mathbf{s}), \quad (13)$$

where $Z(\mathbf{s}) \sim GP(0, K(\cdot; \sigma^2, \phi))$ is a Gaussian process, and $\epsilon(\mathbf{s}) \sim N(0, \tau^2)$ is a white noise process, termed as the nugget (see [Banerjee et al. 2014](#), and references therein). The process parameters are $\boldsymbol{\theta} = \{\boldsymbol{\beta}, \sigma^2, \phi, \tau^2\}$. More generally, we can consider a latent specification for response arising from exponential families, $\alpha(\boldsymbol{\eta}(\mathbf{s})) = \mathbf{x}^\top(\mathbf{s})\boldsymbol{\beta} + Z(\mathbf{s}) + \epsilon(\mathbf{s})$, $Z(\mathbf{s}) \sim GP(0, K(\cdot; \sigma^2, \phi))$ and $Y(\mathbf{s}) \sim \pi(\boldsymbol{\eta}(\mathbf{s}), \cdot)$, where α is a monotonic link function, π is a member of the exponential family and $\boldsymbol{\eta}$ is the natural parameter. Predictive inference on differential processes and curvature wombling proceeds on the latent surface through $P(\mathcal{L}Z \mid \mathbf{Y})$. The joint posterior for differential processes is obtained through, $P(\nabla Z^\top, \text{vech}(\nabla^2 Z)^\top \mid \mathbf{Y}) = \int P(\nabla Z^\top, \text{vech}(\nabla^2 Z)^\top \mid \mathbf{Z}, \boldsymbol{\theta})P(\mathbf{Z} \mid \mathbf{Y}, \boldsymbol{\theta})P(\boldsymbol{\theta} \mid \mathbf{Y}) d\boldsymbol{\theta} d\mathbf{Z}$, while wombling measures $\Gamma_Z(t^*)$ for a curve C_{t^*} within the estimated posterior surface for \mathbf{Z} , are sampled from the posterior, $P(\Gamma_Z(t^*) \mid \mathbf{Y}) = \int P(\Gamma_Z(t^*) \mid \mathbf{Z}, \boldsymbol{\theta})P(\mathbf{Z} \mid \mathbf{Y}, \boldsymbol{\theta})P(\boldsymbol{\theta} \mid \mathbf{Y}) d\boldsymbol{\theta} d\mathbf{Z}$. Customary prior specifications for $\boldsymbol{\theta}$ yield

$$\begin{aligned} P(\boldsymbol{\theta}, \mathbf{Z} \mid \mathbf{Y}) &\propto U(\phi \mid a_\phi, b_\phi) \times IG(\sigma^2 \mid a_\sigma, b_\sigma) \times IG(\tau^2 \mid a_\tau, b_\tau) \times \mathcal{N}_L(\mathbf{Z} \mid \mathbf{0}, \sigma^2 \mathbf{R}_Z) \\ &\times \mathcal{N}_p(\boldsymbol{\beta} \mid \mu_\beta, \Sigma_\beta) \times \prod_{l=1}^L \mathcal{N}_1(Y(\mathbf{s}_l) \mid \mathbf{x}(\mathbf{s}_l)^\top \boldsymbol{\beta} + Z(\mathbf{s}_l), \tau^2), \end{aligned} \quad (14)$$

where IG denotes the inverse-gamma distribution with a shape-rate parameterization, U is a uniform distribution and \mathbf{R}_Z is the correlation matrix corresponding to $K(\cdot; \sigma^2, \phi)$. The resulting full conditionals are $\boldsymbol{\beta} \mid \tau^2, \mathbf{Z}, \mathbf{Y} \sim \mathcal{N}_p(M_\beta m_\beta, M_\beta)$, $\sigma^2 \mid \phi, \mathbf{Z} \sim IG(a_\sigma + \frac{L}{2}, b_\sigma + \frac{1}{2} \mathbf{Z}^\top \mathbf{R}_Z^{-1}(\cdot; \phi) \mathbf{Z})$, $\tau^2 \mid \boldsymbol{\beta}, \mathbf{Z}, \mathbf{Y} \sim IG(a_\tau + \frac{L}{2}, b_\tau + \frac{1}{2} \|\mathbf{Y} - \mathbf{X}\boldsymbol{\beta} - \mathbf{Z}\|_2^2)$, $\mathbf{Z} \mid \mathbf{Y}, \boldsymbol{\theta} \sim \mathcal{N}_L(M_Z m_Z, \tau^2 M_Z)$, where \mathbf{X} is the $L \times p$ matrix with $\mathbf{x}(\mathbf{s}_i)^\top$ as rows, $M_\beta^{-1} = \Sigma_\beta^{-1} + \tau^{-2} \mathbf{X}^\top \mathbf{X}$, $m_\beta = \Sigma_\beta^{-1} \mu_\beta + \tau^{-2} \mathbf{X}^\top (\mathbf{Y} - \mathbf{Z})$, $M_Z^{-1} = \tau^{-2} (\tau^{-2} I_L + \sigma^{-2} \mathbf{R}_Z^{-1}(\cdot; \phi))$, and $m_Z = \mathbf{Y} - \mathbf{X}\boldsymbol{\beta}$. ϕ is updated using Metropolis steps with a normal proposal and an adaptive variance.

Under this setup posterior samples for the differential processes and wobbling measures result from (5) and (6). For each posterior sample of $\{\mathbf{Z}, \boldsymbol{\theta}\}$, we draw $\boldsymbol{\Gamma}_Z(t^*) \mid \mathbf{Z}, \boldsymbol{\theta} \sim \mathcal{N}_2(\mu_{\boldsymbol{\Gamma}_Z}(t^*) - \boldsymbol{\gamma}_{\boldsymbol{\Gamma}_Z}^\top(t^*) \Sigma_{\mathbf{Z}}^{-1} \mathbf{Z}, K_{\boldsymbol{\Gamma}_Z}(t^*, t^*) - \boldsymbol{\gamma}_{\boldsymbol{\Gamma}_Z}^\top(t^*) \Sigma_{\mathbf{Z}}^{-1} \boldsymbol{\gamma}_{\boldsymbol{\Gamma}_Z}(t^*))$, where $\mu_{\boldsymbol{\Gamma}_Z}(t^*)$, $\boldsymbol{\gamma}_{\boldsymbol{\Gamma}_Z}(t^*)$, and $K_{\boldsymbol{\Gamma}_Z}(t^*, t^*)$ are computed from (10) and (11). Algorithms 1 and 2 in the Supplement, Section S4, present further details for posterior sampling. Next, we turn to numerical experiments and data analyses. Codes required for reproducing and emulating the analyses presented in the manuscript are produced for the R statistical programming environment and available for download in the public domain at <https://github.com/arh926/spWombling>.

5 Simulation Experiments

5.1 Data generation

The proposed differential processes are not observed in reality, but are induced by an observed spatially indexed parent process. To evaluate statistical learning of the curvature process we perform simulation experiments within a setup where true values of the differential process and wobbling measures are available. We consider locations $\mathbf{s} = (s_1, s_2)^\top \in \mathbb{R}^2$ over the unit square $[0, 1] \times [0, 1] \subset \mathbb{R}^2$. We generate synthetic data from two distributions: (a) Pattern 1: $y_1(\mathbf{s}) \sim N(10[\sin(3\pi s_1) + \cos(3\pi s_2)], \tau^2)$; (b) Pattern 2: $y_2(\mathbf{s}) \sim N(10[\sin(3\pi s_1) \cdot \cos(3\pi s_2)], \tau^2)$, where the value of $\tau^2 = 1$. Figure 1 presents spatial plots of the generated

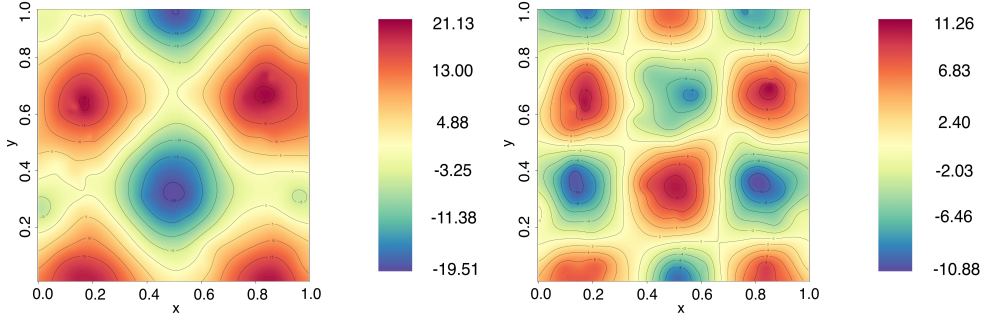


Figure 1: Spatial plots for synthetic patterns, from Pattern 1 (left) and Pattern 2 (right). Scales are shown in the legend alongside.

synthetic response from these patterns. The rationale behind selecting these distributions is: (i) synthetic data is more practical and not from the model in (13), and (ii) true gradient and curvature can be computed at every location \mathbf{s} .

The synthetic patterns chosen feature two different scenarios that may arise. In the first pattern expressions for differentials along the principal directions $\mathbf{e}_1 = (1, 0)^\top$ and $\mathbf{e}_2 = (0, 1)^\top$ are functions of either s_1 or s_2 , $\nabla\mu_1(\mathbf{s}) = 30\pi(\cos(3\pi s_1), -\sin(3\pi s_2))^\top$, $\nabla^2\mu_1(\mathbf{s}) = -90\pi^2\text{diag}\{\sin(3\pi s_1), \cos(3\pi s_2)\}$. The curvature along s_1 does not influence curvature along s_2 , $(\nabla^2\mu_1(\mathbf{s}))_{12} = 0$ for all \mathbf{s} . While $\nabla\mu_2(\mathbf{s}) = 30\pi(\cos(3\pi s_1)\cos(3\pi s_2), -\sin(3\pi s_1)\sin(3\pi s_2))^\top$, $\nabla^2\mu_2(\mathbf{s}) = -90\pi^2 M(\mathbf{s})$, where $M(\mathbf{s})$ is a 2×2 matrix with, $m_{11} = \sin(3\pi s_1)\cos(3\pi s_2)$, $m_{12} = m_{21} = \cos(3\pi s_1)\sin(3\pi s_2)$ and $m_{22} = \sin(3\pi s_1)\cos(3\pi s_2)$ with differentials being functions of both s_1 and s_2 and $(\nabla^2\mu(\mathbf{s}))_{12} \neq 0$ for some \mathbf{s} . While setting up the experiments we vary $L \in \{100, 500, 1000\}$ with 10 replicated instances under each setting.

5.2 Bayesian model fitting

We fit the model in (14) with only an intercept allowing the spatial process to learn the functional patterns in the synthetic response. We use the following hyper-parameter values in (14): $a_\phi = 3/\max\|\Delta\|$, $b_\phi = 30$, $a_\sigma = 2$, $b_\sigma = 1$, $a_\tau = 2$, $b_\tau = 0.1$, $\mu_\beta = 0$ and $\Sigma_\beta = 10^6 I_p$. These choices comprise reasonable weakly informative priors. While a $\text{Uniform}(2, 3)$ prior on ν can be specified (and was implemented as part of this experiment) to ensure the existence

of the curvature process, here our choice of scales in the data generating patterns ensured that $\nu = 5/2$ provided the best model fit when compared with values of $\nu \in \{1/2, 3/2, 5/2\}$. Hence, we present the results with $\nu = 5/2$.

The parameter estimates for $\boldsymbol{\theta}$ are computed using posterior medians and their highest posterior density (HPD) intervals (Chen & Shao 1999, Plummer et al. 2015). For each replicate, we assess our ability to estimate the local geometry of the resulting posterior surface. For this we overlay a grid spanning the unit square. We perform posterior predictive inference for the differential processes at each grid location following Section 2. Posterior predictive medians (accompanied by 95% HPD intervals) summarize inference for the differential processes over the grid locations (Section 5.4 offers supplementary analysis).

5.3 Bayesian wombling with curvature processes

For wombling with curvature processes, or *curvature wombling*, we focus on locating curves that track rapid change within the simulated random surfaces. For example, consider the surface produced by the first pattern. If a curve is provided to us, we can evaluate the posterior distribution of the average or total curvature wombling measures to assess their statistical significance. On the other hand, without a given curve, we consider three different approaches for constructing them from a boundary analysis or wombling perspective: (a) level curves: $C_{y_0} = \{\mathbf{s} : Y(\mathbf{s}) = y_0\}$: Bayesian wombling literature finds that curves parallel to contours often form wombling boundaries (see, e.g., Banerjee & Gelfand 2006) and level curves on a surface are parallel to local contours by definition; (b) smooth curves: produces a smooth curve using Bézier splines (see, e.g., Gallier & Gallier 2000) from a set of *annotated* points that are of interest within the surface; and (c) rectilinear curves: produces a rectilinear curve joining adjacent *annotated* points of interest within the surface using straight lines, performs curvature wombling using a Riemann sum approximation (see (S1) in the Supplement). Curves of types (b) and (c) allow the investigator to specify a region of in-

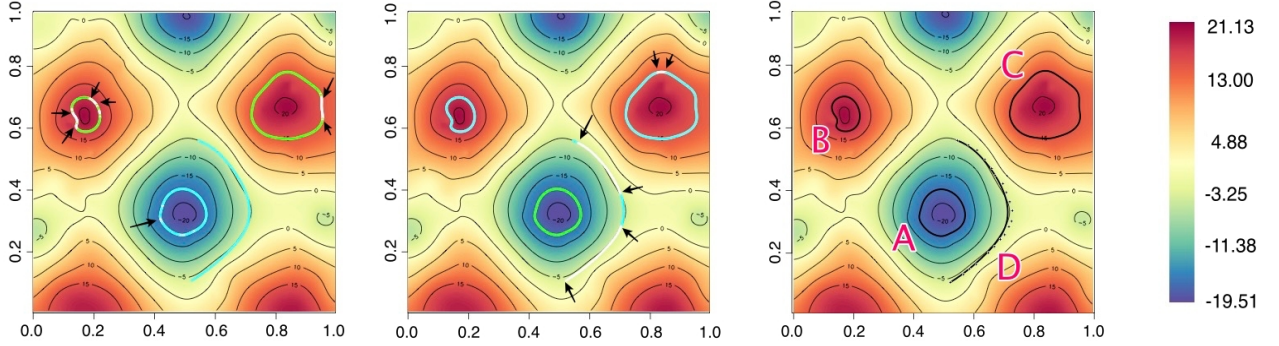


Figure 2: (left) shows color coded directional gradients for segments, (center) shows color coded directional curvature for segments in the direction normal to the curve, (right) shows curves selected for performing curvature wombling. **green** indicates a positive significance, **cyan** indicates negative significance and **white** indicates no significance.

terest that house possible wombling boundaries. For the surface realization produced by Pattern 1, we consider four different types of curves on the response surface, (A) a closed curve enclosing a trough corresponding to a level curve, $C_{y_0=-18}$, (B) a closed curve enclosing a peak corresponding to a level curve, $C_{y_0=+18}$, (C) a closed curve that outlines a contour corresponding to a level curve, $C_{y_0=+15}$ and (D) an open curve along a contour constructed using a Bézier spline. These curves are marked in Figure 2c.

Curvature wombling is performed using methods outlined in Section 3. Referring to the discussion on rectilinear approximation, for each curve, given a partition, we compute t_i and \mathbf{u}_i . Combining the segments produces a vector \mathbf{t} and a matrix of directions, \mathbf{U} that represents the curve. Algorithm 2 in the Supplement, Section S4 devises efficient computation using \mathbf{t} and \mathbf{U} . The total (and average) wombling measures $\bar{\Gamma}(C)$ are sampled from their posteriors using (12). For curves A, B, C and D, we use partitions with sufficiently small norms ($|P|$) to achieve accuracy (3.99×10^{-3} , 3.97×10^{-3} , 4.42×10^{-3} and 2.66×10^{-2} respectively). One and two dimensional line integrals (refer to (10) and (11)) are computed via quadrature using grids of size 10 on $[0, t_i]$, and size 100 on $[0, t_i] \times [0, t_i]$ respectively, for $i = 1, 2, \dots, n_P$. The median of sampled $\bar{\Gamma}(\tilde{C}_P)$ is our estimated wombling measure for the curve. Significance at the curve-segment level is assessed based on the inclusion of 0

Table 1: Results from curvature wombling performed on curves A, B, C and D as shown in Figure 2. The estimated average directional gradient and curvature are accompanied by their respective HPD intervals in brackets. HPD intervals *containing* θ are marked in bold.

Curves (C)	Average Gradient ($\Gamma^{(1)}(C)$)		Average Curvature ($\Gamma^{(2)}(C)$)	
	True	Estimated	True	Estimated
Curve A	-61.54	-64.97 (-92.37, -38.57)	731.94	768.03 (599.30, 913.70)
Curve B	40.85	49.19 (20.45, 73.12)	-808.04	-850.84 (-1066.98, -630.09)
Curve C	84.03	85.65 (59.81, 109.97)	-558.58	-504.98 (-767.55, -241.61)
Curve D	-110.84	-113.27 (-153.23, -77.01)	11.32	-94.64 (-386.94, 233.78)

within the HPD intervals. Our design allows us to compute true values of average wombling measures for each rectilinear segment in the curve. They are computed using, $\mu_{\mathbf{T}}^{true}(\tilde{C}_P) = (\sum_{i=1}^{n_P} t_i)^{-1} \left(\sum_{i=1}^{n_P} \int_0^{t_i} \mathbf{u}_i^{\perp \top} \nabla \mu_1(\mathbf{s}(t)) dt, \sum_{i=1}^{n_P} \int_0^{t_i} \mathbf{u}_i^{\perp \top} \nabla^2 \mu_1(\mathbf{s}(t)) \mathbf{u}_i^{\perp} dt \right)^{\top}$. We compute HPD intervals for the wombling measures at the segment level. Coverage probabilities (CPs) are then constructed by aggregating coverage of true values by HPD intervals over segments.

Curve A encloses a trough and a local minima for the surface, while B and C enclose peaks and local maximums (referring to corresponding locations in Figures S8c and S9c). Along all segments of A we expect negative gradients owing to the decreasing nature of the response in that region, while for B and C we expect positive gradients. Each of them would be expected to yield significant wombling measures for gradients. Referring to the Laplacian surface (see Supplement, Figures S8e and S9e) A, B, and C are located in regions manifesting rapid change in the gradient surface, implying they should yield large positive (curve A) or negative (curves B and C) curvature, forming curvature wombling boundaries. These are all aligned with our findings presented in Table 1, which presents measures of quality assessment for wombling. The magnitude and sign of wombling measures also allow us to differentiate between the type of curvature for the different wombling boundaries. For instance, B is located in a region of higher convexity compared to C, while the nature of convexity for regions enclosed by them are different compared to A. Plots in Figure 2 (left and center) show line segment level inference for average wombling measures. Arrows indicate segments

which were not significant with respect to gradient or curvature, while regions of significance are color coded. D is located in a “relatively flat” region of the surface (see Figures S8e and S9e) and is expected to have gradients but no curvature, which aligns with results shown in Table 1. We conclude by noting that the true values, $\mu_{\mathbf{T}}^{true}(C)$ of the wombling measures for the curves considered, are all covered by the estimated HPD intervals for respective curves. Additionally, at the line segment level we achieved a CP of 1.0 across all curves.

5.4 Supplementary analysis

We present additional results in the online supplement. Tables S1 and S2 present parameter estimates, measures of goodness of fit for the fitted process, and assessment of derivative process characteristics for each pattern considered. We compute root mean square errors (RMSE) across observed locations averaged over 10 replicates for each sample size setting for the fitted process $\widehat{Y}(\mathbf{s}) = \widehat{\beta}_0 + \widehat{Z}(\mathbf{s})$, and $\widehat{\nabla Y}(\mathbf{s})$, $\widehat{vech}(\widehat{\nabla^2 Y}(\mathbf{s}))$. We report standard deviations across replicates. With increasing number of observed locations we are able to effectively learn the underlying process and induced differential processes. Figures S4, S5, S6 and S7 present spatial plots of posterior medians of gradient and curvature processes, for $L = 100$ locations. These plots demonstrate the effectiveness of our methods in learning about the differential processes from the underlying patterns. Similarly plots shown in Figures S8, S9, S10 and S11 demonstrate the same for derived quantities and operators of $\mathcal{L}Y(\mathbf{s})$ —principal curvature (eigenvalues), Gaussian curvature (determinant) (see, e.g., [Spivak 1999](#), [Do Carmo 2016](#)), divergence and Laplacian, which pertain to geometric analysis of curvature for the random surface resulting from the underlying patterns. Statistical significance is assessed at every grid point by checking the inclusion of 0 in their HPD intervals. Significantly positive (negative) points are color coded. We compute average CPs at every grid location to measure the accuracy of our assessment. These CPs are then averaged over replicates. We observed high CPs across the grid for parent and differential processes. Figures S12 and S13 compare

observed against estimated differential processes coupled with their HPD regions.

6 Applications

Frameworks developed for differential assessment and boundary analysis in spatially indexed response are applied to multiple data sets with the aim of locating curvature wobbling boundaries that track rapid change in response. The chosen data arise from varied areas of scientific interest, we briefly describe the origin and significance of each with respect to our methods before performing our analysis. Response is modeled using the hierarchical model in (13). Prior specifications used in (14) are, $\phi \sim \text{Unif}(3/\max_{\mathbf{s} \in \mathcal{S}} \|\Delta\|, 300)$, $\sigma^2 \sim IG(2, 1)$, $\tau^2 \sim IG(2, 1)$ (mean 1, infinite variance), $\boldsymbol{\beta} \sim N(0, 10^6 I_p)$, p being the number of covariates and $\nu = 5/2$ for the Matérn kernel ensuring existence of the differential processes.

Boston Housing: The Boston housing data (see, e.g., [Harrison Jr & Rubinfeld 1978](#)) was collected by the United States Census Service featuring median house prices for tracts and towns in Boston, Massachusetts area. The purpose was to study heterogeneity in the market caused by the need for residents to have clean air. To study such heterogeneity, modern equitable housing policies are incorporating statistical modeling to quantify such behavior. Often they are a result of unobserved effects of rapidly shifting socioeconomic conditions (see, e.g., [Hu et al. 2019](#)). Within a spatial map this manifests as neighboring regions of disparity. Figure 3 shows two such regions: high priced including Downtown Boston, Cambridge, Newton, Wellesley, Brookline etc. and low priced including South and East End. For effective policy implementation, identifying such regions becomes crucial. Spatial variation in the median house prices is evidenced in Figure 4. Curvature wobbling effected on the house price surface would locate regions that feature such change.

The data contains median house price values for 506 census-tracts along with demographic data. Latitude-longitude centers of the census-tracts are used for spatial referencing. To allow $Z(\mathbf{s})$ to capture all the spatial variation, we include only an intercept in the model.

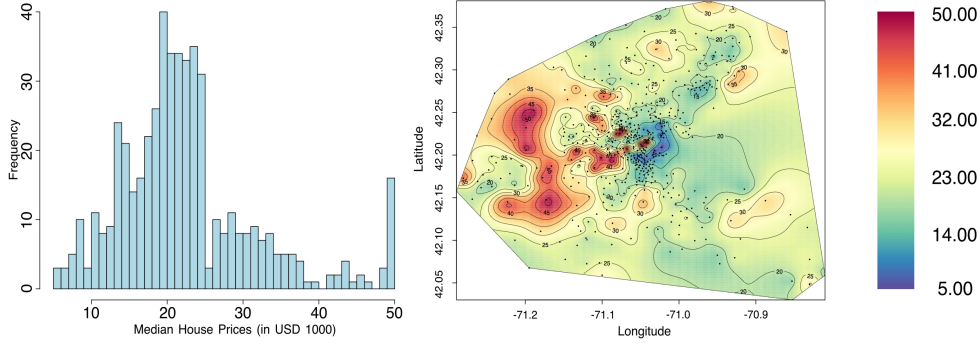


Figure 3: Plots showing (left) probability density of median house prices (in USD 1000) (right) spatial plot of median owner occupied house prices in Boston.

Table 2: Posterior Estimates from the hierarchical linear model in (13) to Boston housing

Parameters (θ)	Posterior Estimates ($\hat{\theta}$)	HPD
ϕ	0.96	(0.83, 1.11)
σ^2	55.18	(43.91, 68.06)
τ^2	14.89	(11.77, 18.71)
β_0	25.58	(24.29, 27.34)

Table 2 shows posterior estimates and HPD intervals for process parameters. We observe that $\frac{\sigma^2}{\sigma^2 + \tau^2} \approx 78.75\%$ —larger portion of total variance being explained by varying location.

Modeled spatial variation in the response is shown in Figure 3 (left). Significance for the estimate, $\hat{Z}(\mathbf{s})$, is assessed using the inclusion of 0 in its posterior HPD. Using posterior samples we estimate the derivative processes for $Z(\mathbf{s})$. A grid, ($\mathcal{G} = \{\mathbf{s}_g : \mathbf{s}_g \in \text{convex-hull}(\mathcal{S})\}$, containing 1229 equally spaced locations) is overlaid over the region with the same purpose. To effect posterior surface analysis on the estimated surface we use

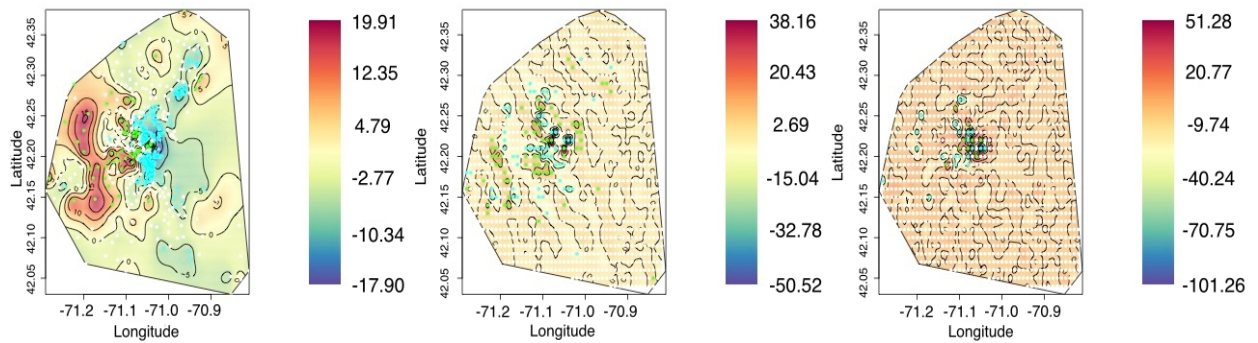


Figure 4: Plots (left to right) showing fitted process, divergence and Laplacian for the median house price surface.

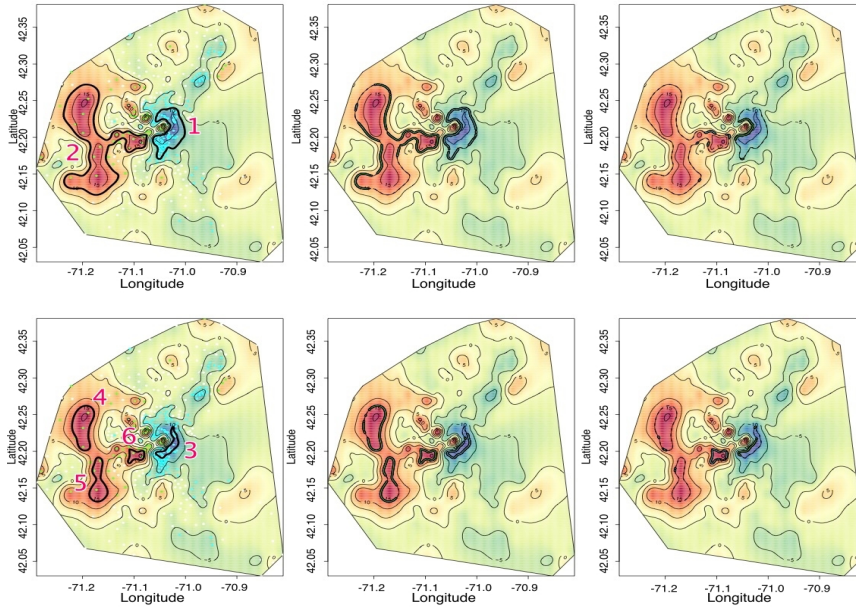


Figure 5: Curvature wombling on the Boston Housing Data.

posterior predictive distributions of $\text{div}(Z)$ and $\Delta(Z)$ revealing zones that manifest rapid change in response and gradients respectively. They are shown in Figures 4 (center and right). Next, we focus on performing curvature wombling on the estimated surface. Strategic posterior surface analysis is used to locate level-sets of interest within the surface that could possibly contain wombling boundaries. We start with contours shown in Figure 5 (left column). Boundary 1 (2) bounds a region where the fitted process has positive (negative) significant estimates. Evidently, the chosen curves should house significant gradients along most segments, but significant curvature should only be detected for segments located at the center (lat-long: $(42.18, 42.23) \times (-71.05, -70.05)$) of the surface in Figures 4 (center and right). Estimated average wombling measures for these curves are shown in Table 3. Figures 5 (center and right) correspond to segment level posterior inference for the curves, line segments with significant directional differentials are indicated in bold. Summarizing, we observe that the gradient, curvature and posterior surface analysis allow us to highlight towns (with census-tracts) within Boston that exhibit heterogeneity in prices. Curvature wombling performed on the surface allows us to delineate zones that house such heterogeneity. For instance, towns located within boundaries 3 (South and East End) and 6 (Newton

and Brookline) show significant change in price gradients, compared to towns within boundaries 4 (Lincoln and Weston) and 5 (Wellesley and Dover). These findings can be verified referring back to price dynamics for real estate in Boston during 1978 (see e.g., [Schnare & Struyk 1976](#)). The same regions are scrutinized for studying segmentation—towns within curves 1 and 3 are accessible to lower income groups willing to sacrifice air quality.

Table 3: Curvature wobbling measures for boundaries in Boston housing accompanied by corresponding HPD intervals in brackets below. Estimates corresponding to HPD intervals containing 0 are marked in bold.

Curve (C)	Average Gradient ($\bar{\Gamma}^{(1)}(C)$)	Average Curvature ($\bar{\Gamma}^{(2)}(C)$)
Boundary 1	-8.91 (-11.31, -6.65)	10.14 (2.84, 18.34)
Boundary 2	6.18 (4.75, 7.49)	-0.09 (-3.45, 3.35)
Boundary 3	-6.47 (-9.74, -3.27)	12.69 (2.65, 22.48)
Boundary 4	6.92 (4.63, 9.19)	1.26 (-5.04, 7.14)
Boundary 5	5.47 (2.95, 7.86)	1.36 (-4.33, 7.42)
Boundary 6	11.82 (7.28, 16.14)	-16.27 (-26.68, -6.57)

Meuse River Data: The Meuse river data features in [Pebesma et al. \(2012\)](#). It provides locations of topsoil heavy metal concentrations, along with soil and landscape variables at the observed locations, collected in a flood plain of the river Meuse, near the village of Stein, Netherlands. The heavy metal concentrations recorded include Cadmium (Cd), Copper (Cu), Lead (Pb) and Zinc (Zn). A distinguishing feature is the naturally occurring boundary—the Meuse. From a boundary analysis standpoint we are interested in examining differentials in heavy metal concentrations along the flood plain of the river to understand the heterogeneous effect of the river on the topsoil. The soils of the floodplain are commonly used for agriculture. Crops grown on the floodplain of the river banks of the Meuse may be consumed by man and/or livestock. The spatial variation in heavy metal concentration can be seen in Figure 6. The path of the Meuse river is shown in each of the spatial plots. Evidently, the heavy metal concentrations decreases with increasing distance from

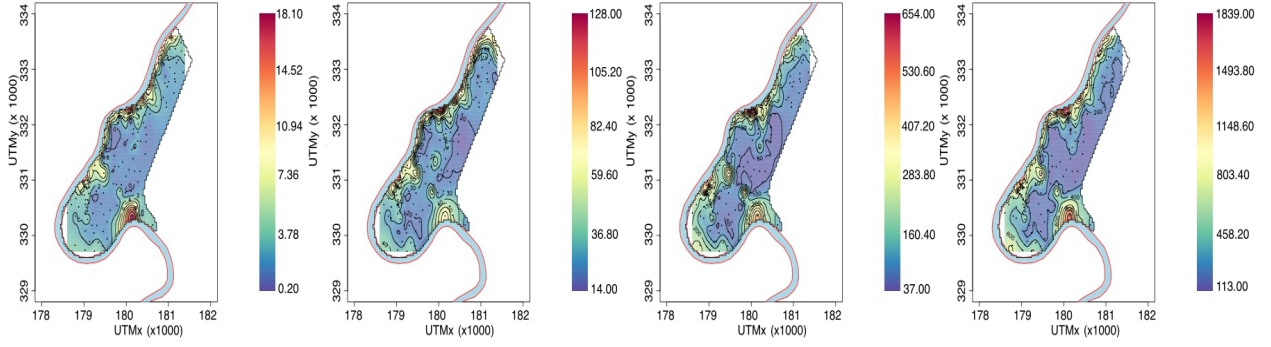


Figure 6: Plots showing heavy metal concentrations in the topsoil of a flood plain at 155 locations for (from left to right) Cadmium (Cd), Copper (Cu), Lead (Pb) and Zinc (Zn) (in mg/kg of soil).

the river. We model the concentrations as independent Gaussian processes. Covariates used are relative elevation above local river bed (`elev`, measured in meters), organic matter (`om` measured in kg/(100kg) of soil), distance to Meuse (`dist`), frequency of flooding, soil type (`soil`), and lime content in soil ($p = 9$). Table 4 shows the posterior estimates of process parameters and model coefficients, β for each of the heavy metals in question. We observe that $\sigma^2/(\sigma^2 + \tau^2) \approx 62.45\%$, 99.79% , 52.09% , 62.29% for Cd, Cu, Pb and Zn respectively, indicating larger portions of total variation being explained by spatial heterogeneity, except for Pb. Variation in Cd and Zn concentration is significantly affected by elevation, organic matter and flooding frequency, while variations in Cu and Pb concentration is significantly affected by elevation, organic matter and flooding frequency and lime content. The estimated residual surface is shown in Figure 7 (left) for Cd concentrations. We observe significant positive gradients with varying curvature depending on segments of the river bed for all heavy metals. We perform curvature wombling on the Meuse using the residual surface, \mathbf{Z} . The results of curvature wombling for cadmium are shown in Figure 7. Results and plots for other metals can be found in the Supplement, Section S7, Figure S14. The accompanying wombling measures are shown in Table 5. We observe sufficient heterogeneity in the signs of the wombling measures, yielding contiguous positive (negative) segments. For example, in Cd concentration, boundaries located for average gradients in the northern and southern region are positive, as opposed to boundaries located in the north western region. Therefore,

Table 4: Posterior estimates of process parameters and covariates for the Meuse river data accompanied by their corresponding HPD intervals in brackets below. Effects with HPDs containing 0 are marked in bold.

Parameters (θ)	Cadmium (Cd)	Copper (Cu)	Lead (Pb)	Zinc (Zn)
ϕ	0.0379 (0.0207, 0.0618)	0.1138 (0.0871, 0.1471)	0.0399 (0.0131, 0.1900)	0.0472 (0.0230, 0.0744)
σ^2	2.9566 (1.2803, 5.2227)	3.2044 (2.3955, 4.0892)	0.9303 (0.2763, 1.7641)	38.3538 (16.7815, 65.1450)
τ^2	1.7771 (0.9107, 2.6328)	0.0067 (0.0012, 0.0244)	0.8555 (0.0010, 1.2280)	23.2226 (9.3743, 35.6867)
Intercept	9.4973 (5.9750, 13.3704)	4.8503 (3.1392, 6.8308)	6.1120 (3.4615, 8.1910)	37.1315 (25.0903, 53.0870)
elev	-0.7672 (-1.2531, -0.3574)	-0.4065 (-0.7418, -0.1656)	-0.5413 (-0.7853, -0.1442)	-2.8781 (-4.7805, -1.2834)
om	0.4011 (0.2616, 0.5233)	0.4293 (0.3276, 0.4728)	0.3434 (0.2490, 0.4253)	0.8606 (0.3681, 1.3166)
dist	-0.0033 (-0.0061, 0.0000)	-0.0025 (-0.0043, -0.0014)	-0.0011 (-0.0029, 0.0006)	-0.0081 (-0.0197, 0.0038)
ffreq (=2)	-1.4176 (-2.3202, -0.3432)	-2.4727 (-3.1794, -1.6716)	-0.8483 (-1.6109, -0.2598)	-4.3182 (-7.9184, -0.6220)
ffreq (=3)	-0.7322 (-2.0520, 0.6248)	-1.4298 (-2.4443, -0.5157)	-0.1865 (-1.2972, 0.6861)	-3.3159 (-7.9307, 1.9128)
soil (=2)	-0.3337 (-1.4661, 0.7491)	0.2236 (-0.7248, 0.9799)	0.5988 (-0.0345, 1.2956)	-2.2213 (-6.1446, 2.0831)
soil (=3)	-0.3884 (-2.0891, 1.2628)	0.6344 (-0.2309, 1.8474)	0.3707 (-0.7108, 1.4029)	-2.9922 (-9.0918, 3.6289)
lime (=1)	0.5752 (-0.3509, 1.4341)	1.3223 (0.7152, 1.9427)	0.7759 (0.1173, 1.4645)	-0.4759 (-3.9057, 2.6510)

while displaying the wobbling measures, in Table 5, we separate them by their sign.

We conclude that effects of river Meuse on regions of the flood plain exhibit significant heterogeneity when considered across heavy metals. Compared to other metals, Pb concentrations are limited to northern regions of the flood plain. Concentrations of Cd and Zn concentrations along the river are similar. Compared to the northern region, in the northwestern region Zn concentrations decrease significantly as we move inland. Studies corroborating such evidence can be found in [Leenaers et al. \(1988\)](#) and [Albering et al. \(1999\)](#).

7 Discussion and Future Work

We developed a fully model-based Bayesian inferential framework for differential process assessment and curvature-based boundary analysis for spatial processes. Introducing the directional curvature process and its associated inferential framework supplements the direc-

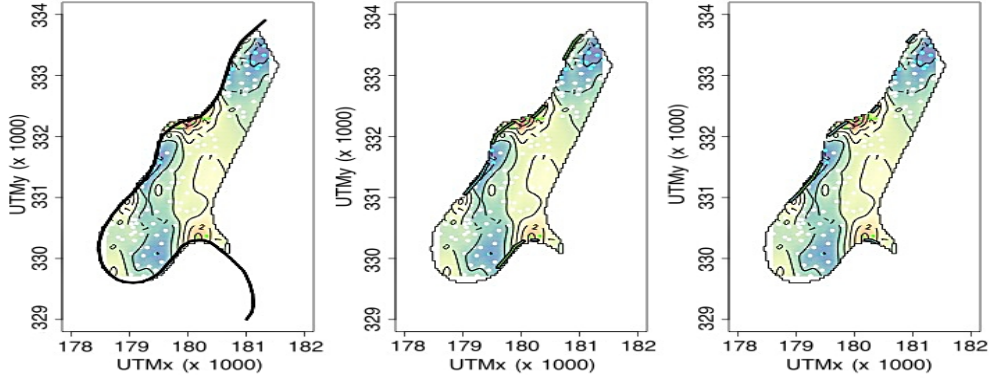


Figure 7: Plots showing results for curvature wombling on the Meuse river for Cadmium (Cd) concentration. Plots showing (left) the resulting fitted process (center) the contiguous segments that display significant gradients (right) the contiguous segments with significant curvature.

Table 5: Curvature wombling measures for the Meuse, separated by zones of positive and negative signs, they are accompanied by their corresponding HPD intervals in brackets below.

Wombling Measures	Cd	Cu	Pb	Zn
$\bar{\Gamma}^{(1)}(> 0)$	0.0510 (0.0298, 0.07401)	0.1273 (0.0913, 0.1729)	0.0375 (0.0019, 0.1561)	0.1984 (0.0876, 0.3162)
$\bar{\Gamma}^{(1)}(< 0)$	-0.0400 (-0.0635, -0.0170)	-0.2561 (-0.3187, -0.1997)	–	-0.1890 (-0.2967, -0.0669)
$\bar{\Gamma}^{(2)}(> 0)$	0.0074 (0.0019, 0.0158)	–	–	0.0422 (0.0111, 0.0879)
$\bar{\Gamma}^{(2)}(< 0)$	-0.0078 (-0.0223, -0.0024)	-0.1247 (-0.1979, -0.0860)	-0.0039 (-0.1076, -0.0006)	-0.0473 (-0.1114, -0.0095)

tional gradients with inference for their rates of change, while its induction into the folds of Bayesian curvilinear wombling allows for further characterization of difference boundaries. Adopting a Bayesian hierarchical model allows for Gaussian calibration when characterizing points, regions and boundaries within a surface. This framework is widely applicable; our applications arise from selected disciplines indicating the utilities of mapping curvature process boundaries to understand spatial data generating patterns. Substantive case studies will be reported separately.

Several avenues hold scope for future developments. A more generalized theoretical framework can be developed for studying joint behavior of the principal curvature (direction of maximum (or minimum) curvature) and the aspect (direction of maximum gradient) (see, e.g., [Wang et al. 2018](#)) leveraging dependent circular uniform distributions (see,

e.g., [Kent et al. 2008](#)). We offer some brief remarks. To obtain the direction of maximum curvature for a spatial surface, we solve $\max_{\mathbf{u} \in \mathbb{R}^2} |\mathbf{u}^\top \nabla^2 Y(\mathbf{s}) \mathbf{u}|$, such that $\|\mathbf{u}\| = 1$, at an arbitrary point \mathbf{s} . Using Lagrange multipliers and denoting $\kappa(\mathbf{u}) = |\mathbf{u}^\top \nabla^2 Y(\mathbf{s}) \mathbf{u}|$, define $\mathcal{O}(\mathbf{u}) = \kappa(\mathbf{u}) - \lambda(\|\mathbf{u}\|^2 - 1)$ hence, $\partial \mathcal{O}(\mathbf{u}) / \partial u_i = \kappa(\mathbf{u})^{-1} (\nabla_{ii}^2 Y(\mathbf{s}) u_i + \nabla_{ij}^2 Y(\mathbf{s}) u_j) - \lambda u_i = 0$, $i, j = 1, 2$. With $u_2/u_1 = \tan \theta_{pc}$, eliminating λ we get $\tan \theta_{pc} = \frac{\nabla_{22}^2 Y(\mathbf{s}) \tan \theta_{pc} + \nabla_{12}^2 Y(\mathbf{s})}{\nabla_{11}^2 Y(\mathbf{s}) + \nabla_{12}^2 Y(\mathbf{s}) \tan \theta_{pc}}$. Defining $h_1 = h_1(\mathbf{s}) = (\nabla_{11}^2 Y(\mathbf{s}) - \nabla_{22}^2 Y(\mathbf{s})) / \nabla_{12}^2 Y(\mathbf{s})$ given $\nabla_{12}^2 Y(\mathbf{s}) \neq 0$ and solving $\theta_{pc} = \tan^{-1} \frac{1}{2} \left[-h_1 \pm \sqrt{h_1^2 + 4} \right]$. If $\nabla_{12}^2 Y(\mathbf{s}) = 0$ then, $\nabla^2 Y(\mathbf{s})$ is diagonal and θ_{pc} corresponds to the direction of $\max\{\nabla_{11}^2 Y(\mathbf{s}), \nabla_{22}^2 Y(\mathbf{s})\}$. We propose that $\Theta = (\theta_{asp}, \theta_{pc})^\top$ follows a dependent circular uniform distribution over $[0, 2\pi] \times [0, 2\pi]$. Further developments with circular regression methods can proceed to examine the effect of covariates on Θ . Multivariate extensions would involve formulating these differential processes on arbitrary manifolds. This requires simulating a Gaussian process on manifolds and inspecting the covariant derivative. Bayesian curvilinear wombling could then be implemented on curves of interest to the investigator. This would not only involve an inferential framework for normal curvature, but also geodesic curvature for such curves. Spatiotemporal curvature processes can build upon [Quick et al. \(2015\)](#) to study evolutionary behavior of the curvature processes with respect to variations in the response across time. Finally, we remark that while there have been substantial recent developments in scalable spatial processes for massive data sets—a comprehensive review is beyond the scope of the current article (see, e.g., [Heaton et al. 2019](#))—not all scalable processes admit the correct degree of smoothness for curvature processes to exist. Constructing scalable processes for curvilinear wombling, and subsequent inference, remains a problem of interest in the wombling community.

Supplementary Materials

The following supplement includes additional theoretical derivations, computing details, additional simulation experiments and wombling for Northeastern US temperatures.

Supplementary Materials for “*Bayesian Modeling with Spatial Curvature Processes*”

Aritra Halder^a, Sudipto Banerjee^b and Dipak K. Dey^c

^aDepartment of Biostatistics,
Drexel University, Philadelphia, PA, USA.

^bDepartment of Biostatistics,
University of California, Los Angeles, CA, USA.

^cDepartment of Statistics,
University of Connecticut, Storrs, CT, USA.

February 13, 2023

8 Review of Directional Gradients and Wombling

8.1 Directional Gradients

For the scalar h and unit vector \mathbf{u} we define $Y_{\mathbf{u},h}^{(1)} = (Y(\mathbf{s} + h\mathbf{u}) - Y(\mathbf{s})) / h$ to be the first order finite difference processes at location \mathbf{s} in the directions of \mathbf{u} . Being a linear function of stationary processes this is well-defined. Passing to limits, we define $D_{\mathbf{u}}^{(1)}Y(\mathbf{s}) = \lim_{h \rightarrow 0} Y_{\mathbf{u},h}^{(1)}(\mathbf{s})$. Provided the limit exist, $D_{\mathbf{u}}^{(1)}Y(\mathbf{s})$ is defined as the directional gradient process. If $Y(\mathbf{s})$ is a mean square differentiable process in \mathbb{R}^d for every $\mathbf{s}_0 \in \mathbb{R}^d$ then $D_{\mathbf{u}}^{(1)}Y(\mathbf{s}) = \mathbf{u}^\top \nabla Y(\mathbf{s})$. Then, if $\mathbf{u} = \sum_{i=1}^d u_i \mathbf{e}_i$, we can compute $D_{\mathbf{u}}^{(1)}Y(\mathbf{s}) = \sum_{i=1}^d u_i D_{\mathbf{e}_i}^{(1)}Y(\mathbf{s})$. The directional gradient process is linear in \mathbf{u} , hence $D_{-\mathbf{u}}^{(1)}Y(\mathbf{s}) = -D_{\mathbf{u}}^{(1)}Y(\mathbf{s})$ and for any vector $\mathbf{w} = \|\mathbf{w}\|\mathbf{u}$, $D_{\mathbf{w}}^{(1)}Y(\mathbf{s}) = \|\mathbf{w}\|D_{\mathbf{u}}^{(1)}Y(\mathbf{s})$. The directional gradient at \mathbf{s}_0 in the direction \mathbf{w} is the slope at \mathbf{s}_0 of the curve traced out by slicing $Y(\mathbf{s})$ in the direction \mathbf{w} (see e.g., [Banerjee & Gelfand 2006](#), Section 2, for more details).

8.2 Wombling Measures

Wombling measures constructed from (7) for total and average gradient are associated with curves to characterize the magnitude of change. To each point $\mathbf{s} \in C$, a directional gradient is associated, $g(\mathcal{L}Y(\mathbf{s})) = D_{\mathbf{n}}^{(1)}Y(\mathbf{s}) = \mathbf{n}(\mathbf{s})^\top \nabla Y(\mathbf{s})$ (also a linear function of $\mathcal{L}_{\mathbf{n}}Y(\mathbf{s})$), along the direction of a unit normal $\mathbf{u} = \mathbf{n}(\mathbf{s})$ to the curve. For a curve tracking rapid change in the surface, choice of the normal direction to a curve is motivated by sharp directional gradients orthogonal to the curve; ℓ is chosen to be the arc-length measure. The rationale behind this choice is to measure change in response with respect to distance traversed on the curve. With reference to (7) the total and average gradients are, $\Gamma^{(1)}(C) = \int_{t_0}^{t_1} \nabla Y(\mathbf{s}(t))^\top \mathbf{n}(\mathbf{s}(t)) \|\mathbf{s}'(t)\| dt$ and $\bar{\Gamma}^{(1)}(C) = \Gamma^{(1)}(C)/\ell(C)$ respectively (see e.g., [Banerjee & Gelfand 2006](#), Section 3, for more details).

9 Interpretation of Spatial Curvature

Pursuits in geospatial analysis generally encounter surfaces which have canonical coordinate systems (e.g. latitude-longitude, easting-northing etc.). This facilitates a parameterization for the surface that leverages the coordinate system, commonly known as the Monge parameterization (also called a Monge patch, named after Gaspard Monge, see e.g., [O'Neill 2006](#), [Pressley 2010](#))—a surface, S , embedded in \mathbb{R}^3 , is parameterized by giving its height Y over some plane as a function of the orthonormal co-ordinates s_1 and s_2 in the plane, $S = \{\mathcal{S} \subset \mathbb{R}^2 \mapsto \mathbb{R}^3 : \mathbf{s} = (s_1, s_2) \mapsto Y(s_1, s_2) = Y(\mathbf{s})\}$. A point is then, $(\mathbf{s}, Y(\mathbf{s})) = (s_1, s_2, Y(s_1, s_2))$. The two tangent vectors at \mathbf{s} are, $\mathbf{E}_1(\mathbf{s}) = (1, 0, \nabla_1 Y(\mathbf{s}))^\top$ and $\mathbf{E}_2(\mathbf{s}) = (0, 1, \nabla_2 Y(\mathbf{s}))^\top$, where $\nabla_i Y(\mathbf{s}) = \frac{\partial}{\partial s_i} Y(\mathbf{s})$, $i = 1, 2$. Let $\nabla Y(\mathbf{s}) = (\nabla_1 Y(\mathbf{s}), \nabla_2 Y(\mathbf{s}))^\top$ denote the gradient vector, consider a unit direction vector, $\mathbf{u} = (u_1, u_2)^\top \in S \subset \mathbb{R}^2$, then $u_1 \mathbf{E}_1(\mathbf{s}) + u_2 \mathbf{E}_2(\mathbf{s}) = (\mathbf{u}^\top, \mathbf{u}^\top \nabla Y(\mathbf{s}))^\top \in T_S(\mathbf{s})$ corresponds to the *directional derivative* of Y along the direction \mathbf{u} , where $T_S(\mathbf{s})$ is the local tangent plane at \mathbf{s} , that is gen-

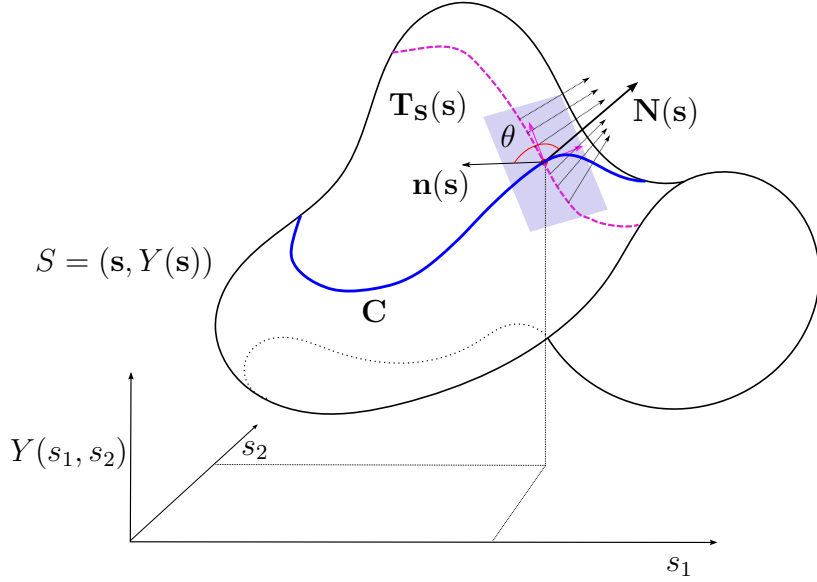


Figure 8: A Monge patch, $S = (s_1, s_2, Y(s_1, s_2))^\top = (\mathbf{s}^\top, Y(\mathbf{s}))^\top$, showing a point \mathbf{s} , a curve C passing through \mathbf{s} , normal to the surface, $\mathbf{N}(\mathbf{s})$, normal to the curve $\mathbf{n}(\mathbf{s})$, θ is the angle between them, and the local tangent plane to the surface, $T_S(\mathbf{s})$. The thin perpendicular pink arrows are tangent vectors, $\mathbf{E}_1(\mathbf{s})$ and $\mathbf{E}_2(\mathbf{s})$. The thin outward pointing black arrows around $\mathbf{N}(\mathbf{s})$ demonstrate change in \mathbf{N} as we move along the direction (dotted line) on the surface.

erated by $\{\mathbf{E}_1(\mathbf{s}), \mathbf{E}_2(\mathbf{s})\}$. The outward pointing normal to the surface S , denoted by $\mathbf{N}(\mathbf{s}) = \mathbf{E}_1(\mathbf{s}) \times \mathbf{E}_2(\mathbf{s}) = (-\nabla_1 Y(\mathbf{s}), -\nabla_2 Y(\mathbf{s}), 1)^\top$, where \times denotes the usual cross-product of vectors. Evidently, $\mathbf{N}(\mathbf{s})$ is orthogonal to the local tangent plane at that point, $T_S(\mathbf{s})$. Quantifying the local geometry of a surface, we are interested in how $\mathbf{N}(\mathbf{s})$ changes (“tips”) as we move in the direction \mathbf{u} from the point \mathbf{s} on the surface—derivatives for $\mathbf{N}(\mathbf{s})$ at the point \mathbf{s} , which lie in $T_S(\mathbf{s})$. This is quantified by the *normal curvature* of S along a direction \mathbf{u} . Before defining normal curvature for a surface, we digress briefly to investigate effects of surface curvature on curves—for a curve parameterized by t , $C = \{\mathbf{s}(t) = (s_1(t), s_2(t)) : t \in [a, b]\}$, passing through \mathbf{s} , if the curvature of C is, κ , the tangent to C at \mathbf{s} , $\mathbf{t}(\mathbf{s})$, and the principal unit normal, i.e. the normal to C on S , $\mathbf{n}(\mathbf{s}) = \mathbf{t}'(\mathbf{s})/\kappa$, then we have, $\mathbf{n}(\mathbf{s}) \cdot \mathbf{N}(\mathbf{s}) = \cos(\theta)$, $\mathbf{t}'(\mathbf{s}) = \kappa \mathbf{n}(\mathbf{s})$, which implies $\kappa \cos(\theta) = \mathbf{t}'(\mathbf{s}) \cdot \mathbf{N}(\mathbf{s})$. We observe that,

$$\mathbf{t}'(\mathbf{s}(t)) = \frac{\partial^2}{\partial t^2} (\mathbf{s}(t), Y(\mathbf{s}(t)))^\top = \frac{\partial}{\partial t} \mathbf{E}_i(\mathbf{s}(t)) s'_i(t) = \mathbf{E}_{ij}(\mathbf{s}(t)) s'_i(t) s'_j(t) + \mathbf{E}_i(\mathbf{s}(t)) s''_i(t) ,$$

since $\mathbf{E}_i(\mathbf{s}) \cdot \mathbf{N}(\mathbf{s}) = 0$, $\kappa \cos(\theta) = \mathbf{t}'(\mathbf{s}) \cdot \mathbf{N}(\mathbf{s}) = (\mathbf{E}_{ij}(\mathbf{s}) \cdot \mathbf{N}(\mathbf{s}))\partial s_i \partial s_j$, $i, j = 1, 2$, where the expression in the parenthesis is a property of the surface, independent of curve C , and is defined as the *second fundamental form*,

$$\Pi(\mathbf{s}) = \begin{pmatrix} \mathbf{E}_{11}(\mathbf{s}) \cdot \mathbf{N}(\mathbf{s}) & \mathbf{E}_{12}(\mathbf{s}) \cdot \mathbf{N}(\mathbf{s}) \\ \mathbf{E}_{21}(\mathbf{s}) \cdot \mathbf{N}(\mathbf{s}) & \mathbf{E}_{22}(\mathbf{s}) \cdot \mathbf{N}(\mathbf{s}) \end{pmatrix} = \begin{pmatrix} \nabla_{11}^2 Y(\mathbf{s}) & \nabla_{12}^2 Y(\mathbf{s}) \\ \nabla_{21}^2 Y(\mathbf{s}) & \nabla_{22}^2 Y(\mathbf{s}) \end{pmatrix} = \nabla^2 Y(\mathbf{s}),$$

where \mathbf{E}_{ij} and $\nabla_{ij}^2 Y$ are the partial differentiation of \mathbf{E} and Y with respect to s_i, s_j respectively, \cdot is the usual dot product for vectors and $\nabla_{12}^2 Y = \nabla_{21}^2 Y$. The second to last equality is obtained under the Monge parameterization. The second fundamental form is invariant with respect to transformations of the local co-ordinate which preserves the sense of \mathbf{N} , i.e. the transformation does not change an outward (inward) pointing normal to an inward (outward) pointing normal for S . Such surfaces are termed as *orientable surfaces*. The Möbius transformation is an example of non-orientable surfaces. The individual terms of Π , quantify the local geometry of a surface (or curvature) along orthonormal coordinates.

Curvature of the C can be attributed to (a) the curvature of the curve itself, and (b) the curvature of the surface on which C lies. κ is the curvature of C , termed as *geodesic curvature*. The curvature of the surface is termed as *normal curvature*, computed along a direction $\mathbf{u} = \mathbf{u}(\mathbf{s})$ is denoted by $\kappa_n(\mathbf{u})$. The normal curvature, which is an intrinsic property of the surface independent of C , is of primary interest to us, $\kappa_n(\mathbf{u}) = \mathbf{u}^\top \Pi(\mathbf{s}) \mathbf{u} / \mathbf{u}^\top \mathbf{u} = \mathbf{u}^\top \Pi \mathbf{u}$, under $\mathbf{u}^\top \mathbf{u} = 1$. $\kappa_n(\mathbf{u})$ is also the *directional curvature* of the Y along \mathbf{u} . For our exploits, $\mathbf{u} = \mathbf{n}$, the normal direction to C . The sign of $\kappa_n(\mathbf{u})$, or equivalently eigen-values of Π inform about the nature of curvature at \mathbf{s} —for example, if κ_1 and κ_2 denote eigenvalues of Π , with $K = \det \Pi = \kappa_1 \kappa_2$, if $K > 0$, it implies that the surface is bending away from $T_S(\mathbf{s})$; depending on whether $\kappa_1, \kappa_2 < 0$ (or > 0), \mathbf{s} can be locally classified as a concave (convex) ellipsoid (for more details see [Stevens 1981](#)).

For a purely differential geometric treatment of this discussion see—[Gauss \(1902\)](#), [Spivak](#)

(1999), Do Carmo (2016), Kreyszig (2019). Figure 8 illustrates this discussion.

10 Examples for selected Covariance Functions

The detailed calculations for closed form expression of selected covariance functions are presented. We start with the power exponential family of isotropic covariance functions, $\tilde{K}(\|\Delta\|) = \alpha \exp(-\phi\|\Delta\|^\nu)$, $0 < \nu \leq 2$. It is clear that $\nabla^4 \tilde{K}(\|\Delta\|)$ and exists only for $\nu = 2$, we have the following form, $\tilde{K}(\|\Delta\|) = \sigma^2 \exp(-\phi\|\Delta\|^2)$. For this choice we have,

$$\begin{aligned}
\left(\nabla \tilde{K}(\Delta)\right)_i &= -2\sigma^2 \phi \exp(-\phi\|\Delta\|^2) \delta_i, \\
\left(\nabla^2 \tilde{K}(\Delta)\right)_{ii} &= -2\sigma^2 \phi \exp(-\phi\|\Delta\|^2) (1 - 2\phi \delta_i^2), \\
\left(\nabla^2 \tilde{K}(\Delta)\right)_{ij} &= 4\sigma^2 \phi^2 \exp(-\phi\|\Delta\|^2) \delta_i \delta_j, \\
\left(\nabla^3 \tilde{K}(\Delta)\right)_{iii} &= 4\sigma^2 \phi^2 \exp(-\phi\|\Delta\|^2) (3 - 2\phi \delta_i^2) \delta_i, \\
\left(\nabla^3 \tilde{K}(\Delta)\right)_{iij} &= 4\sigma^2 \phi^2 \exp(-\phi\|\Delta\|^2) (1 - 2\phi \delta_i^2) \delta_j, \\
\left(\nabla^3 \tilde{K}(\Delta)\right)_{ijk} &= -8\sigma^2 \phi^3 \exp(-\phi\|\Delta\|^2) \delta_i \delta_j \delta_k, \\
\left(\nabla^4 \tilde{K}(\Delta)\right)_{iiii} &= 4\sigma^2 \phi^2 \exp(-\phi\|\Delta\|^2) (3 - 12\phi \delta_i^2 + 4\phi^2 \delta_i^4), \\
\left(\nabla^4 \tilde{K}(\Delta)\right)_{iiij} &= -8\sigma^2 \phi^3 \exp(-\phi\|\Delta\|^2) (3 - 2\phi \delta_i^2) \delta_i \delta_j, \\
\left(\nabla^4 \tilde{K}(\Delta)\right)_{iijj} &= 4\sigma^2 \phi^2 \exp(-\phi\|\Delta\|^2) (1 - 2\phi \delta_i^2) (1 - 2\phi \delta_j^2), \\
\left(\nabla^4 \tilde{K}(\Delta)\right)_{ijkl} &= 16\sigma^2 \phi^4 \exp(-\phi\|\Delta\|^2) \delta_i \delta_j \delta_k \delta_l,
\end{aligned}$$

where $i, j, k, l = 1, 2, \dots, d$. The squared exponential or the Gaussian covariance kernel is the only member of its class that admits such derivatives, although they have been critiqued to produce realizations that are too smooth to be of practical use in modeling (see Stein (1999)).

Turning to the Matérn class we see that with, $\tilde{K}\|\Delta\| = \alpha(\phi\|\Delta\|)^\nu K_\nu(\phi\|\Delta\|)$, where ν is

a parameter controlling the smoothness of realizations, that is mean square differentiability and K_ν is the modified Bessel function of order ν . At $\nu = 3/2$ and $\nu = 5/2$, $\tilde{K}(\|\Delta\|)$ takes the forms,

$$\tilde{K}(\|\Delta\|) = \begin{cases} \sigma^2(1 + \sqrt{3}\phi\|\Delta\|)e^{-\sqrt{3}\phi\|\Delta\|}, & \nu = 3/2 \\ \sigma^2 \left(1 + \sqrt{5}\phi\|\Delta\| + \frac{5}{3}\phi^2\|\Delta\|^2\right) e^{-\sqrt{5}\phi\|\Delta\|}, & \nu = 5/2 \end{cases},$$

where σ^2 is the overall process variance. Matérn with $\nu = 3/2$ is once mean square differentiable, where as Matérn with $\nu = 5/2$ is twice mean square differentiable at 0. As $\nu \rightarrow \infty$, Matérn covariances tend to the Gaussian covariance. Unlike the Gaussian covariance, they do not yield overly smoothed process realizations. For $\nu = 3/2$ we have,

$$\begin{aligned} (\nabla \tilde{K}(\Delta))_i &= -3\sigma^2\phi^2 e^{-\sqrt{3}\phi\|\Delta\|} \delta_i, \\ (\nabla^2 \tilde{K}(\Delta))_{ii} &= -3\sigma^2\phi^2 e^{-\sqrt{3}\phi\|\Delta\|} \left(1 - \sqrt{3}\phi \frac{\delta_i^2}{\|\Delta\|}\right), \\ (\nabla^2 \tilde{K}(\Delta))_{ij} &= 3\sqrt{3}\sigma^2\phi^3 e^{-\sqrt{3}\phi\|\Delta\|} \frac{\delta_i\delta_j}{\|\Delta\|}. \end{aligned}$$

where $i, j = 1, 2, \dots, d$. Since the process is just once mean square differentiable higher order derivatives do not exist. However, for $\nu = 5/2$ we have,

$$\begin{aligned} (\nabla \tilde{K}(\Delta))_i &= -\frac{5}{3}\sigma^2\phi^2 e^{-\sqrt{5}\phi\|\Delta\|} \left(1 + \sqrt{5}\phi\|\Delta\|\right) \delta_i, \\ (\nabla^2 \tilde{K}(\Delta))_{ii} &= -\frac{5}{3}\sigma^2\phi^2 e^{-\sqrt{5}\phi\|\Delta\|} \left(1 + \sqrt{5}\phi\|\Delta\| - 5\phi^2\delta_i^2\right), \\ (\nabla^2 \tilde{K}(\Delta))_{ij} &= \frac{25}{3}\sigma^2\phi^4 e^{-\sqrt{5}\phi\|\Delta\|} \delta_i\delta_j, \\ (\nabla^3 \tilde{K}(\Delta))_{iii} &= \frac{25}{3}\sigma^2\phi^4 e^{-\sqrt{5}\phi\|\Delta\|} \left(3 - \sqrt{5}\phi \frac{\delta_i^2}{\|\Delta\|}\right) \delta_i, \\ (\nabla^3 \tilde{K}(\Delta))_{iij} &= \frac{25}{3}\sigma^2\phi^4 e^{-\sqrt{5}\phi\|\Delta\|} \left(1 - \sqrt{5}\phi \frac{\delta_i^2}{\|\Delta\|}\right) \delta_j, \\ (\nabla^3 \tilde{K}(\Delta))_{ijk} &= -\frac{25\sqrt{5}}{3}\sigma^2\phi^5 e^{-\sqrt{5}\phi\|\Delta\|} \frac{\delta_i\delta_j\delta_k}{\|\Delta\|}, \\ (\nabla^4 \tilde{K}(\Delta))_{iiii} &= \frac{25}{3}\sigma^2\phi^4 e^{-\sqrt{5}\phi\|\Delta\|} \left[3 - 6\sqrt{5}\phi \frac{\delta_i^2}{\|\Delta\|} + \sqrt{5}\phi \left(\sqrt{5}\phi + \frac{1}{\|\Delta\|}\right) \frac{\delta_i^4}{\|\Delta\|^2}\right], \end{aligned}$$

$$\begin{aligned}
\left(\nabla^4 \tilde{K}(\Delta)\right)_{iii} &= \frac{25\sqrt{5}}{3} \sigma^2 \phi^5 e^{-\sqrt{5}\phi\|\Delta\|} \left[\frac{\delta_i}{\|\Delta\|^3} - \frac{1}{\|\Delta\|} \left(3 - \sqrt{5}\phi \frac{\delta_i^2}{\|\Delta\|} \right) \right] \delta_i^2 \delta_j, \\
\left(\nabla^4 \tilde{K}(\Delta)\right)_{iij} &= \frac{25}{3} \sigma^2 \phi^4 e^{-\sqrt{5}\phi\|\Delta\|} \left[\left(1 - \sqrt{5}\phi \frac{\delta_i^2}{\|\Delta\|} \right) \left(1 - \sqrt{5}\phi \frac{\delta_j^2}{\|\Delta\|} \right) + \sqrt{5}\phi \frac{\delta_i^2 \delta_j^2}{\|\Delta\|^3} \right], \\
\left(\nabla^4 \tilde{K}(\Delta)\right)_{ijkl} &= -\frac{25\sqrt{5}}{3} \sigma^2 \phi^5 e^{-\sqrt{5}\phi\|\Delta\|} \left(\sqrt{5}\phi + \frac{1}{\|\Delta\|} \right) \frac{\delta_i \delta_j \delta_k \delta_l}{\|\Delta\|^2},
\end{aligned}$$

where $i, j, k, l = 1, 2, \dots, d$.

The above expressions for entries of the cross-covariance matrices correspond to the joint process, $\mathcal{L}Y(\mathbf{s}) = (Y(\mathbf{s}), \nabla Y(\mathbf{s})^\top, \text{vech}(\nabla^2 Y(\mathbf{s}))^\top)^\top$ with respect to our kernel choices. The following cross-covariance matrices are evaluated at $\|\Delta\| \rightarrow 0$.

1. *Squared Exponential*: In \mathbb{R}^d , we have,

$$V_{\mathcal{L}Y}(\mathbf{0}) = \sigma^2 \begin{pmatrix} 1 & \mathbf{0}^\top & -2\phi \text{vech}(I_d)^\top \\ \mathbf{0} & 2\phi I_d & \mathbf{0} \\ -2\phi \text{vech}(I_d) & \mathbf{0} & 4\phi^2 \text{diag}\{3, 1, \dots, 1, 3, 1, \dots, 1, \dots, 3\} \end{pmatrix},$$

2. *Matérn* ($\nu = 3/2$): For this kernel the existence of only the gradient process is guaranteed, therefore the covariance is for the process, $\mathcal{L}Y(\mathbf{s}) = (Y(\mathbf{s}), \nabla Y(\mathbf{s})^\top)^\top$. In \mathbb{R}^d we

have, $V_{\mathcal{L}Y}(\mathbf{0}) = \sigma^2 \begin{pmatrix} 1 & \mathbf{0}^\top \\ \mathbf{0} & 3\phi^2 I_d \end{pmatrix}$.

3. *Matérn* ($\nu = 5/2$): In \mathbb{R}^d we have,

$$V_{\mathcal{L}Y}(\mathbf{0}) = \sigma^2 \begin{pmatrix} 1 & \mathbf{0}^\top & -\frac{5\phi^2}{3} \text{vech}(I_d)^\top \\ \mathbf{0} & \frac{5\phi^2}{3} I_d & \mathbf{0} \\ -\frac{5\phi^2}{3} \text{vech}(I_d) & \mathbf{0} & \frac{25\phi^4}{3} \text{diag}\{3, 1, \dots, 1, 3, 1, \dots, 1, \dots, 3\} \end{pmatrix}.$$

11 Algorithms

In what follows, we provide the required algorithms for sampling gradients and wombling measures. Although listed separately to highlight the requirement of only posterior samples, the required steps could be included within the MCMC subroutine devised for spatial learning (or fitting the model) of $Y(\mathbf{s})$.

Sampling Gradients and Curvature: The choice for K varies between Gaussian, Matérn with $\nu = 3/2$ and $\nu = 5/2$. There is scope for parallel computation across grid locations. Additionally if the inverse of estimated covariance matrices are stored for the MCMC runs from the model fit, sufficient gains in compilation can be achieved while sampling gradients. If ($\nu = 3/2$) is chosen the ∇^2 terms are not computed.

Algorithm 1: Algorithm for Sampling Gradients and Curvature

Input: \mathcal{S} , A Grid \mathcal{G} spanning \mathcal{S} , posterior MCMC samples $\boldsymbol{\beta}$, $\boldsymbol{\theta}_K = \{\sigma^2, \phi\}$, \mathbf{Z}
Result: Posterior samples for gradients $\nabla Y(\mathbf{s}_g)$ and curvature $\nabla^2 Y(\mathbf{s}_g)$ for $\mathbf{s}_g \in \mathcal{G}$
for $i = 1, 2, \dots, L$ **do**
 for $j = 1, 2, \dots, n_G$ **do**
 $\Delta[i, j] = \mathbf{s}_g[j] - \mathbf{s}[i]$ \triangleright Compute distances of grid locations to observed process
for $i = 1, 2, \dots, n_{\text{MCMC}}$ **do**
 $K[i] = K(\cdot; \boldsymbol{\theta}_K[i])$
 $K.\text{inv}[i] = (K(\cdot; \boldsymbol{\theta}_K[i]))^{-1}$
 for $j = 1, 2, \dots, n_G$ **do**
 $\nabla K[i, j] = (\nabla K(\Delta[i, j]; \boldsymbol{\theta}_K[i])^\top, \text{vech}(\nabla^2 K(\Delta[i, j]; \boldsymbol{\theta}_K[i]))^\top)^\top$
 $V[i, j] = V_{\mathcal{L}Y}(\mathbf{0})$
 $\mu[i, j] = \nabla \mu(\mathbf{s}; \boldsymbol{\beta}[i]) - \nabla K[i, j]^\top K.\text{inv}[i] \mathbf{Z}[i]$ \triangleright $*[\text{r}] \mu(\mathbf{s}; \boldsymbol{\beta}[i]) = \mathbf{X} \boldsymbol{\beta}[i]$
 $\Sigma[i, j] = V[i, j] - \nabla K[i, j]^\top K.\text{inv}[i] \nabla K[i, j]$
 $\mathcal{L}Y[i, j] = \mathcal{N}(\mu[i, j], \Sigma[i, j])$ \triangleright Posterior sample of Gradients and Curvature
return $\mathcal{L}Y$

Sampling Wombling Measures The choices for K are again between Gaussian, Matérn with $\nu = 3/2$ and $\nu = 5/2$. Choices for curves to be evaluated for wombling boundaries range from those outlined in Section 5.2. In case $\nu = 3/2$ wombling measures for curvature are not computed. Choices for approximations include computing Riemann sums replacing

Algorithm 2: Algorithm for Sampling Wombling Measures

Input: \mathcal{S} , A curve C , posterior MCMC samples $\boldsymbol{\beta}$, $\boldsymbol{\theta}_K = \{\sigma^2, \phi\}$, \mathbf{Z}

Result: Posterior samples for wombling measures $\boldsymbol{\Gamma}(\tilde{C}_P)$.

for $j = 1, 2, \dots, (n_P - 1)$ **do**

$t[j] = \|C[j] - C[j + 1]\|$

$\mathbf{u}[j] = (C[j] - C[j + 1])/t[j]$

\triangleright Compute \mathbf{t} and \mathbf{U}

for $i = 1, 2, \dots, L$ **do**

for $j = 1, 2, \dots, n_P$ **do**

$\Delta[i, j] = C[j] - \mathbf{s}[i]$ \triangleright Compute distances of points in curve to observed

 process and norms: $\|\Delta\| [i, j] = \|\Delta[i, j]\|$

for $i = 1, 2, \dots, n_{\text{MCMC}}$ **do**

$K[i] = K(\cdot; \boldsymbol{\theta}_K[i])$

$K.\text{inv}[i] = (K(\cdot; \boldsymbol{\theta}_K[i]))^{-1}$

for $j = 1, 2, \dots, n_P$ **do**

$\nabla K[i, j] = \left(\begin{array}{c} \mathbf{q}_1(0, t[j], D^{(1)}K(\Delta[i, j] + t\mathbf{u}[j]; \boldsymbol{\theta}_K[i])) \\ \mathbf{q}_1(0, t[j], D^{(2)}K(\Delta[i, j] + t\mathbf{u}[j]; \boldsymbol{\theta}_K[i])) \end{array} \right)^\top$,

$V[i, j] = \left(\begin{array}{cc} \mathbf{q}_2(0, 0, t[j], t[j], k_{11}(\boldsymbol{\theta}_K[i])) & \mathbf{q}_2(0, 0, t[j], t[j], k_{12}(\boldsymbol{\theta}_K[i])) \\ \mathbf{q}_2(0, 0, t[j], t[j], k_{21}(\boldsymbol{\theta}_K[i])) & \mathbf{q}_2(0, 0, t[j], t[j], k_{22}(\boldsymbol{\theta}_K[i])) \end{array} \right)$

$\mu[i, j] = \mu_{\boldsymbol{\Gamma}}(t[j]) - \nabla K[i, j]^\top K.\text{inv}[i] \mathbf{Z}[i]$

$\Sigma[i, j] = V[i, j] - \nabla K[i, j]^\top K.\text{inv}[i] \nabla K[i, j]$

$\boldsymbol{\Gamma}[i, j] = \mathcal{N}(\mu[i, j], \Sigma[i, j])$

\triangleright Posterior sample of Wombling Measures

return $\boldsymbol{\Gamma}$

quadrature for line integrals. There is scope for parallel computation with the curve being broken into segments evaluated in parallel for wombling boundaries.

The functions \mathbf{q}_1 and \mathbf{q}_2 denote one and two-dimensional quadrature respectively. In case a Riemann sum (see (15), Section 12) approximation is chosen, the points partitioning C are treated as grid points and the algorithm for sampling gradients and curvature is used for predictive inference on the differential process. The Riemann sums are computed using \mathbf{t} and \mathbf{U} and returned.

12 Proofs and Discussion

For the curvature process formulated in Section 2, we aim to show that the covariance matrix associated with the process $D_{\mathbf{u}, \mathbf{v}}^{(2)} Y(\mathbf{s}) = \mathbf{c}_{\mathbf{u}, \mathbf{v}}^\top \text{vech} \nabla^2 Y(\mathbf{s})$ is valid (pg. 5 last paragraph). We obtain the expression for the covariance matrix by leveraging the directional finite difference

process $Y_{\mathbf{u},\mathbf{v},h}^{(2)}(\mathbf{s})$. For points \mathbf{s}, \mathbf{s}' , we denote $\Delta = \mathbf{s} - \mathbf{s}'$ and \mathbf{u}, \mathbf{v} are unit vectors specifying direction and $\boldsymbol{\delta}(x, y) = \Delta + x\mathbf{u} + y\mathbf{v}$ as a map from $\mathbb{R}^2 \rightarrow \mathbb{R}^d$, after suppressing dependence on Δ and \mathbf{u}, \mathbf{v} , let $g(x, y) = K(\Delta(x, y)) = K(\Delta + x\mathbf{u} + y\mathbf{v})$ denote a map from $\mathbb{R}^2 \rightarrow \mathbb{R}$ we compute the covariance ,

$$\begin{aligned}
C_{\mathbf{u},\mathbf{v}}^{(2)}(\mathbf{s}, \mathbf{s}') &= \lim_{h \rightarrow 0} \lim_{k \rightarrow 0} E \left[Y_{\mathbf{u},\mathbf{v},h}^{(2)}(\mathbf{s}) Y_{\mathbf{u},\mathbf{v},k}^{(2)}(\mathbf{s}') \right], \\
&= \lim_{h \rightarrow 0} \lim_{k \rightarrow 0} \frac{1}{h^2 k^2} [g(h-k, h-k) - g(h-k, h) - g(h, h-k) + g(h, h) \\
&\quad - g(h-k, -k) + g(h-k, 0) + g(h, -k) - g(h, 0) \\
&\quad - g(-k, h-k) + g(-k, h) + g(0, h-k) - g(0, h) \\
&\quad + g(-k, -k) - g(-k, 0) - g(0, -k) + g(0, 0)], \\
&= \lim_{h \rightarrow 0} \frac{g''(h, h) - g''(h, 0) - g''(0, h) + g''(0, 0)}{h^2} = g^{(iv)}(0, 0).
\end{aligned}$$

On repeated application of the chain rule and noting that $\boldsymbol{\delta}_x(x, y) = \mathbf{u}^\top$, $\boldsymbol{\delta}_y(x, y) = \mathbf{v}^\top$ with all other higher order derivatives being 0 we have,

$$\begin{aligned}
g_x(x, y) &= \boldsymbol{\delta}_x(x, y) \nabla K(\Delta(x, y)) = \mathbf{u}^\top \nabla K(\Delta(x, y)), \\
g_y(x, y) &= \boldsymbol{\delta}_y(x, y) \nabla K(\Delta(x, y)) = \mathbf{v}^\top \nabla K(\Delta(x, y)), \\
g_{xx}(x, y) &= \boldsymbol{\delta}_x(x, y) \nabla^2 K(\Delta(x, y)) \boldsymbol{\delta}_x(x, y)^\top = \mathbf{u}^\top \nabla^2 K(\Delta(x, y)) \mathbf{u}, \\
g_{xy}(x, y) &= \boldsymbol{\delta}_x(x, y) \nabla^2 K(\Delta(x, y)) \boldsymbol{\delta}_y(x, y)^\top = \mathbf{u}^\top \nabla^2 K(\Delta(x, y)) \mathbf{v}, \\
g_{yy}(x, y) &= \boldsymbol{\delta}_y(x, y) \nabla^2 K(\Delta(x, y)) \boldsymbol{\delta}_y(x, y)^\top = \mathbf{v}^\top \nabla^2 K(\Delta(x, y)) \mathbf{v}, \\
g_{xxx}(x, y) &= \sum_{i=1}^d \delta_{i,xxx}(x, y) \left(\frac{\partial K}{\partial \delta_i} \right) + 3 \sum_{i,j=1}^d \delta_{i,xx}(x, y) \frac{\partial^2 K}{\partial \delta_i \partial \delta_j} \delta_{j,x}(x, y) \\
&\quad + \sum_{i,j,k=1}^d \delta_{i,x}(x, y) \delta_{j,x}(x, y) \delta_{k,x}(x, y) \frac{\partial^3 K}{\partial \delta_i \partial \delta_j \partial \delta_k}, \\
&= \sum_{i,j,k=1}^d \delta_{i,x}(x, y) \delta_{j,x}(x, y) \delta_{k,x}(x, y) \frac{\partial^3 K}{\partial \delta_i \partial \delta_j \partial \delta_k} = \mathbf{c}_{\mathbf{u},\mathbf{u}}^\top \nabla^3 K(\Delta(x, y)) \mathbf{u}.
\end{aligned}$$

Similarly $g_{xxy}(x) = \mathbf{c}_{\mathbf{u}, \mathbf{u}}^\top \nabla^3 K(\Delta(x, y)) \mathbf{v}$, $g_{yyx}(x) = \mathbf{c}_{\mathbf{v}, \mathbf{v}}^\top \nabla^3 K(\Delta(x, y)) \mathbf{u}$ and $g_{yyy}(x) = \mathbf{c}_{\mathbf{v}, \mathbf{v}}^\top \nabla^3 K(\Delta(x, y)) \mathbf{v}$. Next,

$$\begin{aligned}
g_{xxxx}(x, y) &= \sum_{i=1}^d \delta_{i,xxxx}(x, y) \left(\frac{\partial K}{\partial \delta_i} \right) + \sum_{i,j=1}^d \delta_{i,xxx}(x, y) \frac{\partial^2 K}{\partial \delta_i \partial \delta_j} \delta_{j,x}(x, y) \\
&+ 3 \left[\sum_{i,j=1}^d \delta_{i,xxx}(x, y) \frac{\partial^2 K}{\partial \delta_i \partial \delta_j} \delta_{j,x}(x, y) + \sum_{i,j=1}^d \delta_{i,xx}(x, y) \frac{\partial^2 K}{\partial \delta_i \partial \delta_j} \delta_{j,xx}(x, y) \right. \\
&\quad \left. + \sum_{i,j,k=1}^d \delta_{i,xx}(x, y) \delta_{j,x}(x, y) \delta_{k,x}(x, y) \frac{\partial^3 K}{\partial \delta_i \partial \delta_j \partial \delta_k} \right] \\
&+ 3 \sum_{i,j,k=1}^d \delta_{i,xx}(x, y) \delta_{j,x}(x, y) \delta_{k,x}(x, y) \frac{\partial^3 K}{\partial \delta_i \partial \delta_j \partial \delta_k} \\
&+ \sum_{i,j,k,l=1}^d \delta_{i,x}(x, y) \delta_{j,x}(x, y) \delta_{k,x}(x, y) \delta'_l(x) \frac{\partial^4 K}{\partial \delta_i \partial \delta_j \partial \delta_k \partial \delta_l}, \\
&= \sum_{i,j,k,l=1}^d \delta_{i,x}(x, y) \delta_{j,x}(x, y) \delta_{k,x}(x, y) \delta'_l(x) \frac{\partial^4 K}{\partial \delta_i \partial \delta_j \partial \delta_k \partial \delta_l} = \mathbf{c}_{\mathbf{u}, \mathbf{u}}^\top \nabla^4 K(\boldsymbol{\delta}(x)) \mathbf{c}_{\mathbf{u}, \mathbf{u}}.
\end{aligned}$$

Similarly, $g_{xxyy}(x, y) = \mathbf{c}_{\mathbf{u}, \mathbf{u}}^\top \nabla^4 K(\boldsymbol{\delta}(x)) \mathbf{c}_{\mathbf{u}, \mathbf{v}}$, $g_{yyyx}(x, y) = \mathbf{c}_{\mathbf{v}, \mathbf{v}}^\top \nabla^4 K(\boldsymbol{\delta}(x)) \mathbf{c}_{\mathbf{v}, \mathbf{u}}$, $g_{xxyy}(x, y) = \mathbf{c}_{\mathbf{u}, \mathbf{v}}^\top \nabla^4 K(\boldsymbol{\delta}(x)) \mathbf{c}_{\mathbf{u}, \mathbf{v}}$ and $g_{yyyy}(x, y) = \mathbf{c}_{\mathbf{v}, \mathbf{v}}^\top \nabla^4 K(\boldsymbol{\delta}(x)) \mathbf{c}_{\mathbf{v}, \mathbf{v}}$. Evaluated at $x, y = 0$, i.e. $\boldsymbol{\delta}(0, 0) = \Delta$, g_{xxyy} provides us with the required expression, $C_{\mathbf{u}, \mathbf{v}}^{(2)}(\mathbf{s}, \mathbf{s}') = \mathbf{c}_{\mathbf{u}, \mathbf{v}}^\top \nabla^4 K(\Delta) \mathbf{c}_{\mathbf{u}, \mathbf{v}}$ and $\text{var}(D_{\mathbf{u}, \mathbf{v}}^{(2)} Y(\mathbf{s})) = \lim_{h \rightarrow 0} E(Y_{\mathbf{u}, \mathbf{v}, h}^{(2)}(\mathbf{s}), Y_{\mathbf{u}, \mathbf{v}, k}^{(2)}(\mathbf{s})) = \mathbf{c}_{\mathbf{u}, \mathbf{v}}^\top \nabla^4 K(\mathbf{0}) \mathbf{c}_{\mathbf{u}, \mathbf{v}}$ which exists if $K^{(iv)}(\Delta)$ exists for all Δ , including $\Delta = \mathbf{0}$.

Note: In the above proof we make some abuse of notation for brevity of mathematical expressions involved. To clarify, $\delta_x = \frac{\partial}{\partial x} \delta(x, y)$, $\delta_{xx} = \frac{\partial^2}{\partial x^2} \delta(x, y)$ and so on, $g_x = \frac{\partial}{\partial x} g(x, y)$, $g_{xx} = \frac{\partial^2}{\partial x^2} g(x, y)$ etc., $\sum_{i,j=1}^d = \sum_{i=1}^d \sum_{j=1}^d$ etc.

To derive (2) and the covariance for the directional curvature process, we assume that

$Y(\mathbf{s})$ is isotropic, i.e. $K(\Delta) = \tilde{K}(\|\Delta\|)$ therefore,

$$\begin{aligned} C_{\mathbf{u},\mathbf{u}}^{(2)}(\mathbf{s}, \mathbf{s}') &= \lim_{h \rightarrow 0} \lim_{k \rightarrow 0} E \left[Y_{\mathbf{u},\mathbf{v},h}^{(2)}(\mathbf{s}) Y_{\mathbf{u},\mathbf{v},k}^{(2)}(\mathbf{s}') \right], \\ &= \lim_{h \rightarrow 0} \lim_{k \rightarrow 0} \frac{1}{h^2 k^2} \left[E \left(Y(\mathbf{s} + h(\mathbf{u} + \mathbf{v})) Y_{\mathbf{u},\mathbf{v},k}^{(2)}(\mathbf{s}') \right) - E(Y(\mathbf{s} + h\mathbf{u}) Y_{\mathbf{u},\mathbf{v},k}^{(2)}(\mathbf{s}')) \right. \\ &\quad \left. - E(Y(\mathbf{s} + k\mathbf{v}) Y_{\mathbf{u},\mathbf{v},k}^{(2)}(\mathbf{s}')) + E(Y(\mathbf{s}) Y_{\mathbf{u},\mathbf{v},k}^{(2)}(\mathbf{s}')) \right] \end{aligned}$$

where,

$$\begin{aligned} E \left(Y(\mathbf{s} + h(\mathbf{u} + \mathbf{v})) Y_{\mathbf{u},\mathbf{v},k}^{(2)}(\mathbf{s}') \right) &= \tilde{K}(\|\Delta + (h-k)(\mathbf{u} + \mathbf{v})\|) - \tilde{K}(\|\Delta + (h-k)\mathbf{u} + h\mathbf{v}\|) - \\ &\quad \tilde{K}(\|\Delta + h\mathbf{u} + (h-k)\mathbf{v}\|) + \tilde{K}(\|\Delta + h(\mathbf{u} + \mathbf{v})\|) \\ &\quad - \tilde{K}(\|\Delta + (h-k)\mathbf{u} - k\mathbf{v}\|), \\ E(Y(\mathbf{s} + h\mathbf{u}) Y_{\mathbf{u},\mathbf{v},k}^{(2)}(\mathbf{s}')) &= \tilde{K}(\|\Delta + (h-k)\mathbf{u} - k\mathbf{v}\|) - \tilde{K}(\|\Delta + (h-k)\mathbf{u}\|) \\ &\quad - \tilde{K}(\|\Delta + h\mathbf{u} - k\mathbf{v}\|) + \tilde{K}(\|\Delta + h\mathbf{u}\|) \\ E(Y(\mathbf{s} + k\mathbf{v}) Y_{\mathbf{u},\mathbf{v},k}^{(2)}(\mathbf{s}')) &= \tilde{K}(\|\Delta - k\mathbf{u} + (h-k)\mathbf{v}\|) - \tilde{K}(\|\Delta - k\mathbf{u} + h\mathbf{v}\|) \\ &\quad - \tilde{K}(\|\Delta + (h-k)\mathbf{v}\|) + \tilde{K}(\|\Delta + h\mathbf{v}\|) \\ E(Y(\mathbf{s}) Y_{\mathbf{u},\mathbf{v},k}^{(2)}(\mathbf{s}')) &= \tilde{K}(\|\Delta - k(\mathbf{u} + \mathbf{v})\|) - \tilde{K}(\|\Delta - k\mathbf{u}\|) - \tilde{K}(\|\Delta - k\mathbf{v}\|) + \tilde{K}(\|\Delta\|) \end{aligned}$$

suppressing dependence on Δ , \mathbf{u} and \mathbf{v} , we define $\rho(h, k) = \|\Delta(h, k)\| = \|\Delta + h\mathbf{u} + k\mathbf{v}\|$

and let $g(h, k) = K(\rho(h, k))$. Hence,

$$\begin{aligned} C_{\mathbf{u},\mathbf{v}}^{(2)}(\mathbf{s}, \mathbf{s}') &= \lim_{h \rightarrow 0} \lim_{k \rightarrow 0} \frac{1}{h^2 k^2} [\rho(h-k, h-k) - \rho(h-k, h) - \rho(h, h-k) + \rho(h, h) \\ &\quad - \rho(h-k, -k) + \rho(h-k, 0) + \rho(h, -k) - \rho(h, 0) \\ &\quad - \rho(-k, h-k) + \rho(-k, h) + \rho(0, h-k) - \rho(0, h) \\ &\quad + \rho(-k, -k) - \rho(-k, 0) - \rho(0, -k) + \rho(0, 0)], \\ &= \lim_{h \rightarrow 0} \frac{\rho''(h, h) - \rho''(h, 0) - \rho''(0, h) + \rho''(0, 0)}{h^2} = \rho^{(iv)}(0, 0). \end{aligned}$$

Since, $\rho(0,0) = \|\Delta\|$, from the previous proof we can see that, $\rho^{(iv)}(0,0) = \nabla \tilde{K}(\|\Delta\|)\rho^{(iv)}(0,0) + \nabla^2 \tilde{K}(\|\Delta\|) (4\rho'''(0,0)\rho'(0,0) + 3[\rho''(0,0)]^2) + 6\nabla^3 \tilde{K}(\|\Delta\|)\rho''(0,0)[\rho'(0,0)]^2 + \nabla^4 \tilde{K}(\|\Delta\|)[\rho'(0,0)]^4$.

After some algebra, $\rho'(0) = \frac{\mathbf{u}^\top \Delta}{\|\Delta\|}$, $\rho''(0) = \frac{1}{\|\Delta\|} \left(1 - \frac{(\mathbf{u}^\top \Delta)^2}{\|\Delta\|^2}\right)$, $\rho'''(0) = -3\frac{\mathbf{u}^\top \Delta}{\|\Delta\|^3} \left(1 - \frac{(\mathbf{u}^\top \Delta)^2}{\|\Delta\|^2}\right)$ and $\rho^{(iv)}(0) = \frac{3}{\|\Delta\|^3} \left(5\frac{(\mathbf{u}^\top \Delta)^2}{\|\Delta\|^2} - 1\right) \left(1 - \frac{(\mathbf{u}^\top \Delta)^2}{\|\Delta\|^2}\right)$. Substituting and grouping terms corresponding to $\left(\nabla^2 \tilde{K}(\|\Delta\|) - \frac{\nabla \tilde{K}(\|\Delta\|)}{\|\Delta\|}\right)$, $\nabla^3 \tilde{K}(\|\Delta\|)$ and $\nabla^4 \tilde{K}(\|\Delta\|)$ we get,

$$g^{(iv)}(0) = \frac{3}{\|\Delta\|^2} \left\{1 - 5\frac{(\mathbf{u}^\top \Delta)^2}{\|\Delta\|^2}\right\} \left[1 - \frac{(\mathbf{u}^\top \Delta)^2}{\|\Delta\|^2}\right] \left(\nabla^2 \tilde{K}(\|\Delta\|) - \frac{\nabla \tilde{K}(\|\Delta\|)}{\|\Delta\|}\right) + \frac{6}{\|\Delta\|} \frac{(\mathbf{u}^\top \Delta)^2}{\|\Delta\|^2} \left[1 - \frac{(\mathbf{u}^\top \Delta)^2}{\|\Delta\|^2}\right] \nabla^3 \tilde{K}(\|\Delta\|) + \left(\frac{(\mathbf{u}^\top \Delta)^2}{\|\Delta\|^2}\right)^2 \nabla^4 \tilde{K}(\|\Delta\|),$$

which is the required expression. We discuss validity of the curvature process for surfaces in \mathbb{R}^3 . It can be easily extended to surfaces in \mathbb{R}^d . Define,

$$\begin{aligned} \mathcal{L}_{\mathbf{e}_1, \mathbf{e}_2, h} Y(\mathbf{s}) &= \begin{pmatrix} 1 & 0 & 0 & 0 & 0 & 0 \\ -\frac{1}{h} & \frac{1}{h} & 0 & 0 & 0 & 0 \\ -\frac{1}{h} & 0 & \frac{1}{h} & 0 & 0 & 0 \\ \frac{1}{h^2} & -\frac{2}{h^2} & 0 & \frac{1}{h^2} & 0 & 0 \\ \frac{1}{h^2} & -\frac{1}{h^2} & -\frac{1}{h^2} & 0 & \frac{1}{h^2} & 0 \\ \frac{1}{h^2} & 0 & -\frac{2}{h^2} & 0 & 0 & \frac{1}{h^2} \end{pmatrix} \begin{pmatrix} Y(\mathbf{s}) \\ Y(\mathbf{s} + h\mathbf{e}_1) \\ Y(\mathbf{s} + h\mathbf{e}_2) \\ Y(\mathbf{s} + 2h\mathbf{e}_1) \\ Y(\mathbf{s} + h(\mathbf{e}_1 + \mathbf{e}_2)) \\ Y(\mathbf{s} + 2h\mathbf{e}_2) \end{pmatrix} \\ &= \mathbf{A}_h \mathbf{L}_h(\mathbf{s}) = \left(Y(\mathbf{s}), Y_{\mathbf{e}_1, h}^{(1)}(\mathbf{s}), Y_{\mathbf{e}_2, h}^{(1)}(\mathbf{s}), Y_{\mathbf{e}_1, \mathbf{e}_1, h}^{(2)}(\mathbf{s}), Y_{\mathbf{e}_1, \mathbf{e}_2, h}^{(2)}(\mathbf{s}), Y_{\mathbf{e}_2, \mathbf{e}_2, h}^{(2)}(\mathbf{s})\right)^\top, \end{aligned}$$

as finite difference corresponding to the differential operator $\mathcal{L}Y$ using the expressions of $Y_{\mathbf{e}_i, h}^{(1)}(\mathbf{s})$ and $Y_{\mathbf{e}_i, \mathbf{e}_j, h}^{(2)}(\mathbf{s})$, $i, j = 1, 2$. For every $h > 0$ this defines a linear transformation, since the determinant of \mathbf{A}_h is h^{-8} . We denote the differenced differential process on the right of \mathbf{A}_h , suppressing dependence on $\mathbf{e}_1, \mathbf{e}_2$ by $\mathbf{L}_h(\mathbf{s})$. The associated covariance matrix is given by, $Cov(\mathcal{L}_{\mathbf{e}_1, \mathbf{e}_2, h} Y(\mathbf{s}), \mathcal{L}_{\mathbf{e}_1, \mathbf{e}_2, k} Y(\mathbf{s}')) = \mathbf{A}_h \mathcal{K}_{\mathbf{e}_1, \mathbf{e}_2, h, k}(\Delta) \mathbf{A}_k^\top$, where elements of $\mathcal{K}_{\mathbf{e}_1, \mathbf{e}_2, h, k}(\Delta)$ are obtained from $Cov(\mathbf{L}_h(\mathbf{s}), \mathbf{L}_k(\mathbf{s}'))$. Hence, as $h \downarrow 0$, $\mathcal{L}_{\mathbf{e}_1, \mathbf{e}_2, h} Y(\mathbf{s}) \rightarrow \mathcal{L}Y(\mathbf{s})$ and $\lim_{h \downarrow 0, k \downarrow 0} Cov(\mathcal{L}_{\mathbf{e}_1, \mathbf{e}_2, h} Y(\mathbf{s}), \mathcal{L}_{\mathbf{e}_1, \mathbf{e}_2, k} Y(\mathbf{s}')) = V_{\mathcal{L}Y}(\Delta)$, where the limits operate element-

wise on the matrix $\mathbf{A}_h \mathcal{K}_{\mathbf{e}_1, \mathbf{e}_2, h, k}(\Delta) \mathbf{A}_k^\top$ and, the expression for each element is obtained from previous computations, by setting $\mathbf{u} = \mathbf{e}_1$ and $\mathbf{v} = \mathbf{e}_2$.

For the directional operator, this can be established by observing that the directional differential operator is obtained as follows,

$$\mathcal{L}_{\mathbf{u}, h} Y(\mathbf{s}) = \begin{pmatrix} 1 & 0 & 0 & 0 & 0 & 0 \\ 0 & u_1 & u_2 & 0 & 0 & 0 \\ 0 & 0 & 0 & u_1^2 & 2u_1 u_2 & u_2^2 \end{pmatrix} \mathcal{L}_{\mathbf{e}_1, \mathbf{e}_2, h} Y(\mathbf{s}) = (1 \oplus \mathbf{u}^\top \oplus \mathbf{c}_{\mathbf{u}, \mathbf{u}}^\top) \mathcal{L}_{\mathbf{e}_1, \mathbf{e}_2, h} Y(\mathbf{s}),$$

where \oplus denotes the direct sum for matrices, then as $h \rightarrow 0$, $\mathcal{L}_{\mathbf{u}, h} Y(\mathbf{s}) \rightarrow \mathcal{L}_{\mathbf{u}} Y(\mathbf{s})$. The covariance matrix is obtained following similar arguments presented in the proof for the previous result. In case the covariance is isotropic we have $K(\Delta) = \tilde{K}(\|\Delta\|)$, on repeated differentiation and noting that $\frac{\partial}{\partial \Delta} \|\Delta\| = \frac{\Delta}{\|\Delta\|}$ we have,

$$\begin{aligned} \nabla K(\Delta) &= \frac{\nabla \tilde{K}(\|\Delta\|)}{\|\Delta\|} \Delta, \\ \nabla^2 K(\Delta) &= \frac{\nabla \tilde{K}(\|\Delta\|)}{\|\Delta\|} I - \frac{\nabla \tilde{K}(\|\Delta\|)}{\|\Delta\|^3} \Delta \Delta^\top + \frac{\nabla^2 \tilde{K}(\|\Delta\|)}{\|\Delta\|^2} \Delta \Delta^\top \\ &= \frac{\nabla \tilde{K}(\|\Delta\|)}{\|\Delta\|} I + \left(\nabla^2 \tilde{K}(\|\Delta\|) - \frac{\nabla \tilde{K}(\|\Delta\|)}{\|\Delta\|} \right) \frac{\Delta \Delta^\top}{\|\Delta\|^2}. \end{aligned}$$

Differentiating $\nabla^2 K(\Delta)$ w.r.t. Δ we obtain,

$$\begin{aligned} \nabla^3 K(\Delta) &= \frac{\nabla^2 \tilde{K}(\|\Delta\|)}{\|\Delta\|^2} \text{vech}(I)^\top \otimes \Delta - \frac{\nabla \tilde{K}(\|\Delta\|)}{\|\Delta\|^3} \text{vech}(I)^\top \otimes \Delta \\ &\quad + \left(\nabla^2 \tilde{K}(\|\Delta\|) - \frac{\nabla \tilde{K}(\|\Delta\|)}{\|\Delta\|} \right) \frac{1}{\|\Delta\|^2} \frac{\partial \text{vech}(\Delta \Delta^\top)}{\partial \Delta} \\ &\quad - 2 \left(\nabla^2 \tilde{K}(\|\Delta\|) - \frac{\nabla \tilde{K}(\|\Delta\|)}{\|\Delta\|} \right) \frac{1}{\|\Delta\|^4} \frac{\partial \text{vech}(\Delta \Delta^\top)}{\partial \Delta} \\ &\quad - \left(\nabla^2 \tilde{K}(\|\Delta\|) - \frac{\nabla \tilde{K}(\|\Delta\|)}{\|\Delta\|} \right) \frac{1}{\|\Delta\|^4} \frac{\partial \text{vech}(\Delta \Delta^\top)}{\partial \Delta} \\ &\quad + \nabla^3 \tilde{K}(\|\Delta\|) \cdot \frac{\text{vech}(\Delta \Delta^\top)^\top \otimes \Delta}{\|\Delta\|^3}. \end{aligned}$$

On grouping terms for $\nabla^2 \tilde{K}(\|\Delta\|) - \frac{\nabla \tilde{K}(\|\Delta\|)}{\|\Delta\|}$ and $\nabla^3 \tilde{K}(\|\Delta\|)$ we obtain the required expression,

$$\begin{aligned} \nabla^3 K(\Delta) = & \left(\nabla^2 \tilde{K}(\|\Delta\|) - \frac{\nabla \tilde{K}(\|\Delta\|)}{\|\Delta\|} \right) \left\{ \frac{\text{vech}(I)^\top \otimes \Delta}{\|\Delta\|^2} - 3 \frac{\text{vech}(\Delta\Delta^\top)^\top \otimes \Delta}{\|\Delta\|^4} \right. \\ & \left. + \frac{1}{\|\Delta\|^2} \frac{\partial \text{vech}(\Delta\Delta^\top)}{\partial \Delta} \right\} \\ & + \nabla^3 \tilde{K}(\|\Delta\|) \cdot \frac{\text{vech}(\Delta\Delta^\top)^\top \otimes \Delta}{\|\Delta\|^3} \end{aligned}$$

To obtain $\nabla^4 K(\Delta)$ we differentiate $\nabla^3 K(\Delta)$ w.r.t. Δ , we use notations $A_1 = \frac{\partial \Delta \otimes \text{vech}(I)^\top}{\partial \Delta}$, $A_2 = \frac{\partial \Delta \otimes \text{vech}(\Delta\Delta^\top)^\top}{\partial \Delta}$, $A_3 = \frac{\partial}{\partial \Delta} \left(\frac{\partial \text{vech}(\Delta\Delta^\top)}{\partial \Delta} \right)$ for matricized tensors of order $d(d+1)/2 \times d(d+1)/2$, where the order of matricization conforms to the listing order of the half-vectorization operator vech and A_4 denotes the element-wise product of Δ with $\left(\frac{\partial \text{vech}(\Delta\Delta^\top)}{\partial \Delta} \right)$ in the same order as the matricized tensor.

On differentiating the factor corresponding to the coefficient $\nabla^2 \tilde{K}(\|\Delta\|) - \frac{\nabla \tilde{K}(\|\Delta\|)}{\|\Delta\|}$ we obtain,

$$\begin{aligned} & \frac{1}{\|\Delta\|^2} A_1 - 3 \frac{1}{\|\Delta\|^4} A_2 + \frac{1}{\|\Delta\|^2} A_3 - \frac{2}{\|\Delta\|^4} \text{vech}(\Delta\Delta^\top) \text{vech}(I)^\top \\ & + \frac{12}{\|\Delta\|^6} \text{vech}(\Delta\Delta^\top) \text{vech}(\Delta\Delta^\top)^\top - \frac{2}{\|\Delta\|^4} A_4. \end{aligned}$$

Differentiating $\nabla^2 \tilde{K}(\|\Delta\|) - \frac{\nabla \tilde{K}(\|\Delta\|)}{\|\Delta\|}$,

$$\frac{\nabla^3 \tilde{K}(\|\Delta\|)}{\|\Delta\|} \Delta - \left(\nabla^2 \tilde{K}(\|\Delta\|) - \frac{\nabla \tilde{K}(\|\Delta\|)}{\|\Delta\|} \right) \frac{\Delta\Delta^\top}{\|\Delta\|^2}.$$

Differentiating the factor corresponding to the coefficient $\nabla^3 \tilde{K}(\|\Delta\|)$ we obtain,

$$-3 \frac{\text{vech}(\Delta\Delta^\top) \text{vech}(\Delta\Delta^\top)^\top}{\|\Delta\|^5} + \frac{1}{\|\Delta\|^3} A_2,$$

finally, differentiating $\nabla^3 \tilde{K}(\|\Delta\|) = \nabla^4 \tilde{K}(\|\Delta\|) \frac{\Delta}{\|\Delta\|}$. Grouping coefficients for $\nabla^2 \tilde{K}(\|\Delta\|) -$

$\frac{\nabla \tilde{K}(\|\Delta\|)}{\|\Delta\|}$, $\nabla^3 \tilde{K}(\|\Delta\|)$ and $\nabla^4 \tilde{K}(\|\Delta\|)$ we obtain the required expression, thereby completing the proof.

For proving the result focusing on spectral theory, note that since f is symmetric about 0 by hypothesis,

$$K(t) = \int_{\mathbb{R}} e^{i\lambda t} f(\lambda) d\lambda = \int_{\mathbb{R}} \cos(\lambda t) f(\lambda) d\lambda + i \int_{\mathbb{R}} \sin(\lambda t) f(\lambda) d\lambda = \int_{\mathbb{R}} \cos(\lambda t) f(\lambda) d\lambda.$$

Differentiating w.r.t. t on both sides we have,

$$\nabla K(t) = - \int \sin(\lambda t) \lambda f(\lambda) d\lambda,$$

Since $|\sin(\lambda t) \lambda f(\lambda)| \leq |\lambda| f(\lambda)$ and $\int |\lambda| f(\lambda) d\lambda < \infty$ under hypothesis, differentiation under the integral sign is valid. We repeat the process to obtain,

$$\nabla^2 K(t) = - \int \cos(\lambda t) \lambda^2 f(\lambda) d\lambda, \quad \nabla^3 K(t) = \int \sin(\lambda t) \lambda^3 f(\lambda) d\lambda, \quad \nabla^4 K(t) = \int \cos(\lambda t) \lambda^4 f(\lambda) d\lambda,$$

Next we make the following observations for limits of these derivatives,

$$\lim_{t \rightarrow 0} \left(\nabla^2 K(t) - \frac{\nabla K(t)}{t} \right) = \lim_{t \rightarrow 0} \int \left(\cos(\lambda t) - \frac{\sin(\lambda t)}{\lambda t} \right) \lambda^2 f(\lambda) d\lambda = 0,$$

$$\lim_{t \rightarrow 0} \nabla^2 K(t) = - \lim_{t \rightarrow 0} \int \cos(\lambda t) \lambda^2 f(\lambda) d\lambda = - \int \lambda^2 f(\lambda) d\lambda < \infty,$$

$$\lim_{t \rightarrow 0} \nabla^3 K(t) = \lim_{t \rightarrow 0} \int \sin(\lambda t) \lambda^3 f(\lambda) d\lambda = 0,$$

$$\lim_{t \rightarrow 0} \nabla^4 K(t) = \lim_{t \rightarrow 0} \int \cos(\lambda t) \lambda^4 f(\lambda) d\lambda = \int \lambda^4 f(\lambda) d\lambda < \infty,$$

We evaluate the results obtained above under these observations. Making note of,

$$\left\{ \frac{\text{vech}(I)^\top \otimes \Delta}{\|\Delta\|^2} - 3 \frac{\text{vech}(\Delta \Delta^\top)^\top \otimes \Delta}{\|\Delta\|^4} + \frac{1}{\|\Delta\|^2} \frac{\partial \text{vech}(\Delta \Delta^\top)}{\partial \Delta} \right\}, \quad \frac{\text{vech}(\Delta \Delta^\top)^\top \otimes \Delta}{\|\Delta\|^3}$$

stay bounded as $\Delta \rightarrow 0$ implying $\nabla^3 K(\Delta) \rightarrow 0$ as $\Delta \rightarrow 0$. For $\nabla^4 K(\Delta)$, we observe that the

factors corresponding to $\nabla^2 \tilde{K}(\|\Delta\|) - \frac{\nabla \tilde{K}(\|\Delta\|)}{\|\Delta\|}$, $\nabla^3 \tilde{K}(\|\Delta\|)$ and $\nabla^4 \tilde{K}(\|\Delta\|)$ remain bounded as $\Delta \rightarrow 0$, additionally $\frac{\text{vech}(\Delta\Delta^\top)\text{vech}(\Delta\Delta^\top)^\top}{\|\Delta\|^4} \rightarrow I_{d(d+1)/2}$ as $\Delta \rightarrow 0$. For each diagonal element of $(\nabla^4 K)_{ii} = a_i = \int \lambda^4 f_i(\lambda) d\lambda$ which completes the proof.

For results in page 8, we prove this for $\mathbf{s} \in \mathbb{R}^2$, the proof can be extended to \mathbb{R}^d analogously. Under the hypothesis,

$$Y_1(\mathbf{s}), \sim GP(\mathbf{0}, K(\cdot, \boldsymbol{\theta}_K^1)) \text{ and } Y_2(\mathbf{s}) \sim GP(\mathbf{0}, K(\cdot, \boldsymbol{\theta}_K^2))$$

independently. Without loss of generality, consider the finite difference differential process,

$$\mathcal{L}_{\mathbf{e}_1, \mathbf{e}_2, h} Y_1(\mathbf{s}) = \mathbf{A}_h \mathbf{L}_h^1(\mathbf{s}) = \begin{pmatrix} 1 & 0 & 0 & 0 & 0 & 0 \\ -\frac{1}{h} & \frac{1}{h} & 0 & 0 & 0 & 0 \\ -\frac{1}{h} & 0 & \frac{1}{h} & 0 & 0 & 0 \\ \frac{1}{h^2} & -\frac{2}{h^2} & 0 & \frac{1}{h^2} & 0 & 0 \\ \frac{1}{h^2} & -\frac{1}{h^2} & -\frac{1}{h^2} & 0 & \frac{1}{h^2} & 0 \\ \frac{1}{h^2} & 0 & -\frac{2}{h^2} & 0 & 0 & \frac{1}{h^2} \end{pmatrix} \begin{pmatrix} Y_1(\mathbf{s}) \\ Y_1(\mathbf{s} + h\mathbf{e}_1) \\ Y_1(\mathbf{s} + h\mathbf{e}_2) \\ Y_1(\mathbf{s} + 2h\mathbf{e}_1) \\ Y_1(\mathbf{s} + h(\mathbf{e}_1 + \mathbf{e}_2)) \\ Y_1(\mathbf{s} + 2h\mathbf{e}_2) \end{pmatrix},$$

noting that for every $h > 0$, $\mathbf{L}_h^1(\mathbf{s})$ follows a 6-dimensional normal distribution and $|\mathbf{A}_h| = h^{-8} \neq 0$, making the above linear transformation non-singular. We know from properties of multivariate normal distributions that $\mathcal{L}_{\mathbf{e}_1, \mathbf{e}_2, h} Y_1(\mathbf{s}) \sim \mathcal{N}_5(\mathbf{A}_h \mathbf{0}, \mathbf{A}_h \mathbf{K}_h(\mathbf{0}, \boldsymbol{\theta}_K^1) \mathbf{A}_h^\top)$, where $\mathbf{K}_h(\mathbf{0}, \boldsymbol{\theta}_K^1) = \text{Var}(\mathbf{L}_h^1(\mathbf{s}))$, the cross-covariance matrix for the process $\mathcal{L}_{\mathbf{e}_1, \mathbf{e}_2, h} Y_1(\mathbf{s})$ is $\mathbf{A}_h \mathcal{K}_{h,k}(\Delta) \mathbf{A}_k^\top$, where $\mathcal{K}_{h,k}(\Delta) = \text{Cov}(\mathbf{L}_h^1(\mathbf{s}), \mathbf{L}_k^1(\mathbf{s}'))$, with $\Delta = \mathbf{s} - \mathbf{s}'$. As $h \rightarrow 0$, $\mathbf{A}_h \mathbf{K}_h(\mathbf{0}, \boldsymbol{\theta}_K^1) \mathbf{A}_h^\top \rightarrow V_{\mathcal{L}Y_1}(\mathbf{0})$ and $\mathcal{L}_{\mathbf{e}_1, \mathbf{e}_2, h} Y_1(\mathbf{s}) \xrightarrow{d} \mathcal{L}Y_1(\mathbf{s}) \sim \mathcal{N}_5(\mathbf{0}, V_{\mathcal{L}Y_1}(\mathbf{0}))$, where \xrightarrow{d} indicates convergence in distribution. As $h, k \downarrow 0$ $\mathbf{A}_h \mathcal{K}_{h,k}(\Delta) \mathbf{A}_k^\top \rightarrow V_{\mathcal{L}Y_1}(\Delta)$, implying that $\mathcal{L}Y_1(\mathbf{s}) \sim GP(\mathbf{0}, V_{\mathcal{L}Y_1}(\cdot, \boldsymbol{\theta}_K^1))$. The same arguments can be followed for showing $\mathcal{L}Y_2(\mathbf{s}) \sim GP(\mathbf{0}, V_{\mathcal{L}Y_2}(\cdot, \boldsymbol{\theta}_K^2))$.

1. for (a) consider the associated finite difference operators, $\mathcal{L}_{\mathbf{e}_1, \mathbf{e}_2, h} Y_1(\mathbf{s}) = \mathbf{A}_h \mathbf{L}_h^1(\mathbf{s})$ and $\mathcal{L}_{\mathbf{e}_1, \mathbf{e}_2, h} Y_2(\mathbf{s}) = \mathbf{A}_h \mathbf{L}_h^2(\mathbf{s})$. We note that for every $h > 0$, $\text{Cov}(\mathbf{L}_h^1(\mathbf{s}), \mathbf{L}_h^2(\mathbf{s})) = \mathbf{0}$,

which is the zero matrix (of order 6×6). Now consider the process,

$$\begin{aligned}\mathcal{L}_h^{1,2} &= (\mathcal{L}_{\mathbf{e}_1, \mathbf{e}_{2,h}} Y_1(\mathbf{s})^\top, \mathcal{L}_{\mathbf{e}_1, \mathbf{e}_{2,h}} Y_2(\mathbf{s})^\top)^\top = \mathbf{A}_h \oplus \mathbf{A}_h (\mathbf{L}_h^1(\mathbf{s})^\top, \mathbf{L}_h^2(\mathbf{s})^\top)^\top \\ \mathcal{L}_h^{1,2} &\sim \mathcal{N}_{12}(\mathbf{0}, (\mathbf{A}_h \oplus \mathbf{A}_h)(\mathbf{K}_h(\cdot, \boldsymbol{\theta}_K^1) \oplus \mathbf{K}_h(\cdot, \boldsymbol{\theta}_K^2))(\mathbf{A}_h \oplus \mathbf{A}_h)^\top)\end{aligned}$$

as $h \downarrow 0$, $\mathcal{L}_h^{1,2} \xrightarrow{d} (\mathcal{L}Y_1^\top, \mathcal{L}Y_2^\top)^\top \sim \mathcal{N}_{12}(\mathbf{0}, V_{\mathcal{L}Y_1}(\mathbf{0}) \oplus V_{\mathcal{L}Y_2}(\mathbf{0}))$ which implies $Cov(\mathcal{L}Y_1, \mathcal{L}Y_2) = \mathbf{0}$, and since they jointly follow a multivariate Gaussian this implies that they are independent. Observing that the cross covariance for all $h, k \downarrow 0$, $Cov(\mathbf{L}_h^1(\mathbf{s}), \mathbf{L}_k^2(\mathbf{s}')) = \mathbf{0}$, we can establish that they are independent Gaussian processes.

2. (b) and (c) follow from standard properties of the Gaussian processes.

For the discussion on page 14 preceding (14) we suppress dependence on \mathbf{s} and Y , we denote $g(t) = g(\mathcal{L}Y(\mathbf{s}(t)))$. By definition of the integral, given $\epsilon > 0$, there exists a $\delta_0 > 0$ such that if $|P| < \delta_0$, then

$$\left| \int_a^b g(t) \|\mathbf{s}'(t)\| dt - \sum_{i=1}^{n_P} (t'_i - t'_{i-1}) g(t'_i) \|\mathbf{s}'(t'_i)\| \right| < \frac{\epsilon}{2}, \quad (15)$$

where $\sum_{i=1}^{n_P} (t'_i - t'_{i-1}) g(t'_i) \|\mathbf{s}'(t'_i)\|$ is a *Riemann sum approximation* of the integral. On the other hand, since $g(t)$ is uniformly continuous over $[a, b]$, given $\epsilon > 0$, there exists $\delta_1 > 0$ such that if $x, y \in [a, b]$ with $|x - y| < \delta_1$,

$$|g(x) \|\mathbf{s}'(x)\| - g(y) \|\mathbf{s}'(y)\|| < \frac{\epsilon}{2(b-a)}$$

Set $\delta = \min\{\delta_0, \delta_1\}$, then $|P| < \delta$, using the mean value theorem we obtain,

$$\begin{aligned} & \left| \sum_{i=1}^{n_P} \int_{C_{t_i}} g(t) \|\mathbf{s}'(t)\| dt - \sum_{i=1}^{n_P} (t'_i - t'_{i-1}) g(t'_i) \|\mathbf{s}'(t'_i)\| \right| \\ & \leq \left| \sum_{i=1}^{n_P} (t'_i - t'_{i-1}) \sup g(t) \|\mathbf{s}'(t)\| - \sum_{i=1}^{n_P} (t'_i - t'_{i-1}) g(t'_i) \|\mathbf{s}'(t'_i)\| \right| \\ & \leq \left| \sum_{i=1}^{n_P} (t'_i - t'_{i-1}) \sup |g(t) \|\mathbf{s}'(t)\| - g(t') \|\mathbf{s}'(t')\|| \right| \leq \frac{\epsilon}{2}, \end{aligned}$$

where the first inequality follows from the assumption of C being regular. Together with the inequality in (15) we have,

$$\left| \int_a^b g(t) \|\mathbf{s}'(t)\| dt - \sum_{i=1}^{n_P} \int_{C_{t_i}} g(t) \|\mathbf{s}'(t)\| dt \right| < \epsilon.$$

Finally, almost sure convergence yields for every $\epsilon > 0$,

$$P \left[\left| \int_a^b g(t) \|\mathbf{s}'(t)\| dt - \sum_{i=1}^{n_P} \int_{C_{t_i}} g(t) \|\mathbf{s}'(t)\| dt \right| < \epsilon \right] = 1.$$

Considering a sequence of $\epsilon \downarrow 0$, and using the preceding arguments for each ϵ we can find $\delta \downarrow 0$ such that $|P| < \delta$ which concludes the proof.

13 Tables

Table 6: Table showing results for goodness of fit from the first synthetic experiment where the true response is generated from $y \sim N(10[\sin(3\pi s_1) + \cos(3\pi s_2)], 1)$.

Sample Size	Parameter	Estimate	RMSE					
			Y	$\nabla_1 Y$	$\nabla_2 Y$	$\nabla_{11}^2 Y$	$\nabla_{12}^2 Y$	$\nabla_{22}^2 Y$
$L = 100$	ϕ	2.91 (2.13, 3.81)						
	σ^2	218.35 (69.69, 588.86)	0.05 (0.00)	9.74 (0.23)	9.86 (0.31)	150.82 (4.94)	91.49 (1.94)	180.38 (2.10)
	τ^2 (Truth = 1.00)	0.96 (0.63, 1.39)						
	β_0	0.00 (-0.06, 0.06)						
$L = 500$	ϕ	2.30 (1.88, 2.73)						
	σ^2	367.17 (166.27, 784.53)	0.04 (0.00)	6.66 (0.10)	6.84 (0.12)	127.99 (3.40)	68.11 (2.56)	126.71 (2.69)
	τ^2 (Truth = 1.00)	0.99 (0.86, 1.13)						
	β_0	0.00 (-0.06, 0.06)						
$L = 1000$	ϕ	2.00 (1.60, 2.36)						
	σ^2	553.79 (231.95, 1385.62)	0.03 (0.00)	5.64 (0.18)	6.45 (0.19)	97.16 (2.05)	61.54 (2.27)	114.97 (2.22)
	τ^2 (Truth = 1.00)	1.04 (0.95, 1.14)						
	β_0	0.00 (-0.06, 0.06)						

Table 7: Table showing results for goodness of fit from the second synthetic experiment where the true response is generated from $y \sim N(10[\sin(3\pi s_1) \cdot \cos(3\pi s_2)], 1)$.

Sample Size	Parameter	Estimate	RMSE					
			Y	$\nabla_1 Y$	$\nabla_2 Y$	$\nabla_{11}^2 Y$	$\nabla_{12}^2 Y$	$\nabla_{22}^2 Y$
$L = 100$	ϕ	5.06 (3.69, 6.72)						
	σ^2	38.96 (15.52, 85.33)	0.06 (0.00)	16.12 (0.13)	11.49 (0.22)	258.91 (3.16)	159.54 (1.19)	183.54 (3.70)
	τ^2 (Truth = 1.00)	0.83 (0.53, 1.23)						
	β_0	-3.12 (-0.34, 5.04)						
$L = 500$	ϕ	3.63 (3.05, 4.38)						
	σ^2	114.36 (44.59, 211.47)	0.04 (0.00)	7.04 (0.17)	7.39 (0.17)	179.23 (6.94)	98.39 (3.76)	169.19 (5.16)
	τ^2 (Truth = 1.00)	0.93 (0.80, 1.07)						
	β_0	-0.15 (-2.14, 2.49)						
$L = 1000$	ϕ	2.89 (2.55, 3.26)						
	σ^2	173.19 (94.06, 297.76)	0.03 (0.00)	6.19 (0.26)	6.21 (0.17)	167.27 (10.40)	93.21 (6.75)	163.44 (8.84)
	τ^2 (Truth = 1.00)	1.01 (0.91, 1.10)						
	β_0	-0.22 (-2.03, 2.15)						

14 Plots

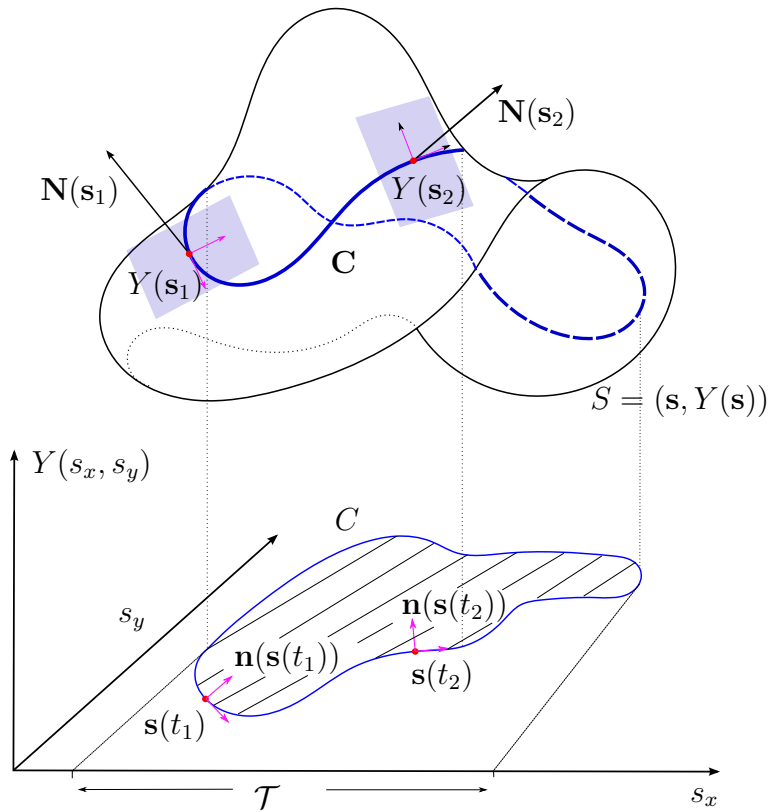


Figure 9: Illustration showing geometric interpretation of curvilinear wobbling. Local tangent planes are shaded around points $\mathbf{s}_1, \mathbf{s}_2$. Normals to the surface are marked as $\mathbf{N}(\mathbf{s}_1)$ and $\mathbf{N}(\mathbf{s}_2)$, locally projected principal unit normals to the projected curve C are marked as $\mathbf{n}(\mathbf{s}(t_1))$ and $\mathbf{n}(\mathbf{s}(t_2))$ respectively. The tangent vectors spanning the local tangent planes are shown with arrows.

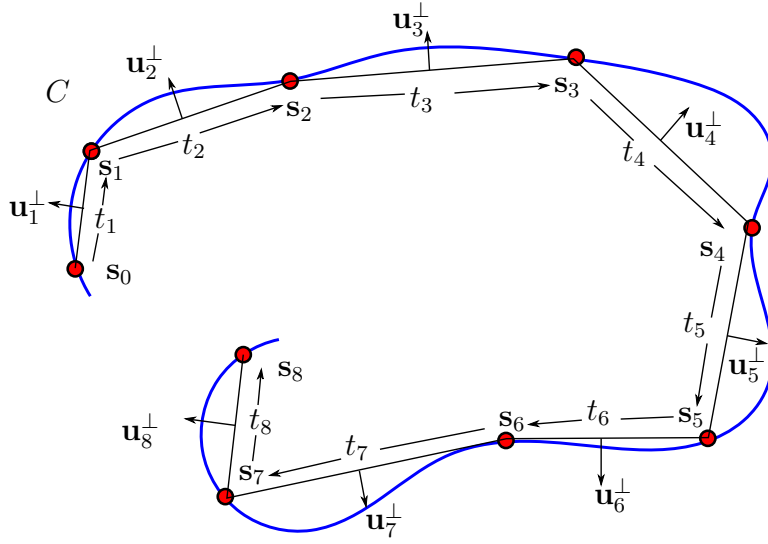


Figure 10: Illustration of rectilinear wombling, showing a curve C , an initial starting point s_0 on the curve, with following points, $\{s_1, s_2, \dots, s_8\}$ corresponding a partition \mathcal{T} , of the parameterized curve. Each linear segment consists of a norm-direction pair (t, \mathbf{u}) , where t specifies the length of the segment and \mathbf{u} the direction of movement. The normal direction for each segment is indicated as \mathbf{u}^\perp .

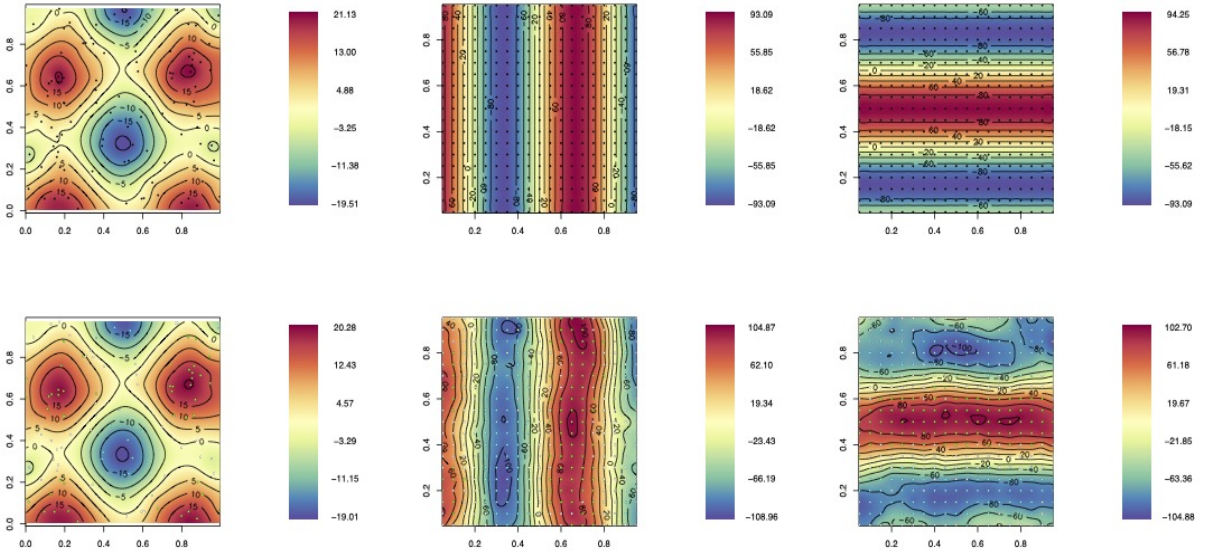


Figure 11: Plots showing the true surfaces for the (a) process, (b) gradients along x -axis, (c) gradients along y -axis, and estimated surfaces for the (d) process, gradients (e), (f) w.r.t. synthetic response generated, $y \sim N(10[\sin(3\pi s_1) + \cos(3\pi s_2)], 1)$

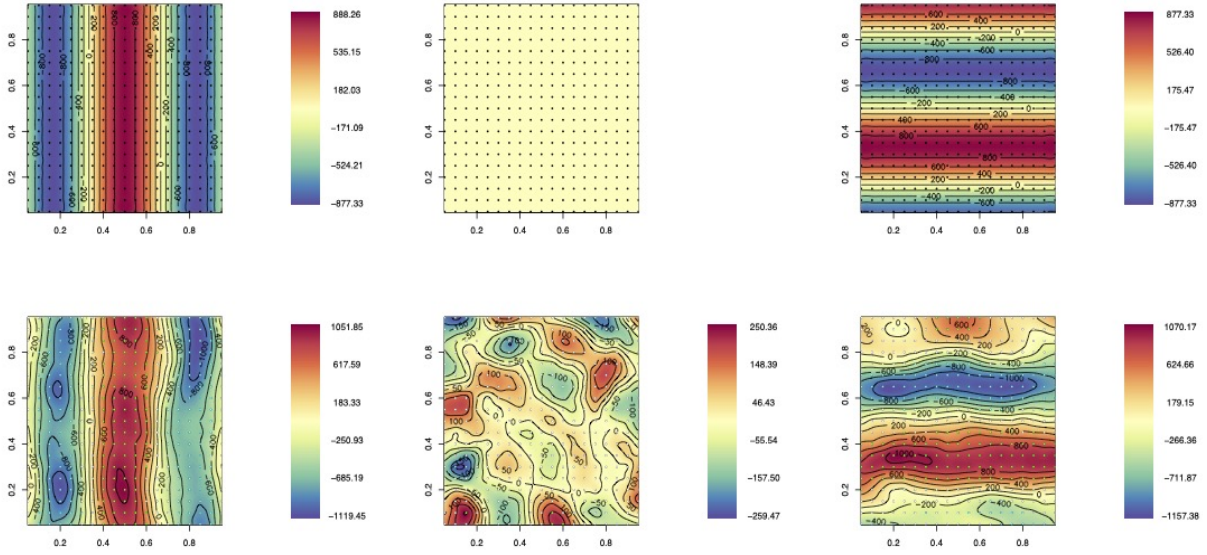


Figure 12: Plots showing the true surfaces for the (a) curvature along x -axis, (b) curvature along x - y -axis, (c) curvature along y -axis, and estimated surfaces for (d) curvature along x -axis, (e) mixed curvature along x - y -axis, (f) curvature along y -axis, for synthetic response generated from, $y \sim N(10[\sin(3\pi s_1) + \cos(3\pi s_2)], 1)$.

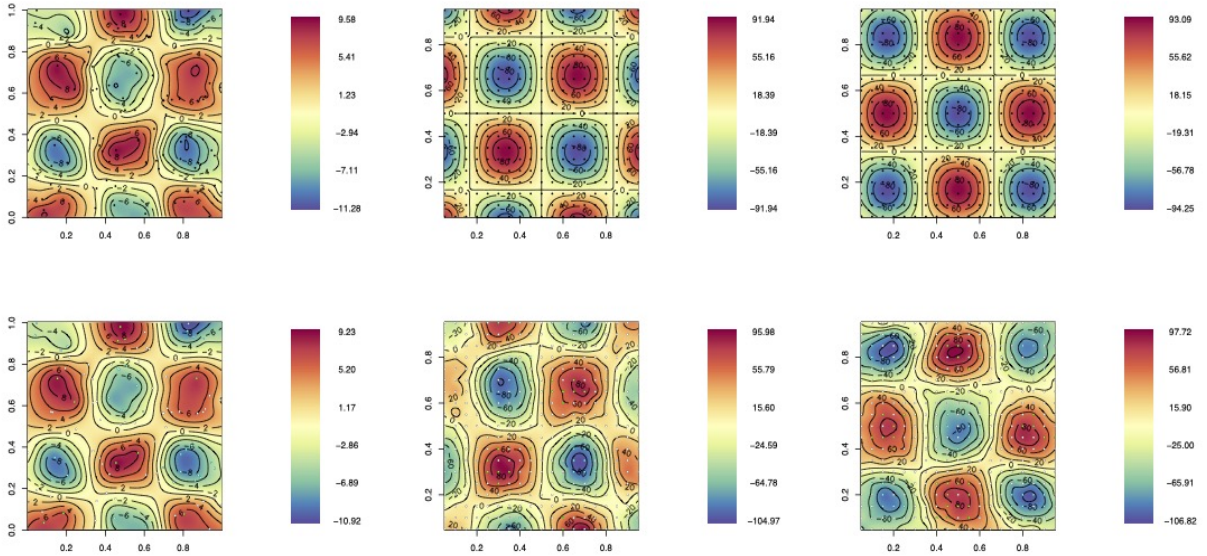


Figure 13: Plots showing the true surfaces for the (a) process, (b) gradients along x -axis, (c) gradients along y -axis, and estimated surfaces for the (d) process, gradients (e), (f) for synthetic response generated from, $y \sim N(10[\sin(3\pi s_1) \cdot \cos(3\pi s_2)], 1)$.

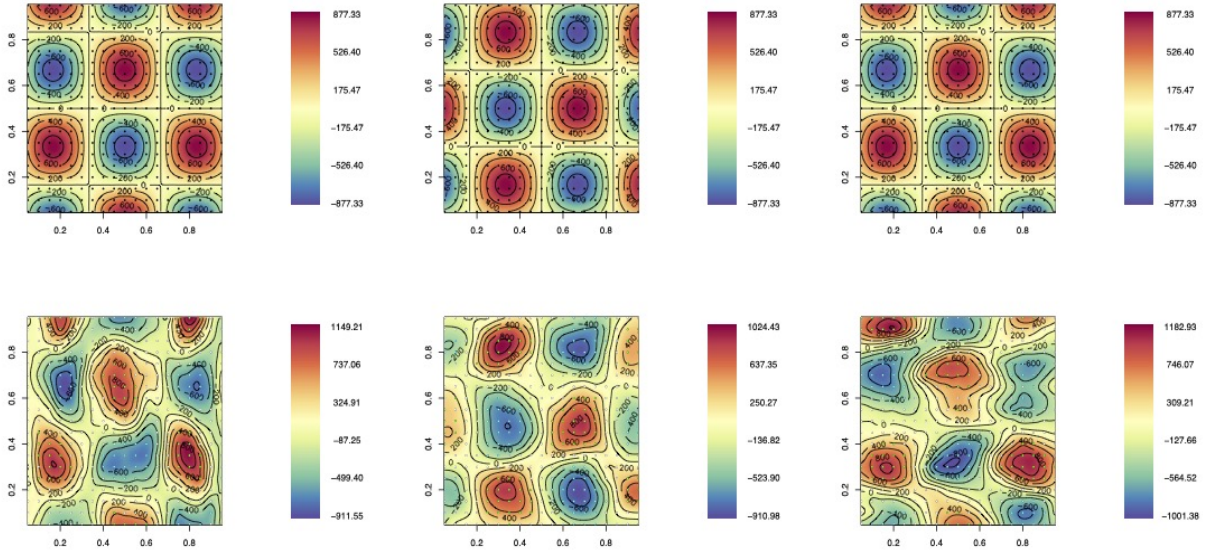


Figure 14: Plots showing the true surfaces for the (a) curvature along x -axis, (b) curvature along x - y -axis, (c) curvature along y -axis, and estimated surfaces for (d) curvature along x -axis, (e) mixed curvature along x - y -axis, (f) curvature along y -axis, for synthetic response generated from, $y \sim N(10[\sin(3\pi s_1) \cdot \cos(3\pi s_2)], 1)$.

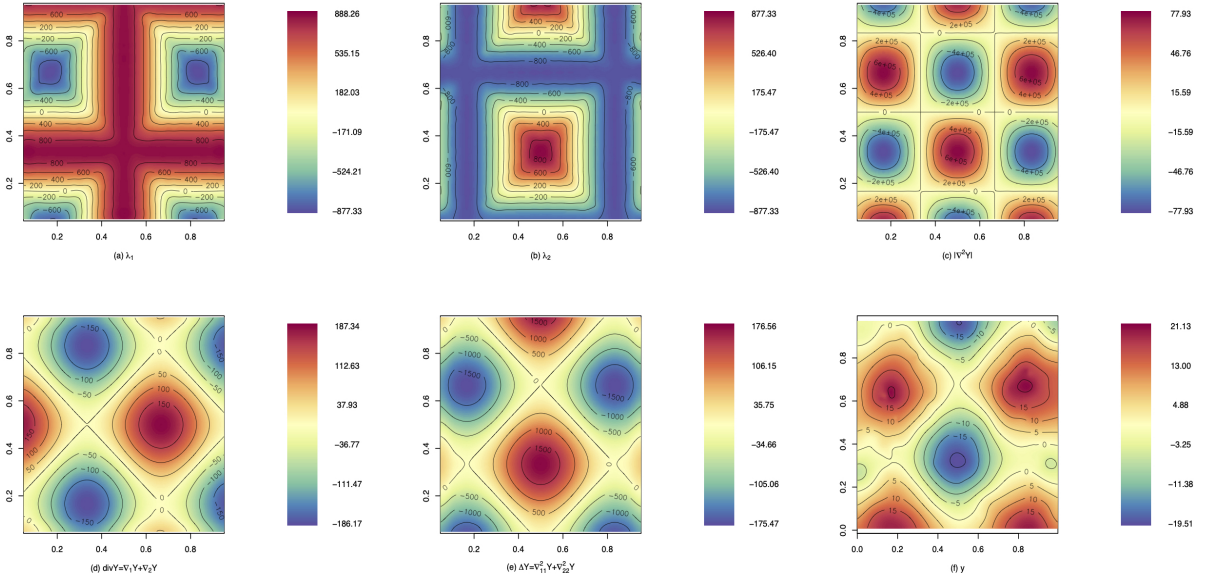


Figure 15: Plots showing the true surfaces for (a) eigen value, λ_1 (b) eigen value λ_2 , (c) Gaussian curvature (scales in $\times 10^4$) (d) divergence (e) Laplacian (scales in $\times 10^1$) over grid points, and (f) fitted process. This is shown for synthetic response generated from, $y \sim N(10[\sin(3\pi s_1) + \cos(3\pi s_2)], 1)$.

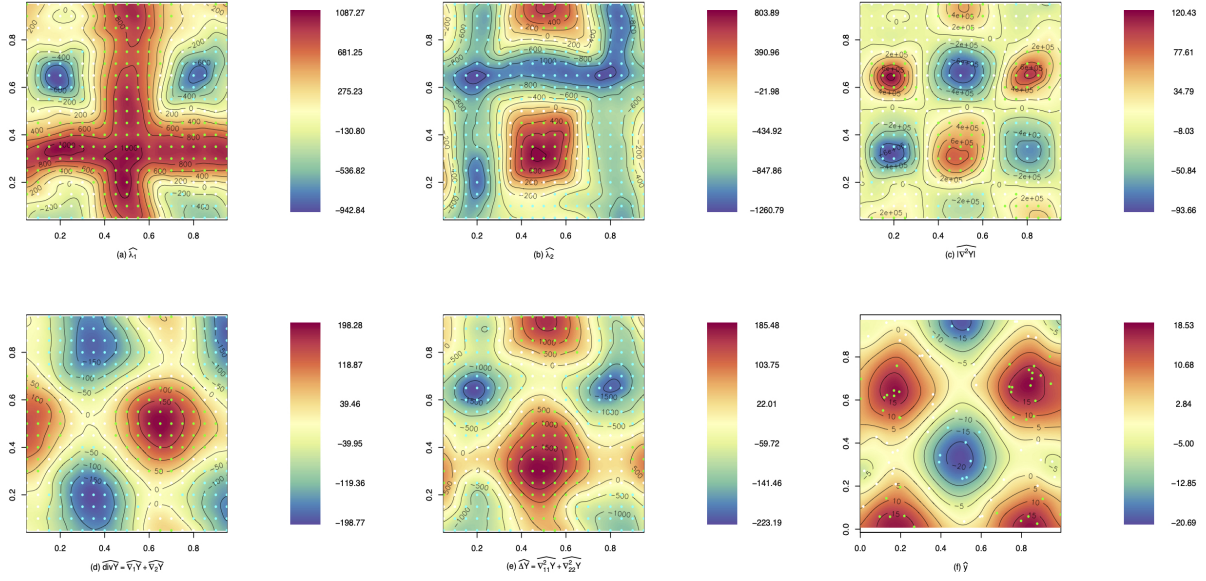


Figure 16: Plots showing the estimated surfaces for (a) eigen value, λ_1 (b) eigen value λ_2 , (c) Gaussian curvature (scales in $\times 10^4$) (d) divergence (e) Laplacian (scales in $\times 10^1$) (f) fitted process over grid points. Each point is color coded; **green** denoting the HPD intervals not containing 0, with positive end points, while **cyan** denotes HPD intervals not containing 0, with negative end points.

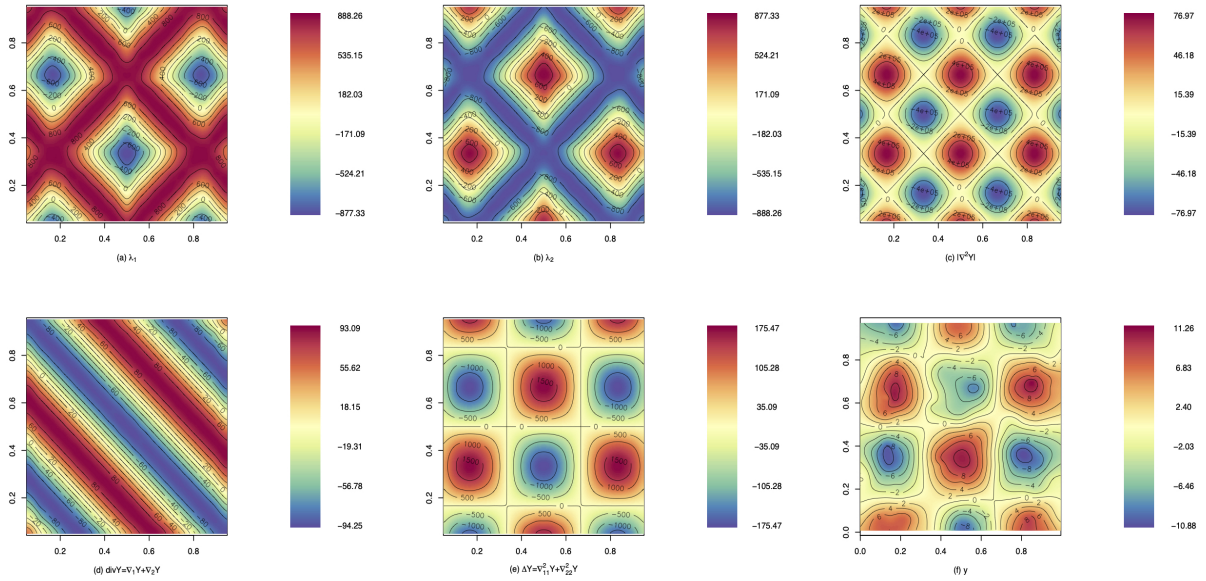


Figure 17: Plots showing the true surfaces for (a) eigen value, λ_1 (b) eigen value λ_2 , (c) Gaussian curvature (scales in $\times 10^4$) (d) divergence (e) Laplacian (scales in $\times 10^1$) (f) fitted process over grid points. This is shown for synthetic response generated from, $y \sim N(10[\sin(3\pi s_1) \cdot \cos(3\pi s_2)], 1)$

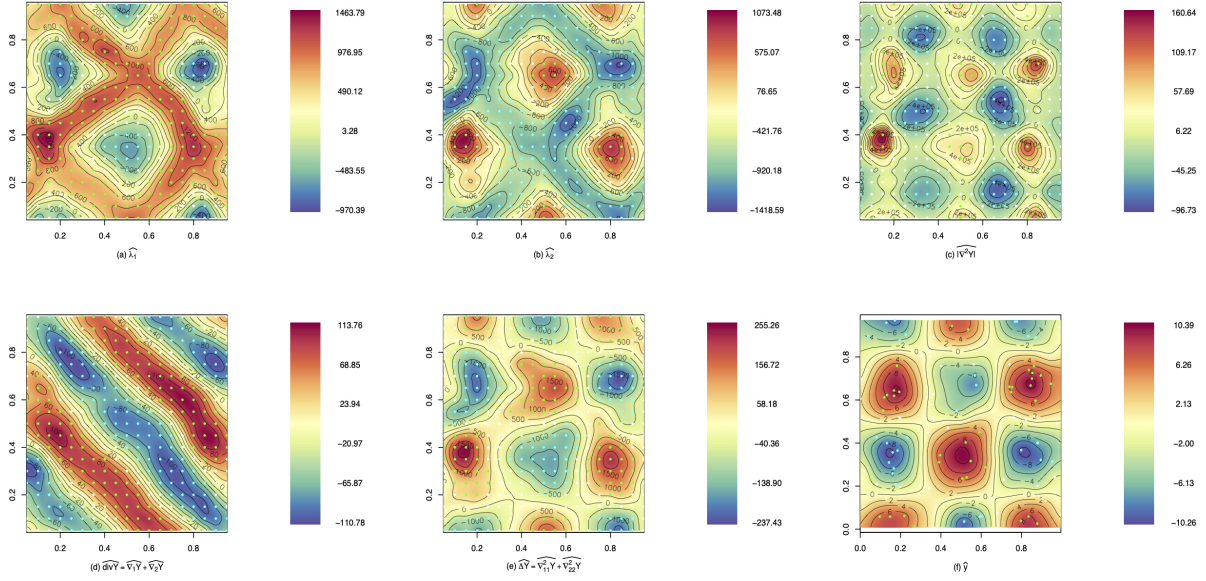


Figure 18: Plots showing the estimated surfaces for (a) eigen value, λ_1 (b) eigen value λ_2 , (c) Gaussian curvature (scales in $\times 10^4$) (d) divergence (e) Laplacian (scales in $\times 10^1$) (f) fitted process over grid points. Each point is color coded; **green** denoting the HPD intervals not containing 0, with positive end points, while **cyan** denotes HPD intervals not containing 0, with negative end points.

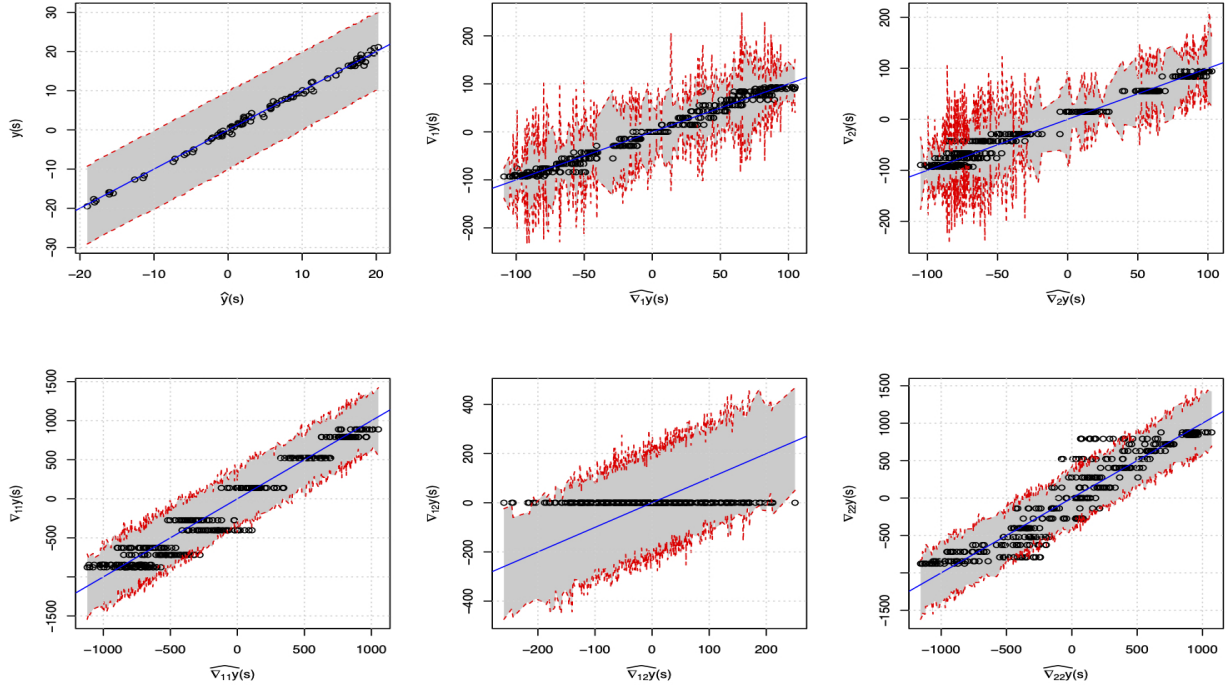


Figure 19: Plots showing observed versus fitted values for (a) the response variable $Y(s)$; (b) gradients with respect to x -axis; (c) gradients with respect to y -axis; (d) curvature with respect to x -axis; (e) mixed curvature over x - y ; (f) curvature for $y \sim N(10[\sin(3\pi s_1) + \cos(3\pi s_2)], 1)$ with respect to y -axis. The gray shades represent the 95% HPD regions for each estimate.

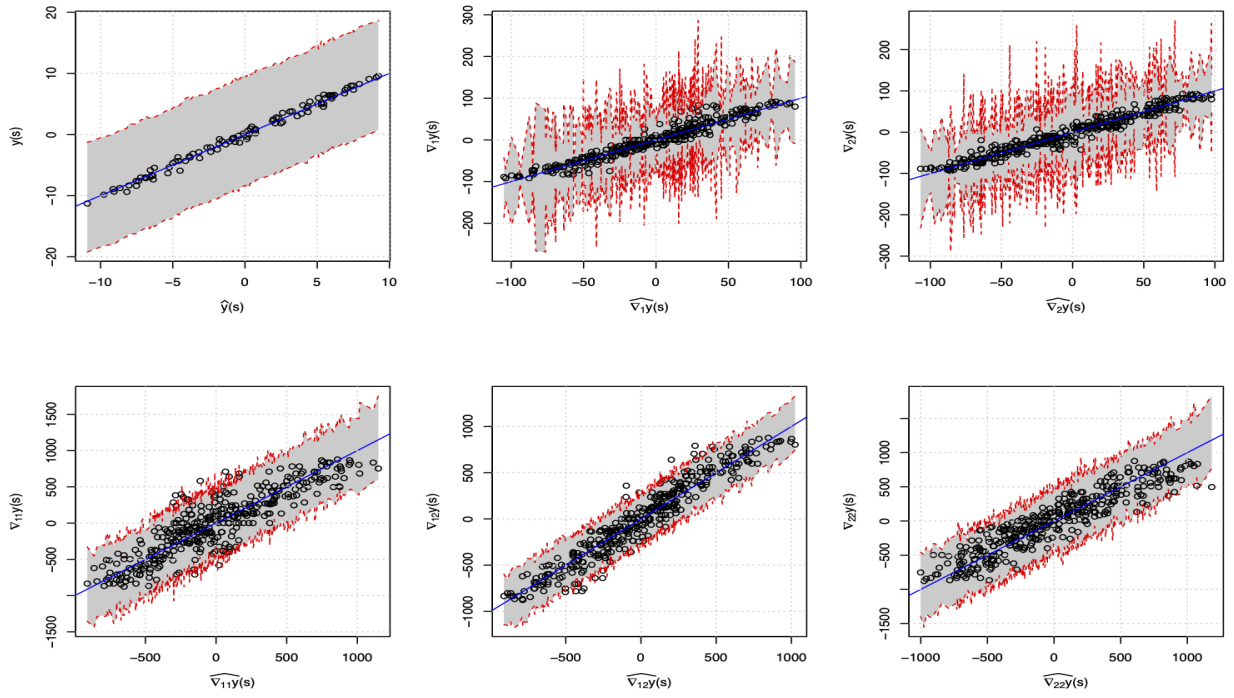


Figure 20: Plots showing observed versus fitted values for (a) the response variable $Y(s)$; (b) gradients with respect to x -axis; (c) gradients with respect to y -axis; (d) curvature with respect to x -axis; (e) mixed curvature over x - y ; (f) curvature for $y \sim N(10[\sin(3\pi s_1) \cdot \cos(3\pi s_2)], 1)$ with respect to y -axis. The gray shades represent the 95% HPD regions for each estimate.

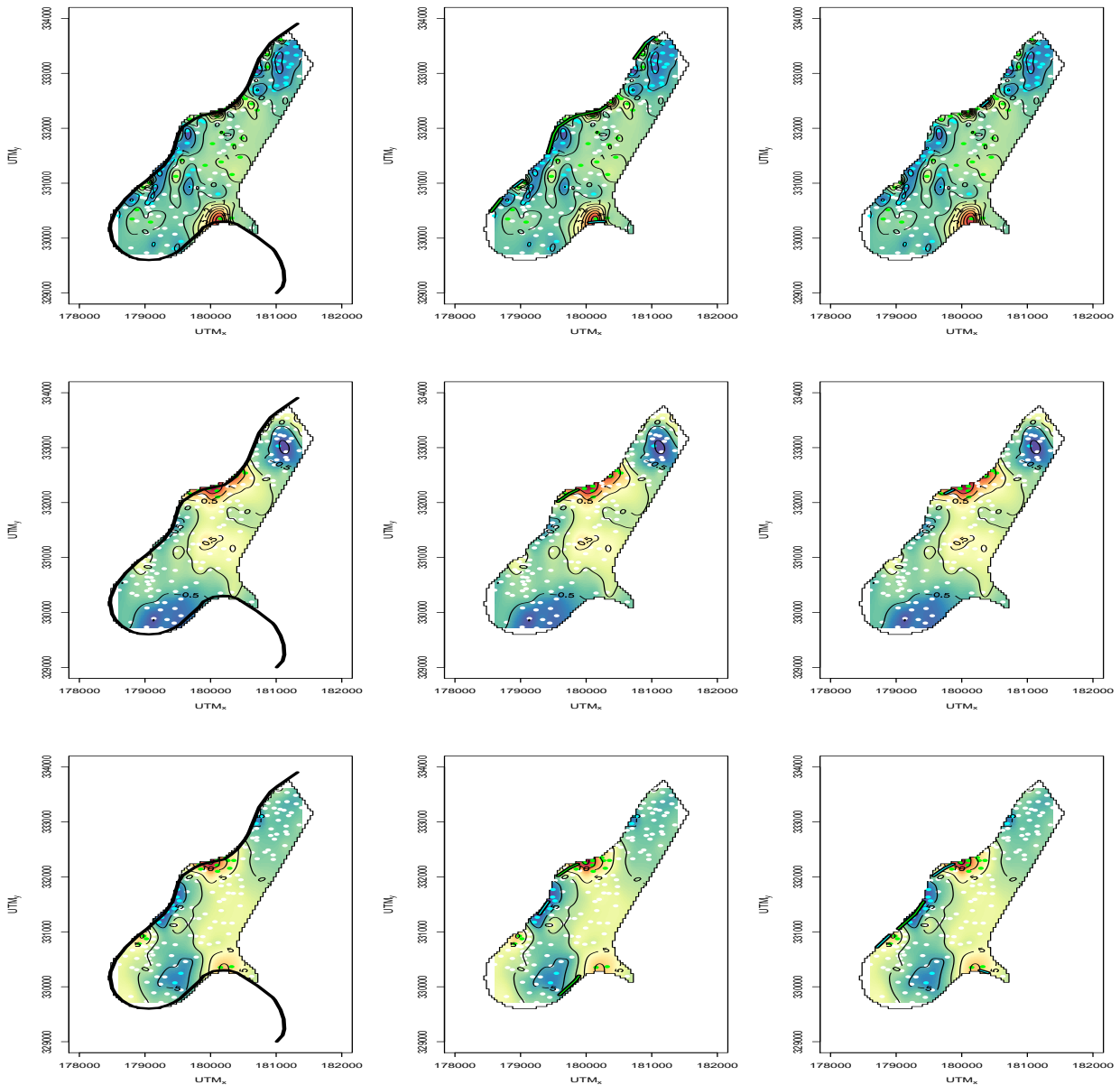


Figure 21: Plots showing results for curvature wombling on the Meuse river (first row) Copper (Cu) (second row) Lead (Pb) (third row) Zinc (Zn).

15 Further Application

15.1 Temperatures in Northeastern US

Temperatures are historically known to exhibit spatial variation. We focus on a data set that records monthly temperatures across weather monitoring stations in the Northeastern United States during January, 2000 from the R-package `spBayes` (Finley et al. 2007). Temperature

gradients and curvature are of interest from an environmental science perspective to track and perform boundary analysis on zones that exhibit significant changes in the surface during a month. Curvature wobbling performed on temperature reveals climate zones featuring rapid atmospheric changes. Quantifying such variations in atmospheric conditions is central to statistical modeling in environmental applications. The data consists of temperatures (in degree Celsius) from 356 weather monitoring stations. The probability distribution for temperatures and interpolated spatial plot is shown in Figure 22. We model the data using the hierarchical model outlined in (13) in the manuscript. We used the following hyper parameters for the model, $\phi \sim \text{Unif}\left(\frac{3}{\max_{s \in S} \|\Delta\|}, 300\right)$, $\sigma^2 \sim \text{IG}(2, 1)$ (mean 1 variance infinite), $\tau^2 \sim \text{IG}(2, 1)$ (mean 1 variance infinite), $\beta_0 \sim N(0, 10^6)$, and $\nu = 5/2$ for the Matérn kernel. We consider 10^4 iterations for MCMC chains, with burn-in diagnosed at 5×10^3 . The posterior estimates from the model fit are shown in Table 8.

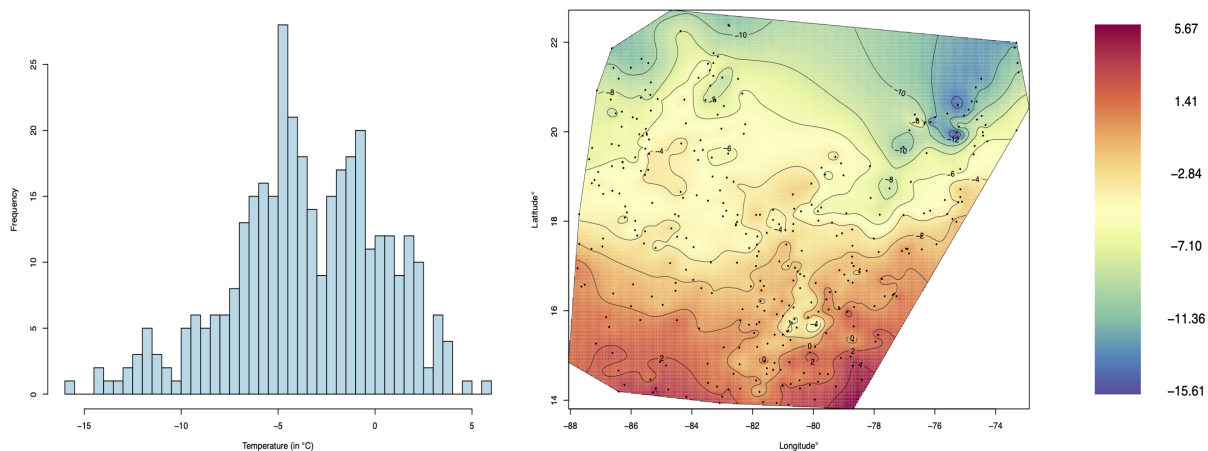


Figure 22: Plots showing (left) probability density of temperatures (in °C) (right) spatial plot of temperatures in Northeastern US during January 2000.

We fit the model with only an intercept, that allows the spatial process $Z(\mathbf{s})$ to capture most of the variation in the data. We observe from Table 8 that $\sigma^2/(\sigma^2 + \tau^2) \approx 95.86\%$. Significance in process parameter estimates is assessed by checking containment of 0 within the HPD intervals. The fitted spatial process, along with significance is shown in Figure 23 (top row, left). For temperature observations falling in the middle no significant spatial effect

is observed, with stations located in the northern and southern regions showing positive and negative spatial effects. This indicates a clear variation in the north-south direction for temperatures in January. The variance of the nugget process τ^2 is small compared to σ^2 . The average estimated temperature is -3.78 °C ($-5.92, -1.69$). Using the posterior estimates

Table 8: Posterior Estimates for Temperatures in Northeastern US. The highest posterior density intervals are shown alongside for respective estimates.

Parameters (θ)	Posterior Estimates ($\hat{\theta}$)	Highest Posterior Density intervals (HPD)
ϕ	0.38	(0.27, 0.51)
σ^2	21.44	(10.11, 41.03)
τ^2	0.92	(0.76, 1.10)
β_0	-3.78	(-5.92, -1.69)

for θ and the spatial process \mathbf{Z} we perform a gradient and curvature assessment over the estimated posterior surface. We use Algorithm 1 outlined in section 11 for sampling gradients and curvature. This is done over a grid encompassing the spatial domain of reference, \mathcal{S} . A grid $\mathcal{G} = \{\mathbf{s}_g : \mathbf{s}_g \in \text{convex-hull}(\mathcal{S})\}$ consisting of 461 points is laid out over the convex-hull of \mathcal{S} . The estimated gradients along x and y -axis are shown in the first row for Figure 23. Elements of the directional curvature process along x and y -axis are shown in the second row. Significance is again indicated by checking containment of 0 within HPD intervals for posterior gradients and curvature. Significant directional curvature is indicative of significant rate of change in temperature gradients along the chosen axis. ∇_{xy}^2 quantifies *interaction* between rates of change in gradients along x and y axis respectively. A significant $\nabla_{xy}^2(\mathbf{s}_g)$ at the grid location \mathbf{s}_g indicates that the rate of change with respect to axis x was significantly influenced by change along y -axis. Regions of local maxima (elliptic points) generally manifest themselves with alternating zones of increasing and decreasing gradients (or curvature) separated by a zone of saddle points (around the location of said maxima). This can be witnessed in the north-eastern region and south-eastern regions where these maxima (minima) occur.

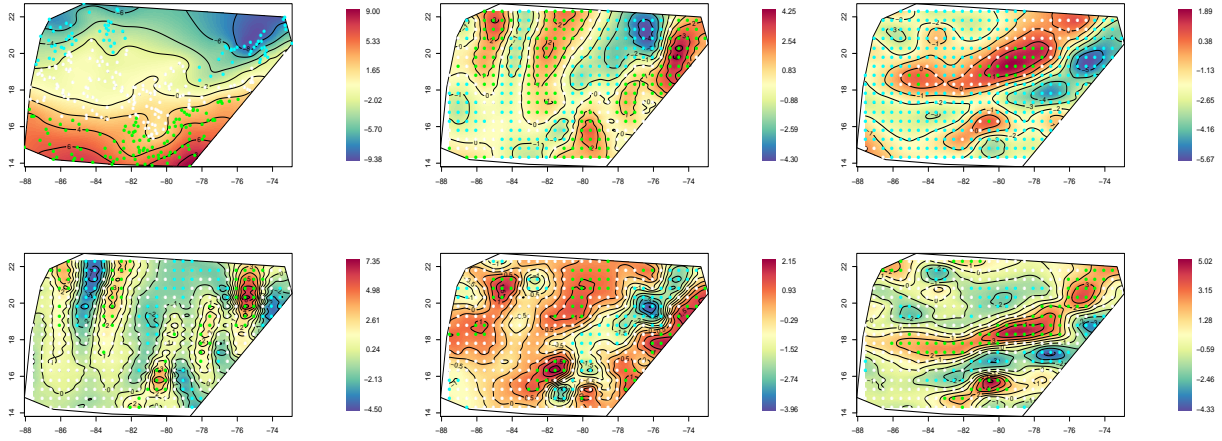


Figure 23: Plots showing (top row) (left) the fitted spatial process (center) the estimated gradient, ∇_x process along x -axis (right) the estimated gradient, ∇_y process along y -axis (bottom row) (left) estimated curvature ∇_{xx}^2 along x -axis (center) estimated curvature, ∇_{xy}^2 (right) estimated curvature, ∇_{yy}^2 along y -axis.

Posterior surface is effected on the same grid \mathcal{G} using the posterior estimates for ∇_{xx}^2 , ∇_{xy}^2 and ∇_{yy}^2 . We leverage these to produce estimated surfaces for the Gaussian curvature (determinant) (shown in left of Figure 24), the divergence operator (shown in center of Figure 24) and Laplacian (shown in right of Figure 24). Posterior surfaces for the Gaussian curvature are indicative of locations/presence of maximas and saddle points, divergence surfaces show regions of rapid change in temperatures while the Laplacian shows regions of maximum change in gradients. Gaussian calibration for these estimate attaches significance allowing us to distinguish between contiguous zones housing significant change.

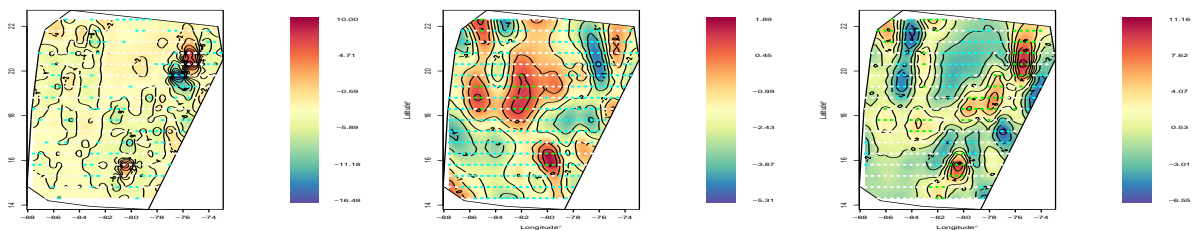


Figure 24: Plots showing surfaces for (left) Gaussian curvature (center) divergence and (right) Laplacian of temperatures in Northeastern US during January 2000.

We perform curvature wombling using inference obtained from the posterior analysis of the surface. Figure 25 and Table 9 show the results for curvilinear wombling on the

Table 9: Curvilinear Wombling measures for boundaries in Northeastern US Temperatures, each measure is accompanied by its corresponding HPD interval in brackets below.

Curve (C)	Average Gradient ($\bar{\Gamma}^{(1)}(C)$)	Average Curvature ($\bar{\Gamma}^{(2)}(C)$)
Boundary 1	2.44 (1.90, 2.97)	-0.38 (-1.48, 0.74)
Boundary 2	2.70 (2.24, 3.18)	-0.40 (-1.67, 0.79)
Boundary 3	2.69 (2.10, 3.28)	-0.34 (-1.71, 0.84)
Boundary 4	2.23 (1.74, 2.72)	-0.31 (-1.67, 1.11)
Boundary 5.1	-2.96 (-4.22, -1.73)	1.13 (-0.88, 3.16)
Boundary 5.2	-3.24 (-4.22, -2.25)	-0.23 (-2.19, 1.69)
Boundary 6.1	1.63 (0.70, 2.58)	-0.23 (-2.96, 2.62)
Boundary 6.2	2.90 (1.93, 3.92)	-0.38 (-3.00, 2.31)

resulting posterior estimates of the surface. The curves chosen are shown in plots on the left for Figure 25. We begin with curves (level sets) “1” and “2” that delineate zones of significant (positive in the south and negative in the north) spatial effects, iteratively proceeding to higher (lower) level sets while inspecting them for curvilinear gradients and curvature. Referring to Table 9, we observe that all curves located with respect to curvilinear gradients, observed from significant average gradients. With respect to directional curvature, we refer to significant segments located in the Figure 25 which show enormous heterogeneity, i.e. changes in directional concavity when traversing the curve, with separated contiguous segments indicating significant changes in concavity. For instance traversing curve “2” in the west-east direction, we observe this clearly. This naturally renders the average directional curvature (shown in Table 9) insignificant when considered along the entirety of curve “2”, which is also the case for other level sets. To be able to detect significance we could only summarize across significant segments (as was done for the Meuse river data).

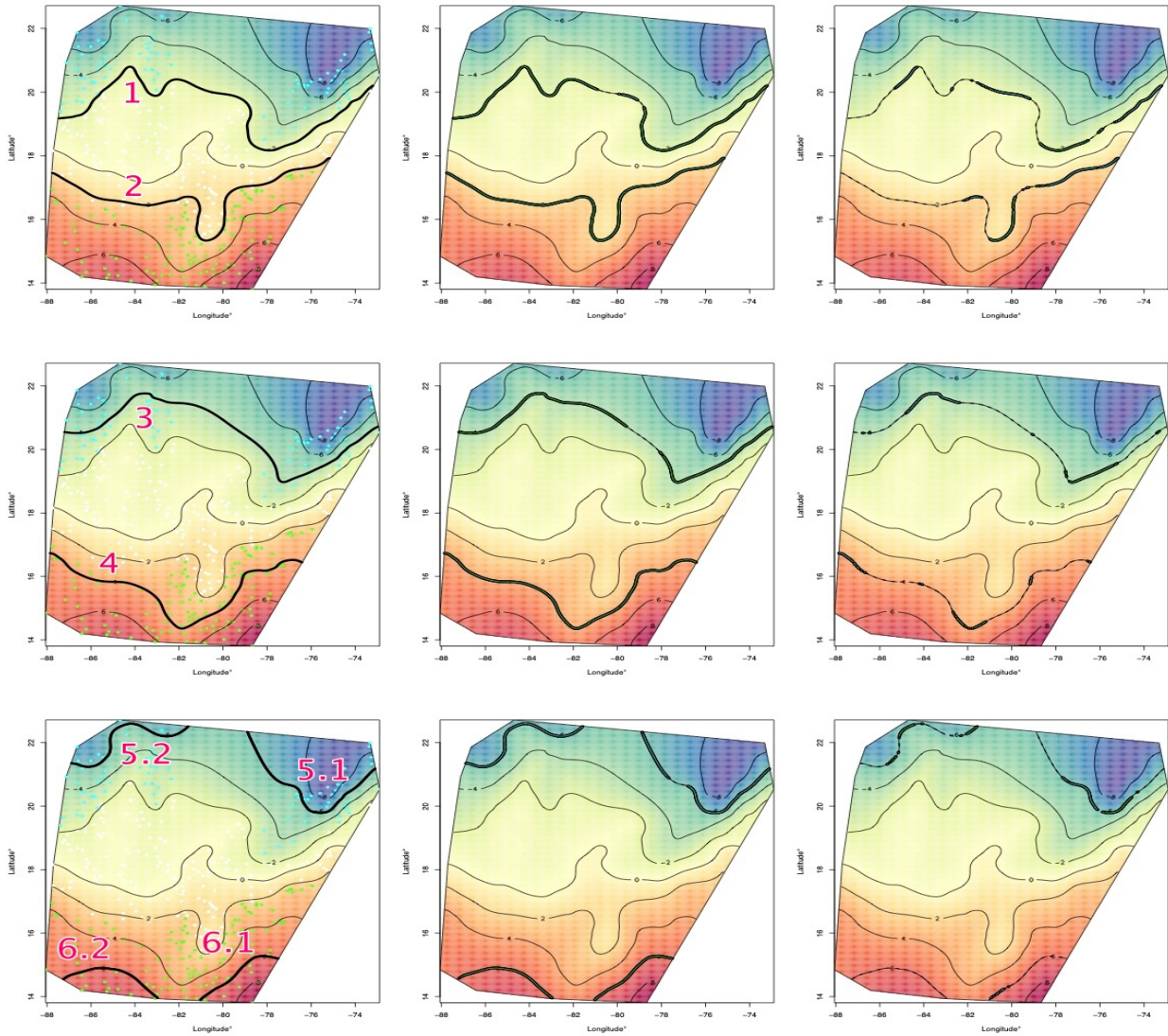


Figure 25: Plots showing curvature wombing on temperatures data. The curves are marked in each row on the figure to the left are to be referenced with Table 9 showing average wombing measures for gradient and curvature for respective curves.

References

- Abramowitz, M., Stegun, I. A. & Romer, R. H. (1988), 'Handbook Of Mathematical Functions With Formulas, Graphs, and Mathematical Tables'.
- Adler, R. J. (1981), *The Geometry Of Random Fields*, SIAM.
- Albering, H. J., Van Leusen, S. M., Moonen, E., Hoogewerff, J. A. & Kleinjans, J. (1999), 'Human Health Risk Assessment: A Case Study Involving Heavy Metal Soil Contamination After The Flooding Of The River Meuse During The Winter Of 1993-1994.', *Environmental Health Perspectives* **107**(1), 37–43.
- Banerjee, S., Carlin, B. P. & Gelfand, A. E. (2014), *Hierarchical Modeling And Analysis For Spatial Data*, CRC press.
- Banerjee, S. & Gelfand, A. (2003), 'On Smoothness Properties Of Spatial Processes', *Journal of Multivariate Analysis* **84**(1), 85–100.
- Banerjee, S. & Gelfand, A. E. (2006), 'Bayesian Wombling: Curvilinear Gradient Assessment Under Spatial Process Models', *Journal of the American Statistical Association* **101**(476), 1487–1501.
- Banerjee, S., Gelfand, A. E. & Sirmans, C. (2003), 'Directional Rates Of Change Under Spatial Process Models', *Journal of the American Statistical Association* **98**(464), 946–954.
- Burrough, P. A., McDonnell, R. A. & Lloyd, C. D. (2015), *Principles Of Geographical Information Systems*, Oxford University Press.
- Chen, M.-H. & Shao, Q.-M. (1999), 'Monte Carlo Estimation Of Bayesian Credible And HPD Intervals', *Journal of Computational and Graphical Statistics* **8**(1), 69–92.

- Chiu, S. N., Stoyan, D., Kendall, W. S. & Mecke, J. (2013), *Stochastic Geometry And Its Applications*, John Wiley & Sons.
- Do Carmo, M. P. (2016), *Differential Geometry Of Curves And Surfaces: Revised And Updated, Second Edition*, Courier Dover Publications.
- Dryden, I. L. & Mardia, K. V. (2016), *Statistical Shape Analysis: With Applications In R*, Vol. 995, John Wiley & Sons.
- Elliot, P., Wakefield, J. C., Best, N. G., Briggs, D. J. et al. (2000), *Spatial Epidemiology: Methods And Applications*, Oxford University Press.
- Finley, A. O., Banerjee, S. & Carlin, B. P. (2007), ‘spbayes: An R Package For Univariate And Multivariate Hierarchical Point-Referenced Spatial Models’, *Journal of statistical software* **19**(4), 1.
- Fitzpatrick, M. C., Preisser, E. L., Porter, A., Elkinton, J., Waller, L. A., Carlin, B. P. & Ellison, A. M. (2010), ‘Ecological Boundary Detection Using Bayesian Areal Wombling’, *Ecology* **91**(12), 3448–3455.
- Gallier, J. & Gallier, J. H. (2000), *Curves And Surfaces In Geometric Modeling: Theory And Algorithms*, Morgan Kaufmann.
- Gao, L., Banerjee, S. & Ritz, B. (2022), ‘Spatial Difference Boundary Detection for Multiple Outcomes Using Bayesian Disease Mapping’, *Biostatistics* . kxac013.
URL: <https://doi.org/10.1093/biostatistics/kxac013>
- Gauss, C. F. (1902), *General Investigations Of Curved Surfaces Of 1827 And 1825*, Princeton University Library.
- Gleyze, J. F., Bacro, J. N. & Allard, D. (2001), Detecting regions of abrupt change: Wombling procedure and statistical significance, *in* P. Monestiez, D. Allard & R. Froide-

- vaux, eds, 'geoENV III — Geostatistics For Environmental Applications', Springer Netherlands, Dordrecht, pp. 311–322.
- Greenwood, J. (1984), 'A Unified Theory Of Surface Roughness', *Proceedings of the Royal Society of London. A. Mathematical and Physical Sciences* **393**(1804), 133–157.
- Haining, R. (1993), *Spatial Data Analysis In The Social And Environmental Sciences*, Cambridge University Press.
- Harrison Jr, D. & Rubinfeld, D. L. (1978), 'Hedonic Housing Prices And The Demand For Clean Air', *Journal of environmental economics and management* **5**(1), 81–102.
- Heaton, M. J. (2014), 'Wombling Analysis Of Childhood Tumor Rates In Florida', *Statistics and Public Policy* **1**(1), 60–67.
- Heaton, M. J., Datta, A., Finley, A. O., Furrer, R., Guinness, J., Guhaniyogi, R., Gerber, F., Gramacy, R. B., Hammerling, D., Katzfuss, M. et al. (2019), 'A Case Study Competition Among Methods For Analyzing Large Spatial Data', *Journal of Agricultural, Biological and Environmental Statistics* **24**(3), 398–425.
- Hu, L., He, S., Han, Z., Xiao, H., Su, S., Weng, M. & Cai, Z. (2019), 'Monitoring Housing Rental Prices Based On Social Media: An Integrated Approach Of Machine-Learning Algorithms And Hedonic Modeling To Inform Equitable Housing Policies', *Land use policy* **82**, 657–673.
- Jones, C. B. (2014), *Geographical Information Systems And Computer Cartography*, Routledge.
- Kent, J. T. (1989), 'Continuity Properties For Random Fields', *The Annals of Probability* pp. 1432–1440.
- Kent, J. T., Mardia, K. V. & Taylor, C. C. (2008), *Modelling Strategies For Bivariate*

- Circular Data, *in* ‘Proceedings of the Leeds Annual Statistical Research Conference, The Art and Science of Statistical Bioinformatics, Leeds University Press, Leeds’, pp. 70–73.
- Kreyszig, E. (2019), *Introduction To Differential Geometry And Riemannian Geometry*, University of Toronto Press.
- Law, A. M., Kelton, W. D. & Kelton, W. D. (2000), *Simulation Modeling And Analysis*, Vol. 3, McGraw-Hill New York.
- Lawson, A. B. (2013), *Statistical Methods In Spatial Epidemiology*, John Wiley & Sons.
- Leenaers, H., Schouten, C. & Rang, M. (1988), ‘Variability Of The Metal Content Of Flood Deposits’, *Environmental Geology and Water Sciences* **11**(1), 95–106.
- LeSage, J. & Pace, R. K. (2009), *Introduction To Spatial Econometrics*, Chapman and Hall/CRC.
- Li, P., Banerjee, S., Hanson, T. A. & McBean, A. M. (2015), ‘Bayesian Models For Detecting Difference Boundaries In Areal Data’, *Statistica Sinica* **25**(1), 385.
- Liang, S., Banerjee, S. & Carlin, B. P. (2009), ‘Bayesian Wombling For Spatial Point Processes’, *Biometrics* **65**(4), 1243–1253.
- Lu, H. & Carlin, B. P. (2005), ‘Bayesian Areal Wombling For Geographical Boundary Analysis’, *Geographical Analysis* **37**(3), 265–285.
- Magnus, J. R. & Neudecker, H. (1980), ‘The Elimination Matrix: Some Lemmas And Applications’, *SIAM Journal on Algebraic Discrete Methods* **1**(4), 422–449.
- Majumdar, A., Munneke, H. J., Gelfand, A. E., Banerjee, S. & Sirmans, C. (2006), ‘Gradients In Spatial Response Surfaces With Application To Urban Land Values’, *Journal of Business & Economic Statistics* **24**(1), 77–90.

- Mardia, K., Kent, J., Goodall, C. & Little, J. (1996), ‘Kriging And Splines With Derivative Information’, *Biometrika* **83**(1), 207–221.
- Matérn, B. (2013), *Spatial Variation*, Vol. 36, Springer Science & Business Media.
- Morris, M. D., Mitchell, T. J. & Ylvisaker, D. (1993), ‘Bayesian Design and Analysis Of Computer Experiments: Use Of Derivatives In Surface Prediction’, *Technometrics* **35**(3), 243–255.
- O’Neill, B. (2006), *Elementary Differential Geometry*, Elsevier.
- Pebesma, E., Bivand, R., Pebesma, M. E., RColorBrewer, S. & Collate, A. (2012), ‘Package “sp”’, *The Comprehensive R Archive Network* .
- Plant, R. E. (2018), *Spatial Data Analysis In Ecology And Agriculture Using R*, CRC Press.
- Plummer, M., Best, N., Cowles, K. & Vines, K. (2015), ‘Package “coda”’, URL <http://cran.r-project.org/web/packages/coda/coda.pdf>, accessed January **25**, 2015.
- Pressley, A. N. (2010), *Elementary Differential Geometry*, Springer Science & Business Media.
- Qu, K., Bradley, J. R. & Niu, X. (2021), ‘Boundary Detection Using A Bayesian Hierarchical Model For Multiscale Spatial Data’, *Technometrics* **63**(1), 64–76.
- Quick, H., Banerjee, S. & Carlin, B. P. (2015), ‘Bayesian Modeling And Analysis For Gradients In Spatiotemporal Processes’, *Biometrics* **71**(3), 575–584.
- Rudin, W. (1976), *Principles Of Mathematical Analysis*, Vol. 3, McGraw-hill New York.
- Santner, T. J., Williams, B. J., Notz, W. I. & Williams, B. J. (2003), *The Design And Analysis Of Computer Experiments*, Vol. 1, Springer.
- Schabenberger, O. & Gotway, C. A. (2017), *Statistical Methods For Spatial Data Analysis*, CRC press.

- Schnare, A. B. & Struyk, R. J. (1976), 'Segmentation In Urban Housing Markets', *Journal of Urban Economics* **3**(2), 146–166.
- Spivak, M. (1999), *A Comprehensive Introduction To Differential Geometry*, number v. 1–5 in 'A Comprehensive Introduction to Differential Geometry', Publish or Perish Inc.
- Stein, M. L. (1999), *Interpolation Of Spatial Data: Some Theory For Kriging*, Springer Science & Business Media.
- Stevens, K. A. (1981), 'The Visual Interpretation Of Surface Contours', *Artificial Intelligence* **17**(1-3), 47–73.
- Terres, M. A. & Gelfand, A. E. (2015), 'Using Spatial Gradient Analysis To Clarify Species Distributions With Application To South African Protea', *Journal of Geographical Systems* **17**(3), 227–247.
- Terres, M. A. & Gelfand, A. E. (2016), 'Spatial Process Gradients And Their Use In Sensitivity Analysis For Environmental Processes', *Journal of Statistical Planning and Inference* **168**, 106–119.
- Vaughan, L. (2018), *Mapping Society: The Spatial Dimensions Of Social Cartography*, UCL Press.
- Waller, L. A. & Gotway, C. A. (2004), *Applied Spatial Statistics For Public Health Data*, Vol. 368, John Wiley & Sons.
- Wang, F., Bhattacharya, A. & Gelfand, A. E. (2018), 'Process Modeling For Slope And Aspect With Application To Elevation Data Maps', *Test* **27**(4), 749–772.
- Wang, X. & Berger, J. O. (2016), 'Estimating Shape Constrained Functions Using Gaussian Processes', *SIAM/ASA Journal on Uncertainty Quantification* **4**(1), 1–25.

Webster, R. & Oliver, M. A. (2007), *Geostatistics For Environmental Scientists*, John Wiley & Sons.

Williams, C. K. & Rasmussen, C. E. (2006), *Gaussian Processes For Machine Learning*, Vol. 2, MIT press Cambridge, MA.

Winkler, G. (2003), *Image Analysis, Random Fields And Markov Chain Monte Carlo Methods: A Mathematical Introduction*, Vol. 27, Springer Science & Business Media.

Wise, S. & Craglia, M. (2007), *GIS And Evidence-Based Policy Making*, CRC Press.

Womble, W. H. (1951), 'Differential Systematics', *Science* **114**(2961), 315–322.